POLITECNICO DI TORINO

Corso di Laurea Magistrale
in Ingegneria Energetica e Nucleare

Specializzazione: *Sustainable nuclear energy*

Tesi di Laurea

Robustness Analysis of Treatment Planning System for Proton Therapy

Relatori

Prof. Gianni Coppa (DET)
Dott.ssa Faiza Bourhaleb (i-See s.r.l.)

Candidato

Michele Raimo
(matr.281430)

Anno Accademico 2022-2023

"Se il risultato conferma l'ipotesi, allora hai appena fatto una misura.
Se il risultato è contrario alle ipotesi, allora hai fatto una scoperta."

Enrico Fermi

Abstract

Proton radiotherapy represents one of the most advanced methods for treating treatment of cancer patients. Treatment with proton beams is a strategy therapy that is receiving considerable interest in the clinical field and in research. The most innovative aspect of proton therapy is the ability to deposit the energy of ionizing radiation in a highly precise and finite way. This advantage, compared with other types of external radiation therapy, is due to the very nature of proton transport in matter. The protons release the greatest amount of energy at the end of their path through the matter. By adjusting the energy of the beam, it is therefore possible to target the tumor mass, significantly limiting the amount of the dose deposited in healthy tissues. Proton therapy is performed thanks to the beam generated by a particles accelerator. The cost and complexity of a facility, capable of generating a beam of protons at very high energies, remain two of the main obstacles to the spread of this oncology treatment technique.
The treatment plan, performed at the beginning of therapy, is evaluated by models of inverse planning that allow the beam characteristics to be defined, in order to perform the correct irradiation of the target. The treatment plan is defined starting from the axial Computed Tomography (CT) scan of the patient and the dose of ionizing radiation intended to be deposited in diseased tissues. The analytical methods that are used, however, are sensitive to physical and physiological uncertainties that may occur in the patient during treatment sessions. It is possible, with the help of algorithms termed 'direct' to verify the distribution of dose obtained from the treatment plan. It is possible to check that any uncertainties do not compromise the effectiveness of the therapy. The direct models are principally two: the analytical method and the method based on a Monte Carlo simulation.
The purpose of this work is to evaluate the effects of uncertainties in the distribution effective dose within the domain. The perturbations are introduced by modifying the density values of the tissues of the patient. By acting on the characteristics of the CT scan, two perturbed scenarios are considered: one, in which the tissues are denser than actual ones, and the other, in which they are less dense. The objective is to verify, through the direct methods, with the same treatment plan, the perturbation of the dose distribution in the two scenarios in which the uncertainties on the density are introduced. In this way, it becomes possible to predict whether the treatment plan is still valid or whether it is compromised. In the second case, it will be necessary to make a new plan. Finally, the purpose is to compare the sensitivity of the direct methods used as a control tool. Starting from the characteristics of the two methods, it is necessary to understand which one is the most suitable for the simulation of cancer treatment.

Estratto

La Radioterapia protonica rappresenta uno dei metodi più avanzati per il trattamento di pazienti oncologici. Il trattamento con fasci di protoni è una strategia terapeutica che riscuote un notevole interesse nel campo clinico e nei progetti di ricerca. L'aspetto maggiormente innovativo della Protonterapia è la capacità di depositare l'energia delle radiazioni ionizzanti in maniera altamente precisa e circoscritta. Questo vantaggio, rispetto ad altre tipologie di radioterapia esterna, è dovuto alla natura stessa del trasporto protonico nella materia. I protoni rilasciano la maggior aliquota di energia alla fine del loro percorso di attraversamento della materia. Regolando l'energia del fascio, è dunque possibile colpire in maniera mirata la massa tumorale, limitando sensibilmente la quota di dose depositata nei tessuti sani. La terapia protonica viene eseguita grazie al fascio generato da un acceleratore di particelle. Il costo e la complessità di un impianto, in grado di generare un fascio di protoni ad energie molto alte, rimangono due dei principali ostacoli alla diffusione di questa tecnica di cura oncologica.
Il piano di trattamento, eseguito all'inizio della terapia, viene valutato da modelli di pianificazione inversa che permettono di definire le caratteristiche del fascio, necessarie al corretto irraggiamento del target. Il piano di trattamento è definito a partire dalla Tomografia Assiale Computerizzata (TAC) del paziente e dalla dose di radiazioni ionizzanti che si intende depositare nei tessuti malati. I metodi analitici che vengono utilizzati risultano, però, sensibili ad incertezze fisiche e fisiologiche che possono presentarsi nel paziente durante le sedute di trattamento.
É possibile, con l'ausilio di algoritmi definiti 'diretti', verificare la distribuzione di dose ottenuta a partire dal piano di trattamento, controllando che eventuali incertezze non compromettano l'efficacia della terapia. I modelli diretti sono principalmente due: il metodo analitico e il metodo basato su una simulazione Monte Carlo.
Lo scopo di questo lavoro è valutare gli effetti delle incertezze nella distribuzione effettiva della dose all'interno del dominio. Le perturbazioni sono introdotte modificando i valori di densità dei tessuti del paziente. Agendo sulle caratteristiche della TAC, si considerano due scenari perturbati: uno, in cui i tessuti sono più densi di quelli reali, e l'altro, in cui sono meno densi. L'obiettivo è di verificare, attraverso i metodi diretti, a parità di piano di trattamento, la perturbazione della distribuzione di dose nei due scenari in cui sono state introdotte le incertezze sui valori di densità. In questo modo, risulta possibile prevedere se il piano di trattamento è ancora valido o se risulta compromesso. Nel secondo caso sarà necessario effettuare un nuovo piano. Infine, si vuole confrontare la sensibilità dei metodi diretti usati come strumento di controllo. A partire dalle caratteristiche dei due metodi, si intende comprendere quale sia il più adatto per la simulazione del trattamento oncologico.

Contents

List of Tables

List of Figures

1 Radiation physics

1.1 Radioactivity

Each nuclide is characterized by an atomic number and a mass number. Considering a neutral nuclide, the atomic number (Z) is defined as the number of electrons or the number of protons. The mass number (A) is defined as the sum of the number of the protons and the number of the neutrons.
It is possible to represent a generic nuclide X as

$$X_Z^A$$

The atomic number is written as a subscript and the mass number as an apex.

The isotopes of an atom present the same atomic number and a different mass number. The atomic number determines the chemical characteristics of a nuclide. This means that the isotopes are considered identically from a chemical point of view. In the next section, it will be clear why this characteristic of isotopes is really important in the nuclides use in patient therapy.

Considering the simple schematic structure of an atom, it is composed of a nucleus and an electronic cloud structured in orbitals around the nucleus. The nucleus is composed of protons and neutrons and it represents the biggest fraction of mass of the whole atom. Protons and neutrons are called "nucleons" and they are held together by a strong force. The protons in the nucleus are subjected to a Coulomb repulsion that increases with the increase of the number of protons present.

$$F = qE = \frac{q_1 q_2}{r^2} k$$

$q1$ and $q2$ are the charge values of the particles. k is the Coulomb constant. r is the distance between the two charged particles. qE is the force that a generic charged particle receives from a generic electrical field.

The neutrons provide stability to the nucleus, especially in case of large nuclei. The balance of the number of protons and the number of neutrons in a nucleus is a key point for the stability of a nuclide.
The Segrè chart (Figure 1) is a 2D plot based on the idea of plotting the nuclides on a xy chart. The x axis represents the number of neutrons and the y axis represents the number of protons.
The black line indicates the stable nuclei. It is possible to see that, for low values of the number of neutrons, the behavior is almost linear. This means that until 20 protons, the same number of neutrons ensures stability to the nuclide.

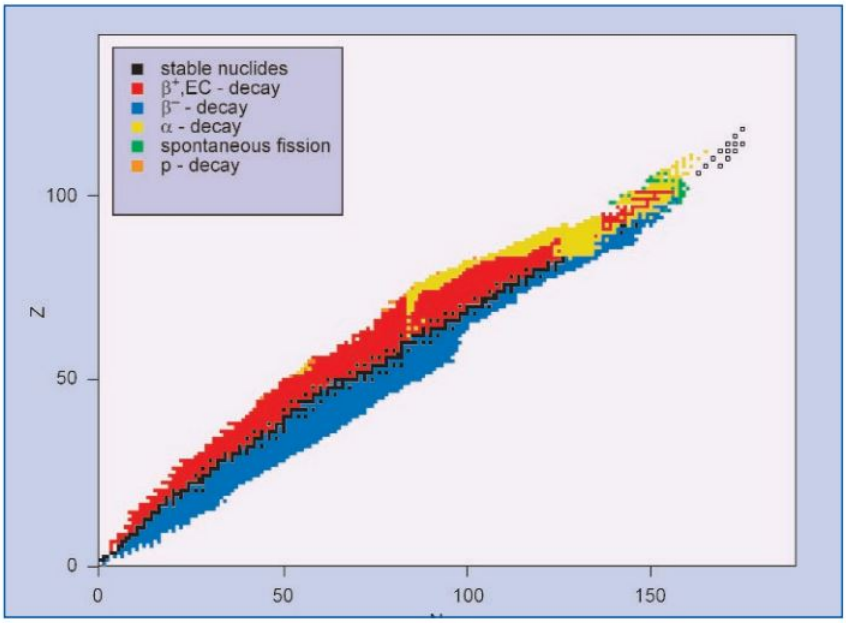

Figure 1: Segrè chart [50]

After around 20 protons, more than 20 neutrons are necessary to counterbalance Coulomb repulsion and ensure stability to the nucleus.
As said previously, the black points represent nuclides in the stability condition. The other colored parts are related to the unstable nuclides. These nuclides, differently to the stable ones, decay in different ways in order to reach a stable condition. In Figure 1, the different colors are related to different types of decay.
The stable condition, that is represented by the stability line, is the end target of each decay process. This graphical reference, on Segrè chart, is called "stability valley". This name is really explanatory in order to give the idea that the unstable nuclei tend all to that condition like rolling stones on the slopes of a steep valley. This qualitative approach results clearly in Figure 2.
Experimental evidence shows that nuclei, with the number of protons and/or number of neutrons equal to "magic numbers", as 2, 8, 20, 28, 50, 82, 126, are particularly stable.
The unstable nuclei, that decay to the stability condition, rearrange nucleons with nuclear reactions releasing and/or absorbing particles. The activity of an unstable nucleus that decays to reach stability is defined as "Radioactivity". It is also possible to define Radioactivity as the spontaneous process in which an unstable nucleus emits particles becoming a more stable nucleus. It is crucial to highlight that not in all cases an unstable nucleus, after a decay event, reaches stability, but at the end of its decay chain it will do. This means that, in some cases, a lot of decay steps are necessary in order to reach the stability valley. In a decay process, the unstable nucleus is called "parent" and the more stable one is called "daughter".

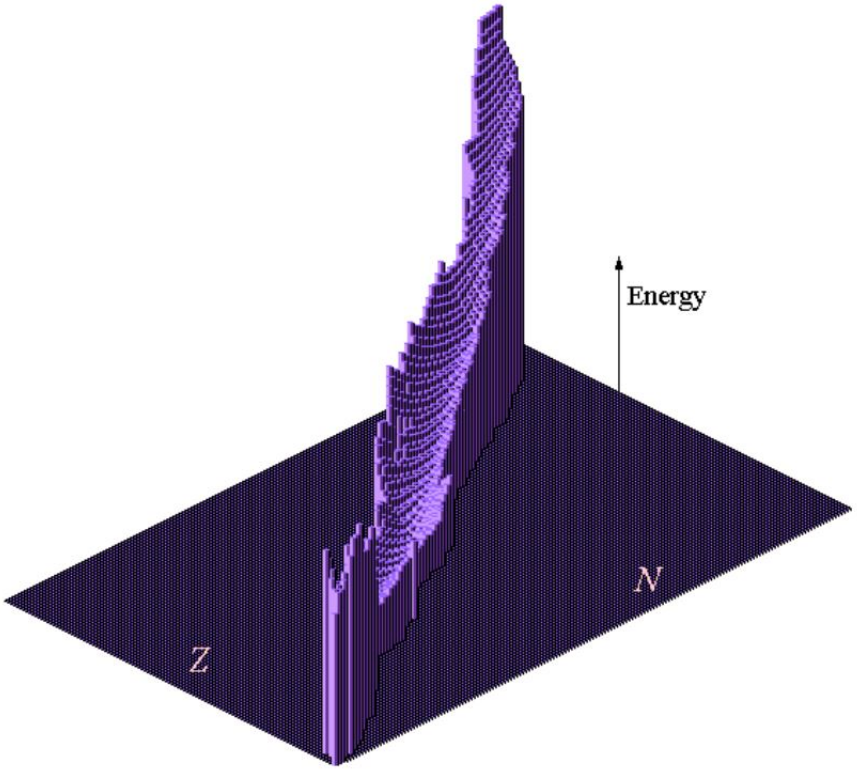

Figure 2: 3D representation of "Stability valley" [76]

When a parent nucleus decays, the daughter one could be stable or unstable. If it is stable, the decay chain stops, if it is still unstable, it will decay generating another daughter, until reaching the stability condition. The unstable atoms are also called "Radionuclides".

Radioactivity is measured in Becquerel (Bq) that is defined as

$$1 \quad Bq = 1 \quad decay \quad per \quad second$$

1 Becquerel is a very small quantity, for this reason, the MBq (10^6 Bq) and the old unit, the Curie, are widely used.

$$1 \quad Curie = 37000 \quad MBq$$

There are different ways of decay, but all of these are characterized by a release of energy. In medical application of the radiation, this energy deposition is used to treat cancers.
Returning to the isotopes, considering two isotopes with the same atomic number, one is stable and the other is unstable. If the radioactive one is intaken in the

body of the patient, it will be physiologically managed as the stable one, because, chemically speaking, isotopes are equivalent. This aspect is very useful in case of internal cancer treatment. It is possible to deposit energy on the malignant cells concentrating the unstable nuclide close to the tumor. An example of this procedure is the thyroid cancer treatment using Iodine-131. The unstable atom of iodine is concentrated in the thyroid in the same way as the stable one. Once reached the thyroid, it decays and deposits energy to the malignant cells of the tumor.

1.2 Law of radioactive decay

Considering a generic decay process, it is possible to obtain the decay law, in order to estimate the concentration of the nuclide in time. $N_P(t)$ is the concentration of a generic parent nuclide as a function of time.

$$N_P(t) = number \quad of \quad parent \quad nuclei \quad at \quad time \quad t$$

$$number \quad of \quad decay \quad events \quad in \quad \Delta t = \lambda N_P(t)\Delta t$$

Δt is a finite time interval and λ is the decay constant related to the decay process. The dimension of λ is the inverse of a time, it describes the frequency of the decay event.

$$\lambda = [T^{-1}]$$

At this point, it is necessary to consider the difference of the numbers of nuclides at the time t and the same quantity at the time $t + \Delta t$.

$$N_P(t + \Delta t) - N_P(t) = -\lambda N_P(t)\Delta t$$

Dividing both sides by Δt

$$\frac{N_P(t+\Delta t)-N_P(t)}{\Delta t} = -\lambda N_P(t)$$

If the time interval Δt is so small that it is possible to assume that it tends to zero

$$\frac{dN_P(t)}{dt} = -\lambda N_P(t)$$

$\lambda N_P(t)$ is the activity and it is measured in Becquerel.

The last equation is a differential equation that is possible to solve separating variables. Considering to know the initial condition of the number of the parent nuclide

$$N_P(t=0) = N_P^0$$

$$N_P(t) = N_P^0 e^{-\lambda t}$$

The exponential equation is the radioactive decay law of an unstable parent nuclide. This law has a decreasing exponential behavior, as it results from Figure 3.

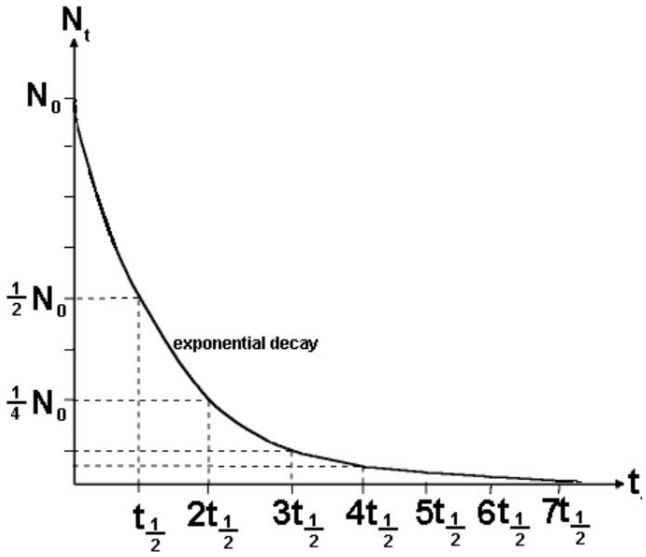

Figure 3: Plot of the Radioactive decay law [44]

In radioactive decay, a very useful quantity is the "half-life". It is defined as the time at which the number of nuclides is the half of the initial one. This quantity is, for example, used in the "Carbon-14 dating" strategy. In order to obtain the formula of the half-life, it is necessary to substitute in the decay law the half of the starting nuclei.

$$\tfrac{1}{2} N_P^0 = N_P^0 e^{-\lambda t}$$

At this point, it is possible to simplify the initial value of nuclides on both sides and explicit the time t.

$$\tfrac{1}{2} = e^{-\lambda t}$$

$$\ln \tfrac{1}{2} = -\lambda t$$

$$\ln 2 = \lambda t$$

$$t_{\frac{1}{2}} = \tfrac{\ln 2}{\lambda}$$

The last equation is the formula of the half-life of a generic decay process. It is possible to see the half-life point in Figure 4.

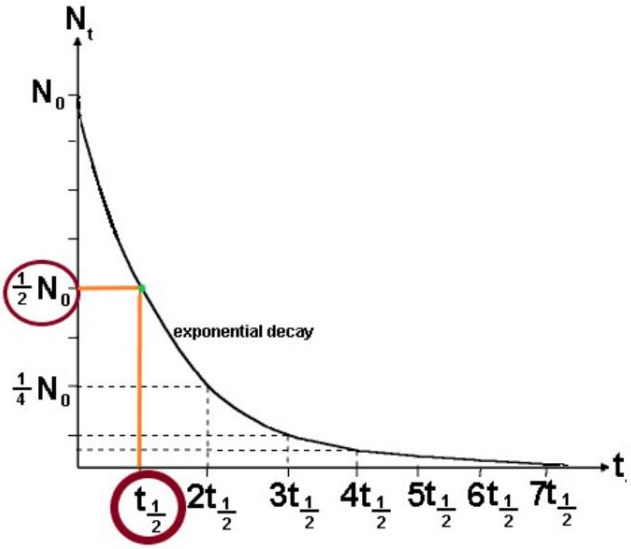

Figure 4: Plot of the Radioactive decay law with the detail on half life [44]

1.3 Radioactive decays

An unstable atom decays into a more stable one trying to reach the stability condition. There are a lot of decay processes, each of these is typical of different radionuclides.
In this section a brief description of each decay process is shown.

1.3.1 Alpha decay

The alpha decay is described by the following equation.

$$X_Z^A = D_{Z-2}^{A-4} + \alpha_2^4$$

It consists of an unstable parent that decays in a more stable daughter nuclide. The daughter has an atomic number decreased by two and a mass number decreased by four. In the alpha decay process, there is the emission of a particle called "alpha particle". The alpha particle is an atom of helium that is characterized by an atomic number equal to two and a mass number equal to four. The alpha particle emitted is used, for example, in some internal radiotherapy applications.
The scheme of the alpha decay is shown in Figure 5.

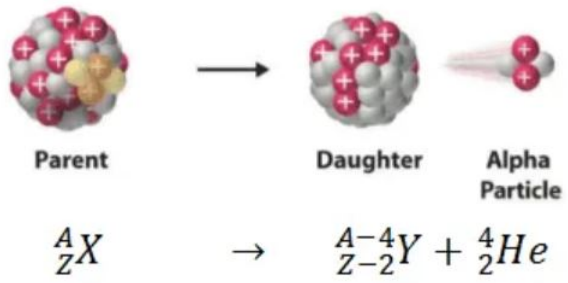

Figure 5: Alpha decay scheme [49]

An example of radionuclide that decays emitting an alpha particle is Radium. The following equation describes its decay chain.

$$Ra_{88}^{226} = Rn_{86}^{226} + \alpha_2^4$$

1.3.2 Beta decay

Another important decay process is the beta decay. It is divided into two cases: the case in which an electron is emitted and the case in which a positron is emitted. The first case is called β^- and the second is called β^+. In both cases, the sum of the atomic number and the mass number remains constant. The two cases of beta decays are described by the following equations.

$$X_Z^A = D_{Z+1}^A + e^- + \bar{\nu_e} \quad (\beta^-)$$

$$X_Z^A = D_{Z-1}^A + e^+ + \nu_e \quad (\beta^+)$$

In the β^- case, the generic parent X decays in a daughter with the atomic number increased by one and the mass number that does not change. In this case, an electron

and an antineutrino are emitted.
In the β^+ case, the parent decays in a daughter with the atomic number decreased by one and the mass number that does not change, as in the previous case. In this case, a positron and a neutrino are emitted. The positron emitted in the β^+ decay is used in the Positron Emission Tomography (PET), for example. A β^+ source is intaken in the patient and the positron is emitted into the body. The positron interacts with the electrons of the atoms doing annihilation. This process generates the emission of two photons that could be detected by the external imaging facility and perform a tomography scan. This procedure is used to individuate the position of the cancer masses.

In Figure 6 and Figure 7 , it is possible to see the scheme of the two beta decays.

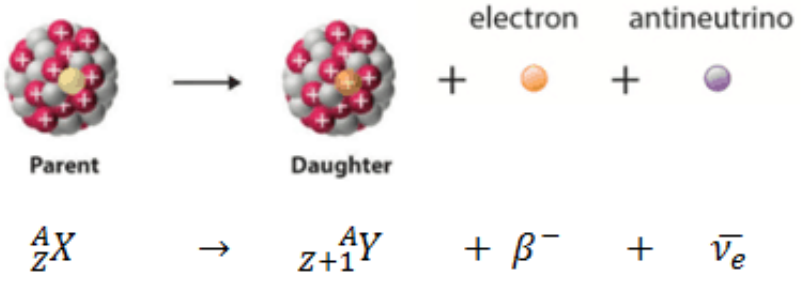

Figure 6: β^- decay scheme[51]

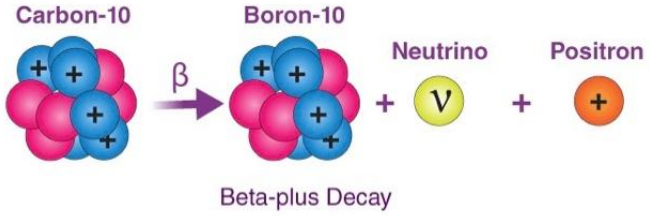

Figure 7: β^+ decay scheme[42]

An example of radionuclide that decays emitting an electron is Phosphorus. The following equation describes its decay chain.

$$P_{15}^{32} = S_{16}^{32} + e^- + \bar{\nu_e}$$

An example of radionuclide that decays emitting a positron is Fluorine. The following equation describes its decay chain.

$$F_9^{18} = D_8^{18} + e^+ + \nu_e$$

1.3.3 Electron capture

The electron capture is described by the following equation.

$$X_Z^A + e^- = D_{Z-1}^A + \nu_e$$

In this case, a proton rich parent catches its own inner shell electron and decays in a daughter with the same mass number and the atomic number decreased by one. A neutrino is emitted. An example of nuclide that decays capturing an electron is the Carbon-11 and its decay reaction is shown in Figure 8.

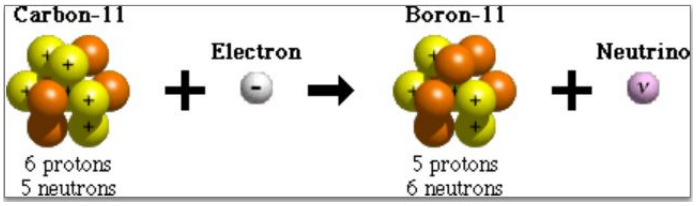

Figure 8: Electron capture decay scheme[35]

1.3.4 Gamma decay and internal conversion

An atom could be in a "metastable" condition. This means that it presents the same mass number and atomic number of the stable isotope, but it has an energy content that makes it not completely stable. This condition is also called an "excited state". This type of radionuclides decays in two ways: gamma decay or internal conversion. In the gamma decay, the excess of energy is released emitting a photon. In the internal conversion, the energy is released to an atomic electron.

The gamma decay and the internal conversion are described by the following equations. The asterisk indicates the metastable condition.

$$X_Z^{*A} = X_Z^A + \gamma(photon)$$

$$X_Z^{*A} = X_Z^A + energy \quad to \quad an \quad atomic \quad electron$$

The emission of the photon, in the gamma decay, usually is instantaneous, but there are some exceptions that are very useful for medical applications, such as Technetium. This radionuclide is used to perform internal radiotherapy and it emits a photon after six hours.

1.3.5 Others decays

There are other three decay mechanisms that are less interesting from an applicative point of view, but that are listed for completeness.
The three processes are the proton emission, the neutron emission and the spontaneous fission.

These three processes are respectively described by the following equations.

$$X_Z^A = D_{Z-1}^{A-1} + p$$

$$X_Z^A = D_Z^{A-1} + n$$

$$X = D_1 + D_2$$

1.4 Interaction of radiation with matter

It is possible to consider radiation as a beam of particles. In order to simplify the mathematical treatment, it is necessary to introduce the hypothesis of homogeneous beam: all the particles have the same velocity and the same energy. The radiation beam is characterized by two quantities: the particle density and the velocity of the particles.

$$n = particle \quad density = [L^{-3}]$$

$$v = velocity = [LT^{-1}]$$

Starting from the density and the velocity definitions, it is possible to estimate the intensity of the beam as follows.

$$I = nv = [L^{-2}T^{-1}]$$

Performing the balance of the particles that cross a generic surface S, it is possible to define the intensity of the beam as the number of particles that cross a generic surface S in a time interval dt divided by the product of S and dt.

$$I = \frac{number \quad of \quad particles \quad that \quad cross \quad S \quad in \quad dt}{Sdt}$$

At this point, it is necessary to consider a generic target with which the particle beam interacts, as it is shown in Figure 9.
Considering two generic points in the target: x and $x + dx$, it is possible to write

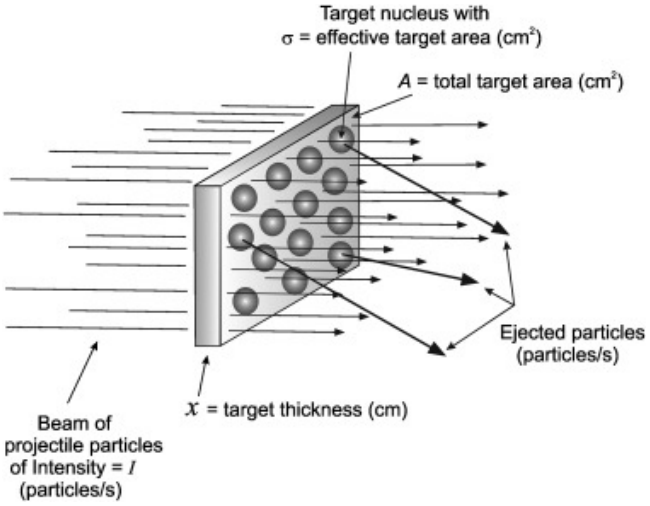

Figure 9: Scheme of the interaction of the radiation with the target [68]

$$I(x + dx) = I(x) - I(x)n_t\sigma dx$$

Where n_t is the density of the target, dx is the distance between the two generic points and σ is the microscopic cross section. σ has the dimension of an area and it is related to the probability, for the radiation, to interact with the particles of the target. The macroscopic cross section μ is the product of σ with the density of the target and it is defined as the probability per unit path that the particles of the beam interact with the target. The macroscopic cross section is also called "attenuation coefficient".

Rearranging the terms of the previous equation and supposing to have an infinitesimal distance between the two generic points considered, it is possible to write

$$\frac{dI}{dx} = -I(x)n_t\sigma$$

This is a differential equation that is possible to solve separating variables. Considering to know the initial value of the intensity of the beam and to have a constant value of μ, it is possible to obtain the following law.

$$I(x) = I(0)e^{-\mu x}$$

This law has a decreasing exponential behavior.
If the attenuation coefficient is not constant and it is a function of x, the equation becomes

$$I(x) = I(0)e^{\int_0^L -\mu(x)dx}$$

2 Effects of radiation

2.1 Ionizing radiation

The radiation could be divided into three categories that are characterized by different levels of energy: non-ionizing, ionizing and inducing artificial radioactivity. These three categories are listed in order of increasing energy. The non-ionizing radiation is characterized by long wavelength and low frequency, while the ionizing one is characterized by higher frequency and shorter wavelength.
Remembering Planck's Law, the energy E associated to an electromagnetic wave is proportional to its frequency ν.

$$E = h\nu$$

$$h = Planck \quad constant = 6.62607015 \cdot 10^{-34} J \cdot s$$

This means that the non-ionizing radiation has a lower energy than the ionizing one.

Ionizing radiation has the capability to create ions at the molecular level and to damage the DNA chain of the cells. Non-ionizing radiation, as the name suggests, is not able to do this, but it can only deposit thermal energy on the tissues causing, for example, skin burns. There are a lot of research studies based on the possible damages to the cells caused by the non-ionizing radiation, but, up to now, there are not experimental evidences.

Some examples of non-ionizing radiation are

- Ultraviolet
- Visible spectrum
- Infrared
- Lasers
- Extremely Low Frequencies (ELF)
- Radio frequencies
- Microwave frequencies

Some examples of ionizing radiation are

- Gamma rays
- X-rays
- Alpha particles
- Beta particles
- Neutrons

In Figure 10, it is possible to see the different types of radiation relating to the energy levels.

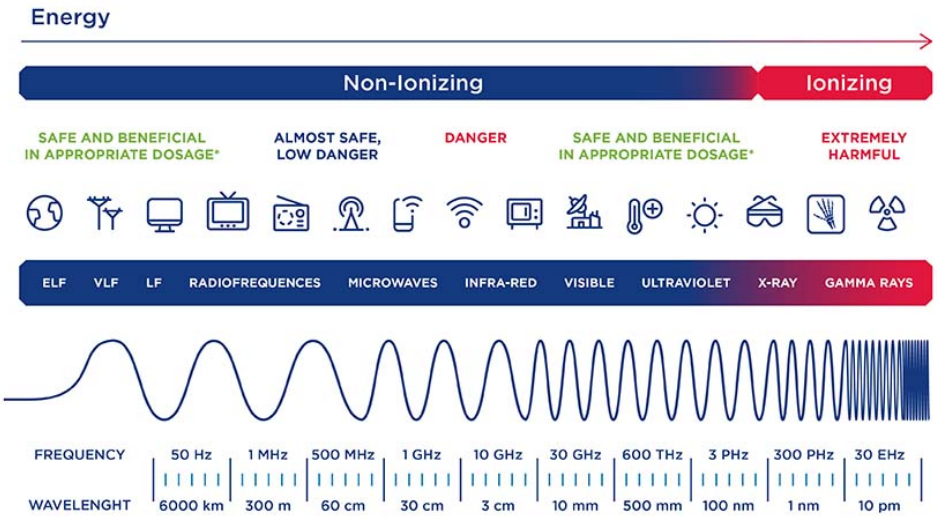

Figure 10: Scheme ionizing and non-ionizing radiation[52]

If the energy of the radiation is very high, a neutron could be captured by a stable atom. Its mass number increases by one, but the atomic number remains constant. This process makes the nuclide unstable and it becomes a radionuclide. This process is defined as "activation" or "radioactivation" and it is related to very high energy radiation. This process is typical of the rich neutron environment as the nuclear reactors. An example of activation reaction is the interaction of the Cobalt-59 with a neutron.

$$n_0^1 + Co^{59} = Co^{60}$$

Cobalt-60 is a radionuclide and it decays in Nichel-60 emitting a beta particle and a photon. The half-life is equal to 5272 years. The scheme of this reaction is reported in Figure 11.

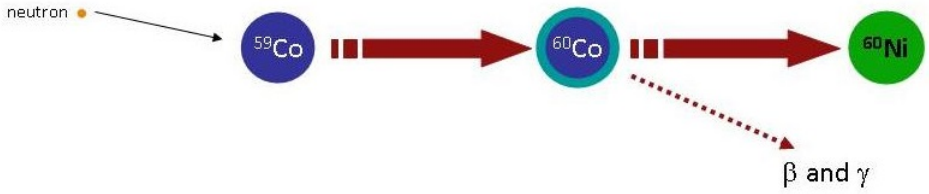

Figure 11: Scheme of the Co-60 activation[32]

Ionizing radiation could be divided into two branches: the directly ionizing radiation and the indirectly ionizing radiation.
The directly ionizing radiation is represented by the condition in which a beam of fast charged particles interacts directly with the charged particles of the matter, with Coulomb interactions.
The indirectly ionizing radiation, instead, is related to the condition in which a beam of uncharged particles, such as photons or neutrons, deposits its energy to the charged particles of the matter and the resulting fast charged particles then deliver their energy to the matter as the directly ionizing radiation case.
These two types of interactions between radiation and matter are shown in Figure 12.

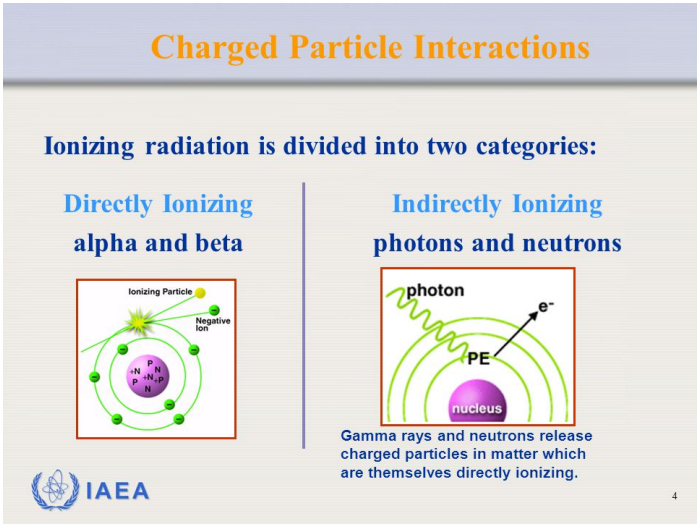

Figure 12: Directly ionizing radiation and Indirectly ionizing radiation[59]

2.2 Radiation measurement quantities

There are a lot of useful quantities that are used to estimate the energy deposition in the matter and its effects on the tissues. In the following sections, the main ones are presented.

2.2.1 ϵ_{tr} and ϵ

The first two quantities, related to the energy deposition, are the transferred energy (ϵ_{tr}) and the imparted energy (ϵ). The transferred energy is defined as the energy transferred from photons to charged particles. It is the sum of initial kinetic energies of all the charged particles released by uncharged ionizing radiation from an amount of material of mass m. The imparted energy is defined as the total energy deposited by the charged particles in a volume element of mass m. These two quantities are necessary to define two widely used quantities: the dose and the kerma.

2.2.2 Dose and Kerma

The dose is, probably, the most used quantity to estimate the magnitude of the radiation effects in the matter. It is defined as the ratio between the imparted energy and the mass of the target. Its dimension is [J/kg]. The unit of measure of the dose is the Gray (Gy) or the older one, the Rad (Absorbed Radiation Dose).

$$D = Dose = \frac{\epsilon}{m} = [J/kg]$$

$$1 \quad J/kg = 1 \quad Gy = 100 \quad Rad$$

The dose is, more precisely, called "Absorbed dose", in order to avoid confusing it with the effective dose and the equivalent dose.

The kerma k (Kinetic Energy Released to MAtter) is defined, by the ICRU (International Commission on Radiation Unit and measurement), as the ratio between the transferred energy and the mass of the target. Also in this case, the unit of measurement is an energy divided by a mass.

$$k = \frac{\epsilon_{tr}}{m}$$

2.2.3 Equivalent dose

The absorbed dose is not sufficient to describe the radiation effects on the tissues. The first limit of the absorbed dose definition is the fact that the same value of dose of two different types of radiation causes different effects. The absorbed dose does not take into account the type of radiation.

The equivalent dose H is based on the absorbed dose value, but it also takes into account, with the introduction of a weighting factor W_R, the type of radiation. This factor is called "Radiation weighting factor". It is a dimensionless number. The unit of measurement of the equivalent dose is the Sievert (Sv).

$$H = D \cdot W_R \quad [Sv]$$

The factor W_R depends on how the energy release of the radiation is distributed along the path in the tissues. This aspect is estimable with a very important quantity, the LET (Linear Energy Transfer). The unit of measurement of LET is $KeV/\mu m$. Higher is the value of LET and more energy is released in a short distance, lower is the value of LET and less energy is released distributed over a long distance. Radiations with high values of LET, such as protons or alpha particles, are related to high values of W_R. In this case, these types of radiation release more energy in a short path. Radiations with low values of LET, such as X-rays or beta particles, are related to low values of W_R. In Table 1, the values of W_R of the most common particles are shown.

Radiation type and energy range	W_R
photons - all energies	1
electrons - all energies	1
protons - with E>2MeV	5
Alpha particles	20

Table 1: Radiation Weighting factors [60]

2.2.4 Effective dose

In order to estimate the biological effects of the radiation on human tissues, the equivalent dose is still not sufficient. The same value of equivalent dose deposited on different organs or tissues could cause different damages. Not all organs are equally sensitive to radiation. For example, if a radiation hits the entire body in a homogenous way, the effects are limited with respect to the case in which the same

radiation beam hits a single organ in a precise way. In order to take into account both the type of radiation and the type of tissues on which the dose is delivered, the effective dose is necessary.

The effective dose E has the same dimension of the equivalent dose. It is calculated by multiplying the equivalent dose by a weighting factor W_T, called "Tissues weighting factor". It takes into account the resistance of each organ or tissue in order to weight the effect of the radiation with respect to the biological characteristics of the target. Also W_T is a dimensionless number.

$$E = H \cdot W_T = D \cdot W_R \cdot W_T$$

Higher is the value of W_T and more sensitive is the tissue to the radiation. Lower is the value of W_T and more resistant is the tissue to the radiation. In Table 2, the values of W_T of the most commonly considered organs and tissues are shown.

Tissue or body part	W_T
Gonads	0.20
Bone marrow	0.12
Colon	0.12
Lung	0.12
Stomach	0.12
Bladder	0.05
Breast	0.05
Liver	0.05
Oesophagus	0.05
Thyroid	0.05
Skin	0.01
Bone surface	0.01

Table 2: Tissues Weighting factors[60]

2.3 Biological effects

As explained in the previous section, the effects of the radiation on the tissues depends on the type of the radiation, the tissue of the target and the magnitude of the dose. The radiation interacts with the DNA damaging it, in two different ways: directly and indirectly. In the direct case, the radiation interacts directly with the DNA chains causing damages and the death of the cell. In the indirect case, the radiation interacts with water generating free radicals that damage the DNA structure and causing the death of the cell. In Figure 13, these two different mechanisms are shown.

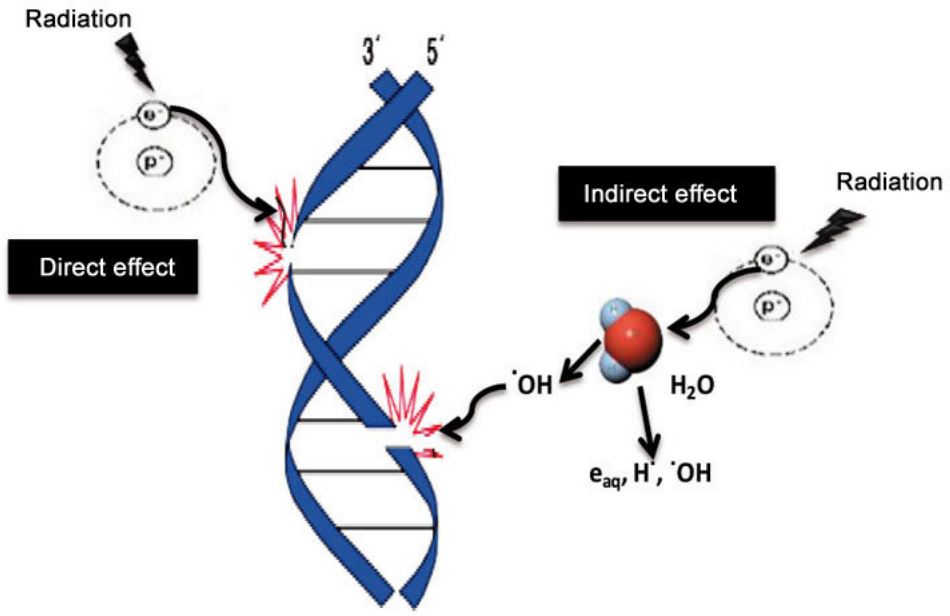

Figure 13: Direct and Indirect interaction between radiation and DNA[85]

Regarding the effects on the human body, they are mainly of two different types: stochastic and non-stochastic. Stochastic effects are further divided in stochastic hereditary effects and stochastic somatic effects. The stochastic hereditary effects do not appear on the exposed individual, but on its future generations. These types of effects are mainly light genetic and somatic effects. Some examples are one eye a different color from the other or, more grossly, one limb shorter or missing. These effects are caused by a lot of factors and radiation is only one of these. The probability to present stochastic hereditary effect is directly proportional to the absorbed dose. The stochastic somatic effects are manifested on the exposed individual as cancer appearance induction. As for the hereditary effects, cancer appearance is caused by a lot of different factors, radiation is only one of these and the probability is directly proportional to the absorbed dose. The extra cancer risk, due to radiation, is estimable with statistical methods, but it is a very difficult estimation. Stochastic effects have no threshold dose below which effects will not occur. This means that there is not a minimum dose under which the exposed individual is sure to avoid stochastic effects for him or for his future generations.
The non-stochastic effects, also called "deterministic", appear in the highly exposed individual. These effects are known as acute effects of radiation. Some examples of the symptoms are skin burns, hair loss, sterility, vomiting and diarrhea. For the deterministic effects, a threshold dose value exists. These symptoms were detected, for the first time in history, after the Hiroshima and Nagasaki bombardments. In

Table 3, dose thresholds related to some organs are shown.

Threshold dose (Gy)	**Area irradiated**	**Effect**
> 0.15	Testes	Temporaly sterility
> 0.5	Eye	Cataracts
> 2	Skin	Burns
> 2.5	Gonads	Permanent sterility
> 20	CNS	Death in hours

Table 3: Threshold dose for different organs[60]

The scheme of the effects are shown in Figure 14.

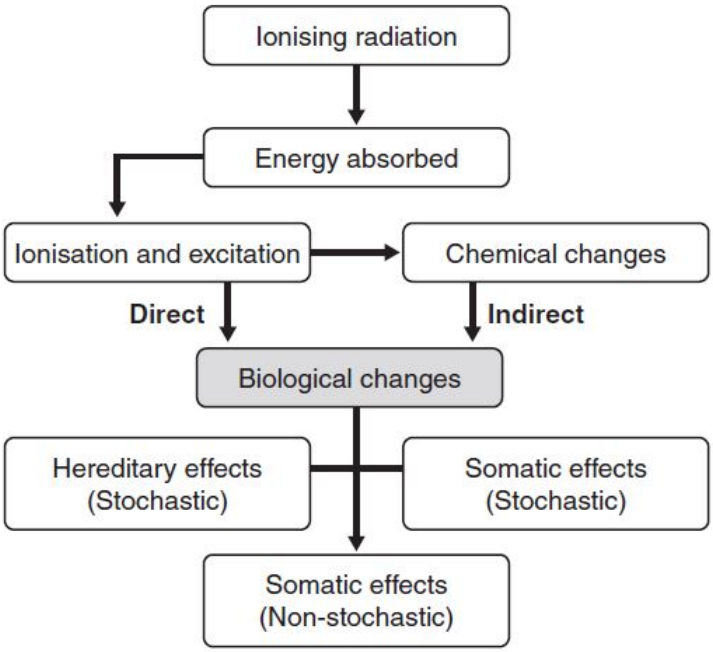

Figure 14: Scheme of radiation effects[74]

Considering a generic dose D, it is possible to estimate the effects on the cells evaluating the probability of death of them.

$$p_{death} = f(D)$$

In order to have quantitative information on the function f, it is possible to obtain a mathematical relation. As said before, the interaction of the radiation with the

cells consists of the damage to the DNA strands. Considering the double strand structure of the DNA, there are three possible cases.

The first case is characterized by a particle of the beam that breaks only one strand of the DNA. In this case, the other chain works as back-up and the repair of the DNA structure is performed.
The second case is characterized by a particle of the beam that breaks the two strands. This event is very rare and it is also called "magic bullet". In this condition, the repair of the DNA is not possible.
Finally, the third case is characterized by two particles of the beam that break one strand each. This case is represented also by the situation in which each of the two particles breaks a strand in different moments, but the interval time between the first and the second particle is shorter than the repair time. Also in this last case, the repair is not possible.
In Figure 15, two of the three cases listed above are shown.

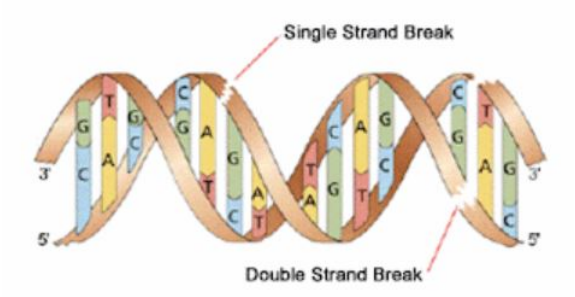

Figure 15: Interaction of the particles with the DNA[55]

At this point, considering a particle that hits a cell, it is possible to define

$$p_1 = probability \quad that \quad one \quad strand \quad is \quad broken$$

$$1 - p_1 = probability \quad to \quad survive$$

Considering N particles, it is possible to define the probability of survival to N particles as

$$p_N = (1 - p_1)^N$$

Considering that $p_1 << 1$, it is possible to do the following approximation.

$$(1 - p_1)^N \simeq e^{-p_1 N}$$

Remembering that

$$D = \epsilon N$$

$$N = \frac{D}{\epsilon}$$

It is possible to define

$$e^{-p_1 N} = e^{-\frac{D}{\epsilon}p_1} = probability \quad of \quad survival \quad for \quad 1 \quad strand = p_{1,str,surv.}$$

At this point, it is possible to estimate the magic bullet case.

$$probability \quad to \quad survive \quad to \quad magic \quad bullet = e^{-\frac{D}{\epsilon}p_2} = p_{mb,surv}$$

Redefining

$$\frac{p_1}{\epsilon} = \alpha_1$$

$$\frac{p_2}{\epsilon} = \alpha$$

Rewriting the probability of survival equations

$$p_{1,str,surv} = e^{-\alpha_1 D}$$

$$p_{mb,surv} = e^{-\alpha D}$$

It is necessary to estimate the probability to break one strand.

$$p_{1str,break} = 1 - e^{-\alpha_1 D}$$

At this point, it is possible to estimate the probability to break two strands.

$$p_{2str,break} = (1 - e^{-\alpha_1 D})^2$$

It is necessary to estimate the probability to not break the two strands.

$$p_{2str,surv} = 1 - (1 - e^{-\alpha_1 D})^2$$

Considering the probability to not break the two strands and the probability to survive to the magic bullet event, it is possible to estimate the total probability to survive.

$$p_{surv}(D) = [1 - (1 - e^{-\alpha_1 D})^2]e^{-\alpha D} = e^{-\alpha D}e^{-\beta D^2}$$

This law is defined as "Linear quadratic formula for the cell survival probability". As it is clear from the formula, the behavior of the survival probability, with respect to the dose, is decreasing exponential. Starting from this solution, it is possible to obtain the plot of the fraction of survival cells with the increase of the dose. This plot is shown in Figure 16.

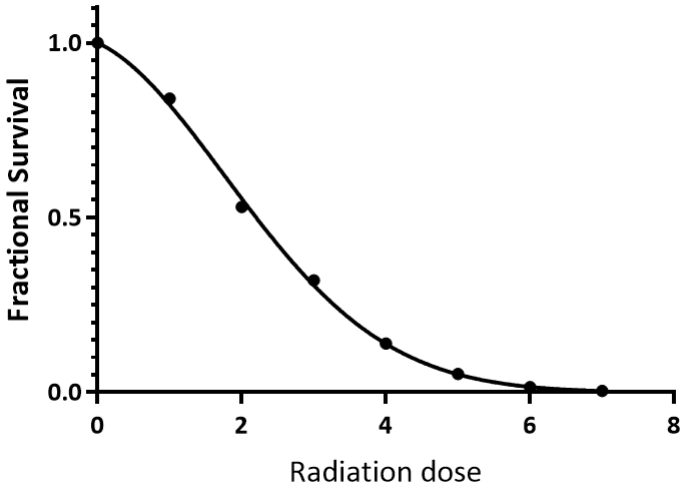

Figure 16: Fraction of survival cells[7]

2.4 Dose limits

In order to avoid damages or side effects related to the ionizing radiation exposure, dose limits are imposed for the population. These limits are set to totally avoid non-stochastic effects and to minimize the probability of the stochastic ones. It is important to remember that a threshold does not exist for stochastic effects to the ionizing radiation exposure. The dose limits are usually imposed by the regulating radiation protection commission of each state and they may be slightly different from state to state. The dose limits are often expressed in terms of effective dose, specifying the value for each organ or tissue. The values have, as unit of measurement, the Sievert.

An example of dose limit, related to the absolute whole body limit per year for the population, is 50 mSv. This limit is, as an example, related to the value imposed by the Nuclear Regulatory Commission (NRC) in the USA. It is important to underline that the radioprotection commission of each state gives a very detailed report on the dose limits imposed, differentiating the dose limit for the different categories of the population. The categories are set considering the fragility of the individuals of each category. For example, particular attention is spent to under 18 years old individuals and for women of childbearing age.

In the Table 4, it is possible to see some dose limits related to the values imposed by the NRC in the USA. The values reported are in [mSv].

	Class. workers	**Unclass. workers**	**Public**
Whole body	20	6	1
Individual organ	500	150	50
Lens of eye	150	50	15
Fetus of pregnant workers	1	1	/

Table 4: Dose limits for workers and public[74]

Regarding Table 4, the dose limits are different for three categories: classified workers, unclassified workers and members of the public. The unclassified workers are those individuals that are not exposed to ionizing radiation during their working day and, for this reason, they are not medically checked to verify if they are suitable to receive a higher dose with respect to the public. The classified workers, instead, are people that, during their working day, are exposed to a higher dose with respect to the public. An example of classified workers is the radiotherapist. These workers are subjected to medical checks in order to ensure that they are quite healthy to receive that dose.

In the previous table, there are different values for the whole body, for individual organs, for the fetus and for the lens of the eye. It is necessary to consider that these values are related to the effective dose. For this reason, each organ is differently radiosensitive according to its structure. The two factors that determine the radiosensitivity of an organ or a tissue are the mitotic index and the specificity of the cells. The higher the mitotic index and the specificity of the cells, the more radiosensitive the organ. It is interesting to underline that, in case of treatment of a patient with radiotherapy or imaging sessions using ionizing radiation, there is not a dose limit. This aspect is very important because, in a clinically compromised condition, in which a lot of imaging sessions or radiotherapy are necessary, the responsibility to find the trade-off between the absorbed dose and the benefits is of the doctor.
In order to respect limits imposed, especially for classified workers, it is necessary to perform both integral measures of the dose and instantaneous ones. The tools used to perform measures are called “dosimeters”. There are different types of dosimeters

that are based on different physical phenomena. The integral dosimeters perform the measure of the absorbed dose during a time interval of exposure, they are useful to estimate the dose received by a worker during a work session. The instantaneous dosimeters measure the dose in that moment and they are useful, for example, to screen some critical areas or to find "hot-spots".

3 Monte Carlo methods

3.1 The Monte Carlo approach

The Monte Carlo approach is a resolutive method widely used in different fields of application. It gives the possibility to obtain a numerical solution of very complex multidimensional problems. This type of approach is applied, for example, in mathematical analysis, financial economics, particle physics, fluid dynamics, optics and medical physics. In each of these application fields, the phenomena of interest are completely different, but the procedure approach is the same. It is important to underline that the Monte Carlo method is not a discretization method based on an analytical approach. It represents a revolutionary way of thinking based on the generation of a large number of random events. The methodology is characterized by a statistical and probabilistic way of resolution. In order to understand the Monte Carlo procedure, it is useful to think about a physical experiment of interest. Considering wanting to investigate a physical phenomenon of which the analytic law is unknown, the only possible way is to perform a lot of experiments. When a sufficient large number of experiences is reached, it is possible to extrapolate general informations on the phenomenon of interest. The Monte Carlo approach is based on this type of procedure, but experiments are performed virtually on a computer. The statistical method, based on obtaining general information starting from a large number of collected data, is called "statistical inference".
Monte Carlo codes are very reliable, in order to solve complex systems, but a large number of experiments is necessary. Generally speaking, Monte Carlo codes require a great deal of computational effort. As it is clear from Figure 17, the more the complexity of the problem increases, the more competitive the Monte Carlo approach becomes with respect to deterministic methods.

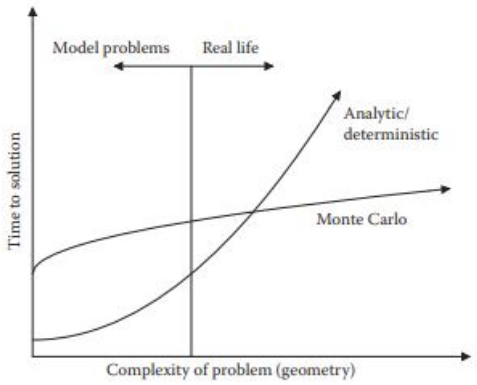

Figure 17: Time to solution trend using Monte Carlo and deterministic/analytic approaches [97]

The main advantage of this type of approach is to understand the behavior of complex systems starting from the simulation of basic physical phenomena. The collected data must be generated randomly in the domain of interest, according to the probability distribution of the phenomenon. A very important aspect, during the generation of random data, is represented by the requirement that the random events must describe all the possible different samples that are related to the domain. A distorted sampling of the domain cases compromises all the results obtained by a model. On the computer implementation of a Monte Carlo code, it is not possible to generate pure random numbers. For this reason, "pseudorandom algorithms" are used in order to ensure an independent generation of data. For brevity, data created are usually defined as "random data" although they do not derive from a purely random generation.

A classical example that is effective to present the Monte Carlo algorithm is the estimation of the PI Greek value. Considering a square extended from -1 to 1 in both directions with an inscribed circle of radius one, as it is shown in Figure 18, it is possible to create an uniform distribution of points in the square.

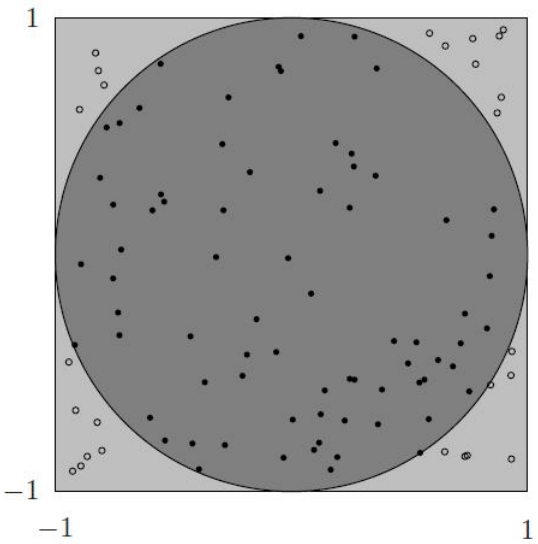

Figure 18: Geometry scheme of the PI Greek estimation example [63]

Defining P as the probability that the point is in the circle, it is possible to write

$$P = \frac{A_{circle}}{A_{square}} = \frac{\pi \cdot r^2}{l^2} = \frac{\pi}{4} \qquad (1)$$

From (1), it is possible to get the PI Greek relation

$$\pi = P \cdot 4 \qquad (2)$$

Calling N_{in} and N_{tot} , respectively the number of points inside the circle and the number of total points in the square, it is possible to write a relation for the estimation of the probability P.

$$P \simeq \frac{N_{in}}{N_{tot}} \qquad (3)$$

Substituting the (3) equation in the (2) one, the approximated formula for PI Greek is obtained.

$$\pi \simeq \frac{N_{in}}{N_{tot}} \cdot 4 \qquad (4)$$

Increasing the number of points generated in the square, the estimation of PI Greek becomes more precise.

3.2 Pseudo-random generation of numbers

As anticipated in the previous section, Monte Carlo algorithms are based on the generation of random numbers. Implementing the models on a computer, it is impossible to obtain a purely random set of numbers. The computer, in order to generate random numbers, needs a suitable algorithm and it starts the generation from an initial value. This procedure is intrinsically not purely random. For this reason, these types of algorithms are called "pseudo-random numbers generators" or more briefly "PRNG". A way to understand why an algorithm is not capable of generating purely random numbers is focusing the attention on the scheme procedure that it follows. There are a lot of types of PRNG, but they are mainly based on a mathematical formula that links the previous number with the value of the next one. It is clear that this procedure could start only with the imposition of an initial value, called "seed". The seed is usually chosen by the user, but in some cases a default value is just implemented in the algorithm. The aspect, that the generation of the numbers is dependent on the seed value, shows clearly that the procedure is intrinsically not purely random. The sequence of numbers is strictly linked to the initial guess.

In order to understand the generation method, it could be useful to consider a very general and simple case. Considering to start from an initial state S_0 (the seed), a finite set S of states is calculated by a function f that calculates the next number starting from the previous one.

$$f : S \to S$$

At this point, considering a function g, an output space U is generated starting from the finite set S.

$$g : S \to U$$

According to these steps, it is possible to write:

$$S_n = f(S_{n-1})$$

$$U_n = g(S_n)$$

$$n = 1, 2, 3...$$

This very simple schematic example could be useful to understand that the sequence of numbers is related to the initial value and to the choice of the generating functions. In order to obtain a reliable Monte Carlo simulation, the quality of the PRNG is one of the "load-bearing" pillars. The more the succession of numbers is close to a purely random generation, the higher the quality of the PRNG. If the generation of pseudo-random numbers is not very similar to a purely random one, there could be some distortions in the results of the Monte Carlo model. There are a lot of types of PRNG, some examples are the linear congruential generator, the multiple-recursive generator and the combining generator. In order to ensure a reliable PRNG, it is possible to do some tests to rank the different methods. The detailed analysis of these tests are beyond the purposes of this work, but a very qualitative approach is available.

Considering a X_n sequence of randomly distributed variables, it is possible to estimate a sequence of random values Y_n.

$$Y_n = f(x_1, x_2, ...x_n)$$

According to the Central Limit Theorem (CLT), the distribution of Y_n must tend to the standard normal distribution. It is clear that this step is only a qualitative and raw method, but it represents a useful check. As it results in Figure 19, the distribution of Y_n tends to the standard normal one increasing the number of samples.

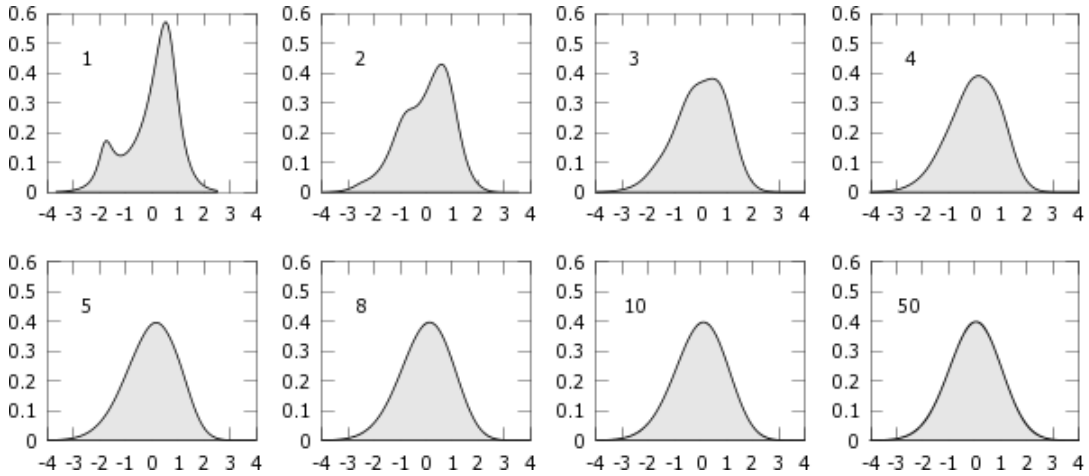

Figure 19: Random variables distribution increasing the number of samples [82]

3.3 Some historical references

The modern version of Monte Carlo methods was born in the last years of the second World War, in the "Manhattan project" in Los Alamos, during the development of the nuclear bomb. The name "Monte Carlo" was used to indicate some revolutionary mathematical methods used for the first time, in the nuclear weapon project, by some mathematicians such as Stanislaw Ulam, John von Neumann and Nicholas Constantine Metropolis. This approach was used for the first time to solve some physical processes about neutron diffusion. The characteristic name was chosen by Ulam referring to the randomness linked to the game of poker in the Monte Carlo casinò.
Enrico Fermi, another important scientist of the Manhattan project, in the 1930s, had applied some solution methods to the problem of neutron diffusion. The type of approach he had used was very similar to the one later defined by Ulam as the "Monte Carlo method".
It is possible to conclude that, in the 20th century, the Monte Carlo algorithm was born thanks to the necessity to solve particle transport in the matter.
Before the Fermi application, Comte de Buffon, in 1777, used a method that was very similar to a pseudo-Monte Carlo algorithm. He wanted to estimate the probability that a needle thrown on a sheet, marked by four equidistant lines, would fall on the sheet crossing one of the four lines. In order to get this result, he tossed, as it is shown in Figure 20, a large number of needles to obtain a mean value of probability. One hundred years later, Pierre Simon Laplace, in 1886, demonstrated that the experiment performed by Buffon was suitable to estimate the PI Greek value.

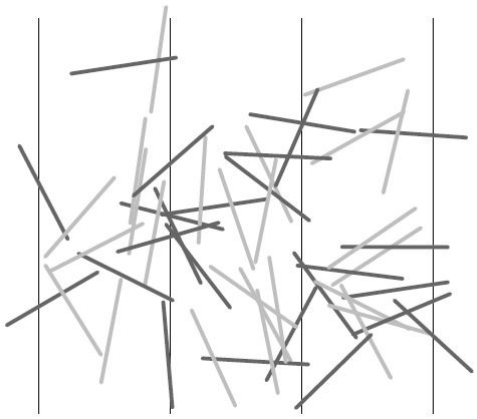

Figure 20: Scheme of the Buffon experiment [63]

3.4 Medical physics applications

The Monte Carlo method, as mentioned above, is used in many different fields. The first practical applications were used in the problems of interaction of particles with matter. Increasing the number of experiments of the free flight of a particle, it is possible to describe the behavior of a particle beam. This aspect confirms that Monte Carlo algorithms are very suitable in medical physics applications, in particular for radiotherapy and radiation dosimetry. Treating the radiation as a beam of particles, it is possible to evaluate the interaction with the matter of a lot of types of particles such as photons, electrons, positrons, neutrons, protons and heavy ions. These classes of particles are widely used in radiotherapy applications. The main purposes of the Monte Carlo simulations are to plan a correct treatment strategy for a therapy session and to estimate the dose received by the patient. This type of approach is essential to perform more accurate radiotherapy. The Monte Carlo method, generally speaking, is applicable both to internal and external radiotherapy.
One of the first fields of application of this kind of method was the study of the photon beam generated by a Linear Accelerator used for external radiotherapy. The important purposes were to evaluate the dose absorbed by the patient and to predict the quality of the beam produced.

A very simple example is the interaction of a photon with the matter. The following equation is the attenuation law of a generic particle.

$$p(s)ds = \mu(E)e^{-\mu(E)s}ds$$

It is crucial to remember that $p(s)$ is the probability that the photon interacts with the matter after a path s and $\mu(E)$ is the linear attenuation coefficient. The

coefficient depends on the structure of the medium and on the energy of the incident photon. This law links the physics of the phenomenon to the probability information, that is crucial in the Monte Carlo model to generate random events.

In external radiotherapy, the Monte Carlo model is used to simulate the photons or electrons beam generated by clinicals Linear Accelerators. For the calculation of the patient dose, the physics of the process is based on the particle transport and on the energy deposition in a heterogeneous medium, the patient body. The body is defined as a radiation detector, in order to estimate the damages to the tissues. In internal radiotherapy, the Monte Carlo approach is applied in Brachytherapy, for example, to evaluate the dose distribution around the sealed source and to set an appropriate treatment planning. An important field of application of Monte Carlo packages, as Geant4 developed by CERN, is the radionuclide therapy that is better described in the following section. The dose prediction and the simulation of the current radiotherapy phenomena, with the Monte Carlo approach, is so effective that also the advanced studies on the future radiotherapy systems are simulated using this kind of methods.

3.5 External Radiotherapy applications

The most common type of radiotherapy performed is currently the external radiotherapy. It consists of a radioactive source that is located outside of the patient. The radiation beam hits the patient, depositing energy on its tissues. The purpose of this type of therapy is to deposit energy on the malignant cells in order to kill them. A more detailed description of the characteristics of the external radiotherapy and the differences between the different types of treatment are shown, in this work, in the following sections.
Generally speaking, there is always a part of healthy cells that will be hitted by the particle beam, but the main purpose of the therapy planning is to minimize the amount of energy deposited on the healthy cells. The goal of the radiotherapy doctor is to reach, in a proper way, the cancer mass, reducing as much as possible the dose received by the healthy tissues. The particles mainly used in external radiotherapy are three: photons, electrons and hadrons.
The first type of external treatment that was performed was based on a photon beam produced by LINAC (LINear ACcelerator). The traditional external radiotherapy is divided in two subcategories: the high energy photons beam therapy, that uses photons with energies of 4-25 Mev, and the low energy photons beam one. The most diffused type is the high energy one.
The traditional treatment presents some drawbacks that will be presented in the next sections, for this reason, a very innovative radiotherapy strategy is actually performed, the Proton therapy, or more generally Hadron therapy. It is characterized by a beam composed of positive ions or protons and it presents some revolutionary advantages.

Considering an historical reference, the first simplified models of photons beam for LINACs was developed from the 1970s to 1990s.
The most powerful tool to analyze radiotherapy planning is the Monte Carlo simulations because they are very reliable to model particle transport problems.
The radioactive source, used in external radiotherapy, is a beam of particles and, for this reason, it is necessary to model a particle transport case. The resolutive approach is based on the tracking of the particle transport estimating the energy deposition of each particle. The geometry case is composed by a fixed radioactive source and a hitten detector, the patient body. In the Monte Carlo model, it is necessary to set a virtual radiation source in order to estimate the virtual detector response. It is clear that, generally speaking, in the radiotherapy simulations, the construction of the virtual patient body detector is a challenging step.

In Figure 21, it is possible to see the results of a Monte Carlo simulation of a proton therapy treatment.

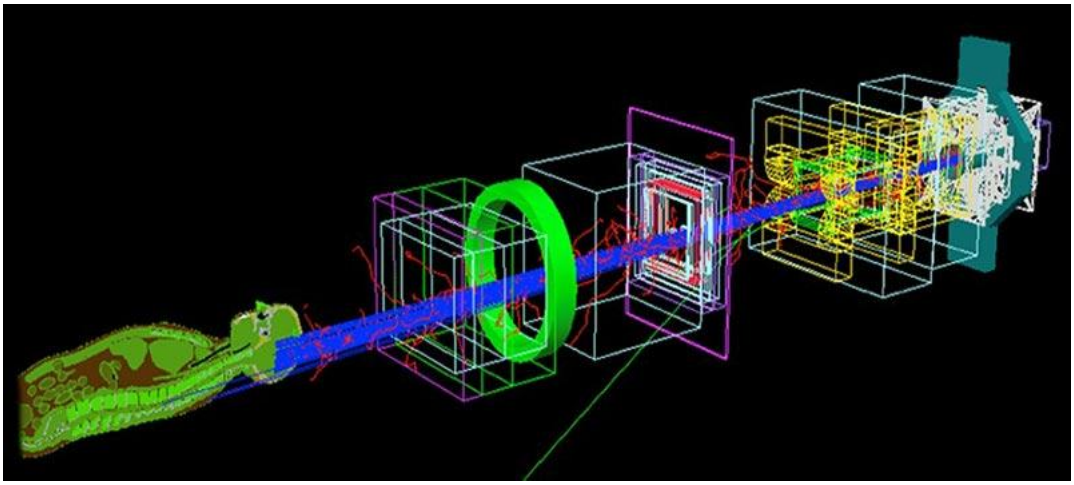

Figure 21: Graphic result of M.C. simulation of a proton therapy treatment[33]

3.6 Internal Radiotherapy applications

In some cases of cancer treatment, external irradiation is not sufficient. In these cases, a possible strategy is to intake a radionuclide in a radiopharmaceutical, in order to hit the tumor cells with an internal source. In this condition, the deposition of energy, due to the radiation effect, is done near the malignant cells exploiting the concentration of the radionuclide in the area of interest. The radionuclide could be intaken orally or intravenously and they are usually alfa or beta emitters.
An example of internal radiotherapy is the treatment of thyroid cancer. The therapy

is performed intaking iodine. The Iodine-131 is naturally concentrated in the thyroid cells by the biological processes.
There are some important aspects to consider during the planning of an internal radiotherapy. The first aspect to consider is that, during this type of therapy, the radioactive source, once intaken, continues to emit following its decay law. Unlike an external treatment, it is not possible to interrupt the energy deposition by removing the patient from the particle beam path or by switching off the radioactive source. The radiopharmaceutical emits particles, according to its decay, for the whole period from the intake to the complete depletion. The decay law, in this case, is related to two different phenomena: the radioactive decay of the radionuclide and the decay related to the biological removal of the human body. For these applications, an effective decay constant is calculated, in order to consider both phenomena. Another complication is linked to the fact that each patient absorbs the radiopharmaceutical in a different way and at different times. For this reason, a lot of simulations are necessary to understand the real distribution of the radiopharmaceutical in the body. The last aspect to underline is the fact that the radiopharmaceutical must be concentrated in the right place and in the right moment in order to deposit a big quantity of energy on the malignant cells, trying to reduce the component released to the healthy cells. In order to respect this requirement, it is necessary to choose the radionuclide with a proper decay constant, the right quantity and the right intake position. As said before, a lot of predictive simulations are necessary to understand in a proper way the distribution of the radionuclide in the human body during the treatment. For this purpose, Monte Carlo simulations are useful and reliable.
The problem is complex, because it is necessary to link the radiation emission of the radionuclide with the absorption and the diffusion of the drug in the body. The solution of this complex condition will help doctors to carry out the best possible therapy, optimizing the use of the radiopharmaceutical on malignant cells. In this way, it could also be possible to control the eventual deposition of energy in areas where it is not required.

3.7 GPU-based Monte Carlo simulations

3.7.1 Introduction

The Monte Carlo simulations are a very suitable tool to obtain a precise solution of complex particle transport problems. This aspect makes this method suitable for radiotherapy simulations. For example, the Monte Carlo model is considered as the most accurate method for dosimetric dose calculations, but it is very suitable also in Proton therapy and radiopharmaceutical therapy simulations. This approach is based, as previously explained, on a stochastic process that requires a big number of particle experiments and a heavy computational effort. In the standard Monte Carlo models, the simulation is implemented on CPU (Central Processing Unit), but in

this case, the computation time is usually long and it is not compatible with routine clinical applications. This aspect limits the Monte Carlo use in the radiotherapy field.
In order to obtain an efficient and fast simulation, it is necessary to perform parallel processing techniques optimizing the computation time. In the last few years, the main strategies adopted are the implementation on CPU clusters, cloud computing and GPU (Graphical Processing Unit). The parallelization strategies are crucial to perform more than one particle fly simultaneously and to increase the speed of the Monte Carlo simulation. A very interesting and cheap possibility is to implement the simulation model on the GPU, taking advantage of the large number of cores of which it is composed.

3.7.2 CPU and GPU

CPU and GPU are two fundamental parts of a computer, they have a similar physical construction, but they perform different works. Both are silicon-based microprocessors and both handle data, but they are constructed for different purposes. The CPU is often considered as the brain of the computer and its work is related to the computer operation and to the processes needed for the operating system. It is composed of a small number of cores that often are concentrated on a single activity, in order to maximize the execution velocity. It has a broad spectrum of work on very varied activities. These features make the CPU fast and versatile and suitable for serial processing.
The GPU is composed of many more cores than the CPU. It is structured in hundreds of small cores and they are designed for very specialized activity. Its structure is suitable for dividing the workload between the different cores. The graphical processing unit was originally developed for 3D rendering tasks and for implementing graphical user interfaces, but in recent years the latest models are very flexible. The GPU remains a fundamental element for advanced graphic applications, but it could be used in a lot of different fields as parallel processors. Being very suitable for parallel computing, it represents a cost-effective alternative to CPU clusters.
It is crucial to evaluate if the algorithm, that it is necessary to implement on the GPU, is suitable for that. Not all algorithm types can be implemented on a GPU. GPU manufacturers, such as Nvidia for example, are trying to stimulate this widespread use of their products, by developing some toolkits that make it possible to write C and C++ code in a way that is directly implementable on a Graphics Processing Unit. The toolkit developed, for example, by Nvidia is CUDA (Compute Unified Device Architecture). A very effective definition was provided by Nvidia in a response letter to an Intel lawsuit: “The CPU is the brain of the computer, the GPU its soul”.

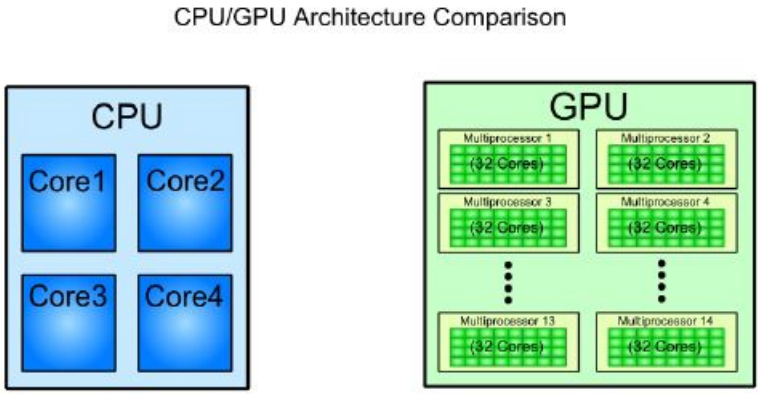

Figure 22: CPU/GPU architecture comparison [53]

3.7.3 Applications

In the first decade of the 2000s, the idea of implementing a particle transport Monte Carlo code on a GPU was born to try to reduce the computation time of the standard simulations by exploiting GPU parallel processing capability.
The first idea was to develop some simplified models with the same base code of a standard CPU-based Monte Carlo model. The main advantage of the GPU implementation is that, exploiting the parallel processing and the multi-core architecture, it is possible to generate a lot of particles simultaneously on the different cores, increasing the speed of the Monte Carlo simulations.
In 2008, the article "Parallel computing with graphics processing units for high-speed Monte Carlo simulation of photon migration", written by Erik Alerstam, Tomas Svensson and Stefan Andersson-Engels, presented a very simple case study. It was a simple ray-tracing model for photons migration with a very simple detector geometry: a semi-infinite slab geometry, homogeneously scattering, and non-absorbing media. The comparison of the results is performed between three Monte Carlo simulations: the WMC simulation (using a double precision) used as reference, the CPU simulation and the GPU simulation. In order to compare the CPU and the GPU results, both the simulations are performed using single precision. In this way, the simulations performed with CPU and GPU are statistically equivalent and the comparison of the computation times is consistent. As it results clear from Figure 23, the results of the three simulations are very similar, so the quality of the results of the different simulations could be considered comparable.

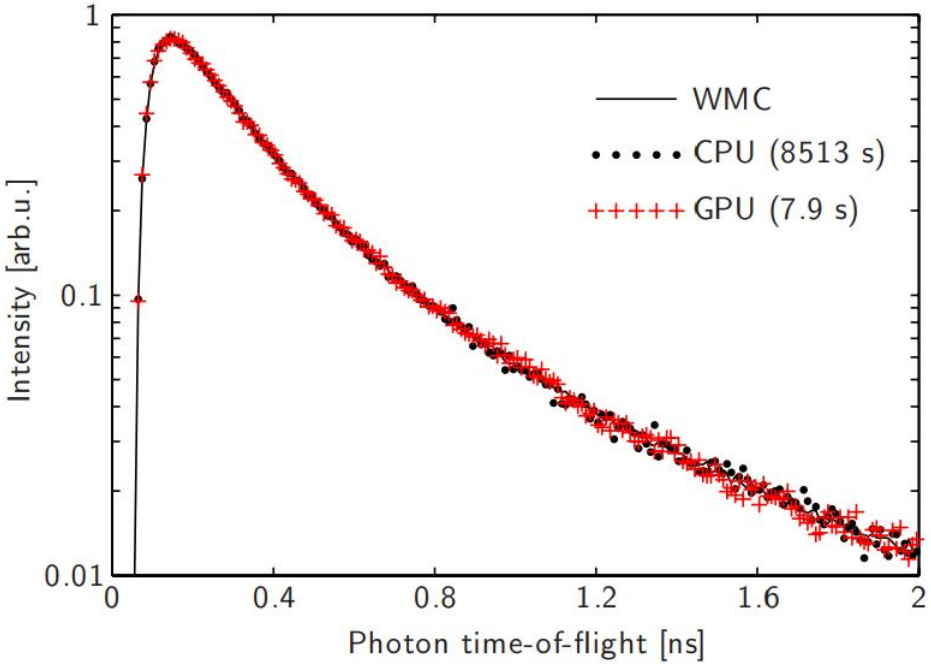

Figure 23: Intensity of the photon beam respect the photon time of flight, comparison between the three simulations[24]

Considering the CPU and the GPU simulations, the computation time related to the GPU one results 1080 times shorter than the CPU one. This very interesting analysis confirms that, if the Monte Carlo model is suitable, the implementation on the Graphic Processing Unit is a very good and cheaper choice to reduce computation time of a particles transport simulations.
In this type of GPU-based simulations, the particle generation is so fast that the standard pseudo-random numbers generator could show some problems. If the RNG is seeded with a timestamp, during the parallel generation of particles, the simultaneously generated events could have exactly the same characteristics. This aspect is a big problem for a Monte Carlo simulation because the samples generated are not uniform over the domain of interest. The main problem is that the number of parallel processes is large and, consequently, the number of random numbers requested is too large, considering the short period of the RNG. In order to solve this problem, it is possible to use random number generators with an extremely large period, that are memory-hungry, or to adopt alternative and innovative strategies for RNG suitable for GPU-based simulations, as the MWC (multiply-with-carry) RNG used in the previous example.

Another very recent example of GPU-based Monte Carlo simulation is a GPU-accelerated simulation of a CBCT (Cone-Beam Computed Tomography) performed by researchers of University of Massachusetts Lowell with some international col-

laborations [73]. This work is an example in which Monte Carlo simulation is used to create an X-rays image, called "Computed Tomography". The structure of the case study is an X-rays source that, with a photon beam, hits the virtual phantom (patient body). After the interaction of the particles with the phantom, the residual photons are used to create the image. The photons released from the source are called "primary photons" and the photons detected after the interaction are called "secondary photons". The comparison between the CPU-based simulation and the GPU-based one, in this case, is performed using an hybrid strategy. The computation time comparison is done between a pure CPU implemented simulation and an hybrid approach in which the generation of photons is implemented on the CPU and the interactions of the particles with the phantom is performed on the GPU. The GPU part is composed by a Geant4-based code implemented on an Nvidia Tesla V100 GPU card.
The hybrid simulation framework is structured as follows. The primary photons are generated by the CPU and emitted towards the phantom. Once reached the phantom surface, the photons are saved in a user-defined batch until it is full. The photon batch is saved in the GPU memory. At this point, the GPU is composed of four kernels: the first treats the photon angle, the second manages the transport of the photons through the phantom and the third and the fourth generate the projection image from the photons. The projection is saved in the CPU that after this sequence could start with a new photon batch. The scheme of this procedure is shown in Figure 24.

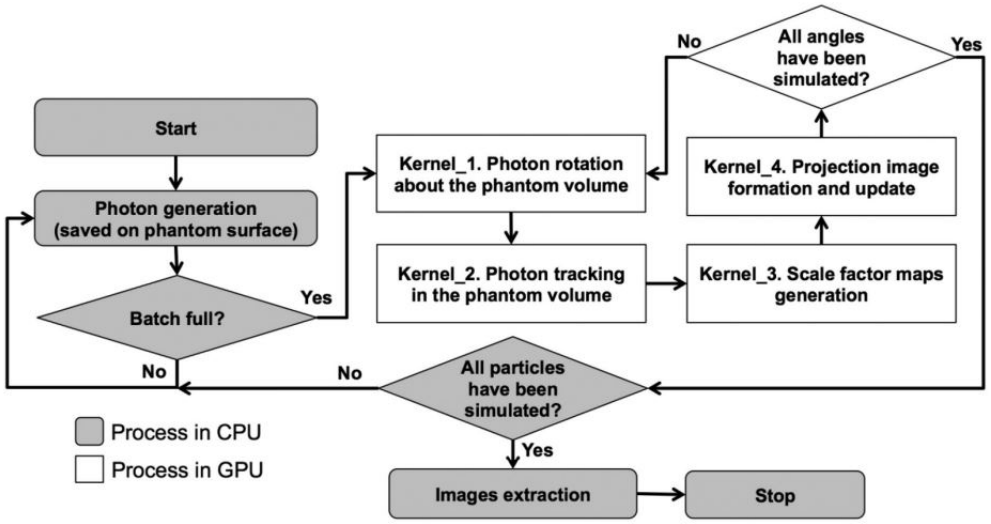

Figure 24: Workflow of the GPU implementation of MV-CBCT simulation[73]

The comparison between the images generated by the CPU-based simulation and by the hybrid simulation are in agreement. The image quality is not compromised,

but the most important aspect is that the use of the four kernels of the GPU causes an acceleration factor of the simulation of values between 900 and 2300.

Another example recently developed is GGEMS (Gpu GEant4-based Monte carlo Simulations). It is born from a French collaboration between CHRU-Brest and the INSERM. It is a Monte Carlo simulation platform based on the well validated Geant4 physics model. GGEMS is written in C++ and it is able to be implemented both on the CPU architecture and the GPU one thanks to the use of the OpenCL library. The aim of the developers is to provide a faster alternative to the traditional Geant4 simulations. This tool could be reliable in different radiotherapy applications such as external radiation, brachytherapy, CT (computed tomography) imaging, PET (positron emission tomography) and SPECT (Single Photon Emission Computerized Tomography).

3.8 Benchmarking and Validation

As previously described, a Monte Carlo simulation is the most accurate method to perform the prediction of the dose distribution in a patient geometry case. The large computational effort requested by a Monte Carlo algorithm justifies the development of optimization-based algorithms or simplified Monte Carlo codes.
The simulations based on the Monte Carlo approach are characterized by the extrapolation of information from a large number of experiments performed, virtually, according to the probability of the physical phenomena that it is necessary to simulate. If the code is developed in a proper way, the results are predictive of the real behavior because they are obtained starting from the real probability of the phenomenon. Generally speaking, in order to be sure to obtain a very precise prediction, the benchmarking and validation of the Monte Carlo model are necessary. The results of the simulation must be compared to the data obtained by a pre-validated model that simulates the same physical phenomenon.
The benchmarking procedure, in this type of application, is defined as the comparison of the dose distribution calculated by a Monte Carlo code with the corresponding values estimated by pre-validated codes or obtained experimentally. The two sources that are used to perform benchmarking are data measured during an experimental trial or the results of a simulation which has already been validated.
In case of simulations that estimate the dose distribution in a given domain, the comparison is usually performed using the relative values of the dose. The results are normalized to a reference dose level in order to get a more effective analysis. The dose values, in the profile plots, are usually normalized to either the maximum value at peak or to the plateau value at low depth. For example, the results, in the case presented below, are normalized to the maximum value obtained. The case studies used during the benchmarking could be created artificially, as a virtual target, or could derive from real patient cases.

In Figure 25, it is possible to see the results of a validation study [18] performed by a

group of Australian researchers. The validation approach is based on the comparison of the results of a Monte Carlo code developed with the toolkit Geant4 and a pre-validated code. The case study is the particle transport in the Microbeam Radiation Therapy (MRT). The MRT is a therapy strategy to treat tumors that is based on the use of a high-intensity beam produced in a synchrotron facility.

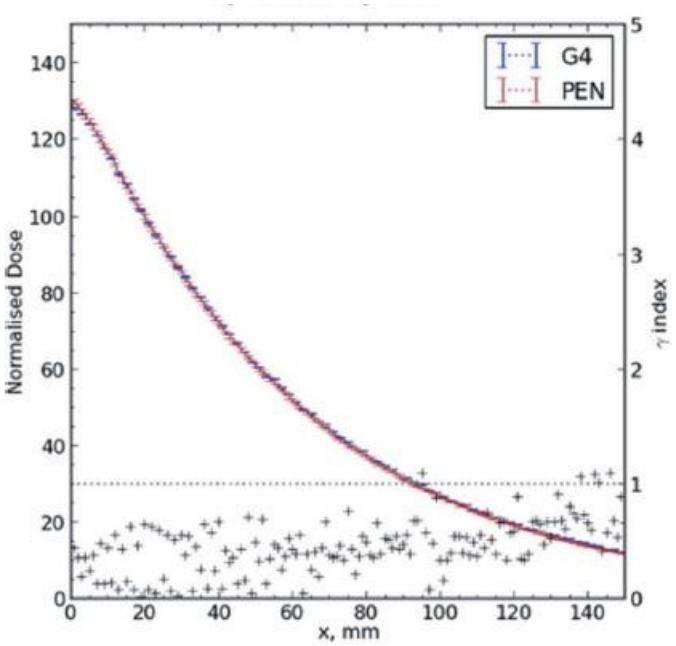

Figure 25: Benchmarking study of a Monte Carlo simulation for dose distribution in MRT[18]

In this case, the fitting of the results of the two models is very evident. On the x-axis the penetration depth of the beam in the tissues is reported and on the y-axis there is the dose normalized to a fixed value taken as a reference.

4 Geant4

4.1 General characteristics

The Monte Carlo algorithms could be used in several ways. In order to obtain a user-friendly result, they are usually implemented in commercial softwares with an intuitive interface. This form is suitable for the final user that gives in input the problem characteristics and that obtains the results, without being interested in the structure of the code. For developer users, there are toolkits that can be written in different types of code such as Fortran, C++, Java etc.
As previously anticipated, the Monte Carlo applications used in this work are developed with Geant4.
Geant4 is a free toolkit package developed by CERN with a lot of international collaborators and it is developed in order to solve problems related to the interaction of the particles with matter. It is written in C++ and it is based on the object-oriented approach. This kind of approach is very flexible and suitable for the definition of very complex problems. Geant4 is composed of structured classes, in order to define all the characteristics of the problem that the user wants to solve.
Geant4 gives the possibility to visualize the problem geometry and the particle beam shape. This tool is very useful for obtaining a qualitative and visually striking result. In Figure 26, an example of the graphical result of a very basic problem is shown. The package is open source and it is based on the collaboration of the users. Each of them could report any bugs or defects and the report is shared with the entire community of users. The user support is composed by an internet based forum and a FAQs section on the Geant4 website.
From the 2021, CERN has published five documents that are useful to support the user from the first steps in the basic examples to the most advanced applications. Currently, the toolkit is available for UNIX, LINUX, Mac OS X and Windows systems.

The history of Geant starts in 1993 with the birth of Geant3. This first release was the result of the collaboration of CERN with the Japanese KEK (High Energy Accelerator Research Organization) and it was structured with the programming language Fortran. Geant3 was the milestone of this project and it began to be used for modeling particle beams produced by accelerators. Comparing the experimental data measured in the accelerators with the Geant3 results, it was possible to improve the performance of the code in order to perform a validation of the simulation results. In the late 90s, especially after 1998, thanks to a large international collaboration, Geant4 was born. It was developed with a different programming language, C++.

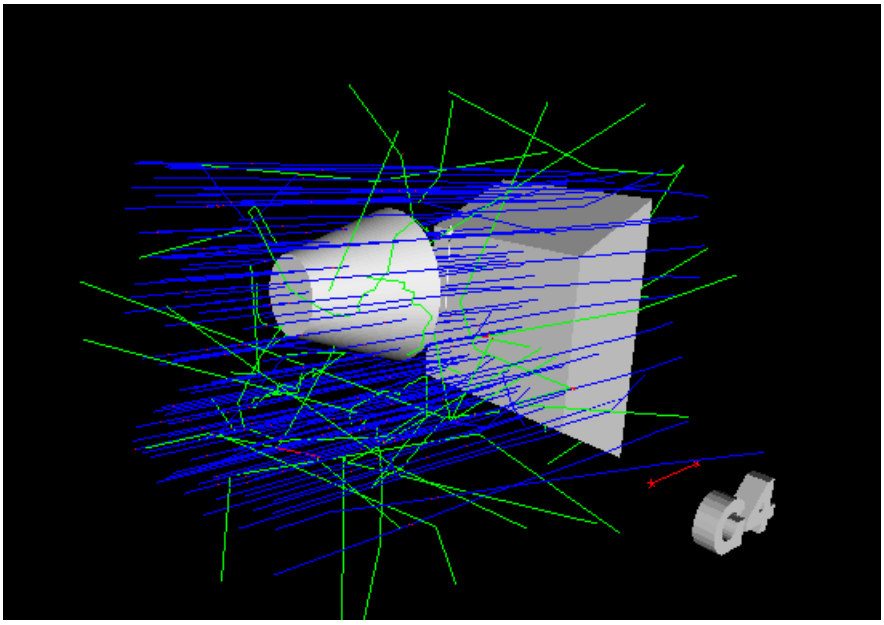

Figure 26: Graphic result of a simple simulation on Geant4 [38]

4.2 Model definition

The purpose of this section is not to explain the detailed procedure for defining a particle transport problem on Geant4, but it may be useful to highlight the main problem characteristics to be defined.
The physical definition of a Geant4 model is mainly based on three steps: the detector geometry definition, the particle definition and the physic process specification. It could be useful to imagine a generic model as composed by two macroscopic elements: the particle beam and the detector. Following this approach, it is necessary to set the characteristics of the two elements and the physical process that describes the behavior of the particles interaction. In order to define the physical characteristics of each element, suitable classes are implemented.
Starting from the definition of the detector geometry, the main characteristics to set are:

- Shape
- Material
- Name
- Position
- Orientation

The material could be chosen from a database or defined following three possible methods: the molecule definition, a mixture material defined according to fractional masses and a simple material composed by only one element.

Considering the particle definition, there are two possibilities: the first is to choose a pre-defined particle from a database and the second is to introduce a new particle defining the physical properties. The main characteristics to set in order to define a new particle are:

- Atomic mass
- Atomic number
- Excitation energy

The last aspect to set is the physic process. It is possible to choose from a database with a lot of different interaction processes. Some examples of physical processes are:

- Electromagnetic
- Hadronic
- Transportation
- Decay
- Optical

Obviously, in order to be able to construct a whole Geant4 model, a thorough study of each class is necessary.

5 Particles therapy

5.1 Introduction to external radiotherapy

The external radiotherapy is a form of therapy treating cancers using a beam to deposit energy on the malignant cells. As previously said, the conventional external radiotherapy is based on the use of photons or electrons beam, produced by LINACs. The conventional radiotherapy is widely used and it represents a consolidated technology. The photons beam, thanks to its high penetrating capability, is used to treat deep-seated tumors in the patient body. The electrons beam are adopted in case of surficial cancers.
The facility used in the conventional radiotherapy is a linear particle accelerator that is capable of producing photons and electrons beams with energy that are included between 2 and 25 MeV.
A LINAC is a structure that is composed of a series of couples of electrodes. Electrons are generated by an electron gun thanks to the thermionic effect. Once an electron is produced, it is accelerated by the electrical field of each couple of electrodes. The energy reached by the electron is proportional to the value of voltage tension between the two electrodes. Considering that the maximum values of voltage difference that are possible to produce are of the order of 100 KeV, in order to reach energy levels of the order of tens of MeV, a series of electrodes is necessary. Electrodes are supplied by an oscillating electric source, an AC generator. This aspect is necessary in order to invert the polarity at each step of acceleration.
In Figure 27 , the LINAC structure based on the series of accelerating electrodes is shown.

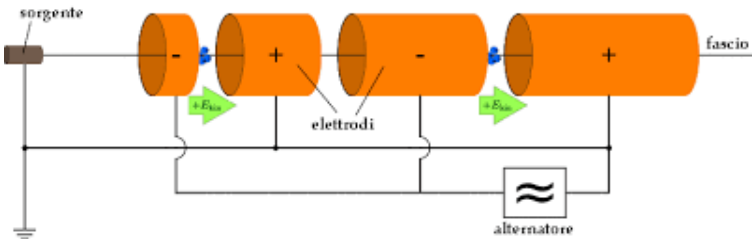

Figure 27: Scheme of LINAC accelerating stages [56]

Once the electrons have reached a sufficiently high level of energy, they are directed on a metallic target that emits X-rays. If the purpose is to perform the treatment with the electrons beam, the last step is jumped. The photon beam, at this point, is collimated and homogenized in order to hit the patient in a precise way.
In Figure 28, it is possible to see the photon beam generation phase and the collimation of the beam directed to the patient.

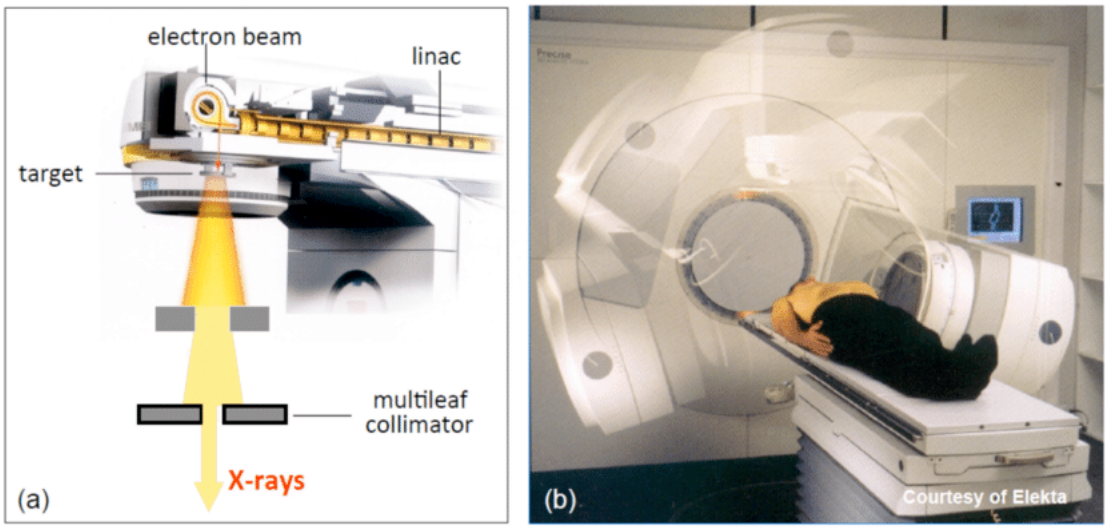

Figure 28: Graphic LINAC representation [77]

Particles therapy is an alternative approach to external radiotherapy, it is considered as an advanced alternative to the conventional one performed using photons and electrons. Particles therapy, as the same as the X-rays one, is based on the deposition of energy on the malignant cells of the tumor, but, in this case, the cancer mass is hitten with a beam of particles such as neutrons, protons and, generally speaking, heavy ions.
The most promising and advanced therapy is that performed with protons and heavy ions, it is called Hadron Therapy. This approach presents a very important advantage regarding conventional radiotherapy. In order to treat a deep-seated tumor in the body of a patient, the photons beam releases its energy during all the transport path and the main part of energy is deposited in the first part of the region of interaction with the tissues. This aspect is one of the main drawbacks related to the photons radiotherapy, a relevant part of the dose is released before reaching the tumor cells risking to damage healthy cells. This problem is often reduced by moving the photons source around the patient, in order to minimize the dose deposited on the healthy cells. This problem is almost negligible in case of superficial tumors, but it is a non-negligible limitation for the treatment of internal tumors.

Considering the plot in Figure 29, it is possible to notice that, in case of Hadron Therapy treatment, the main part of the dose is released at the end of the path.

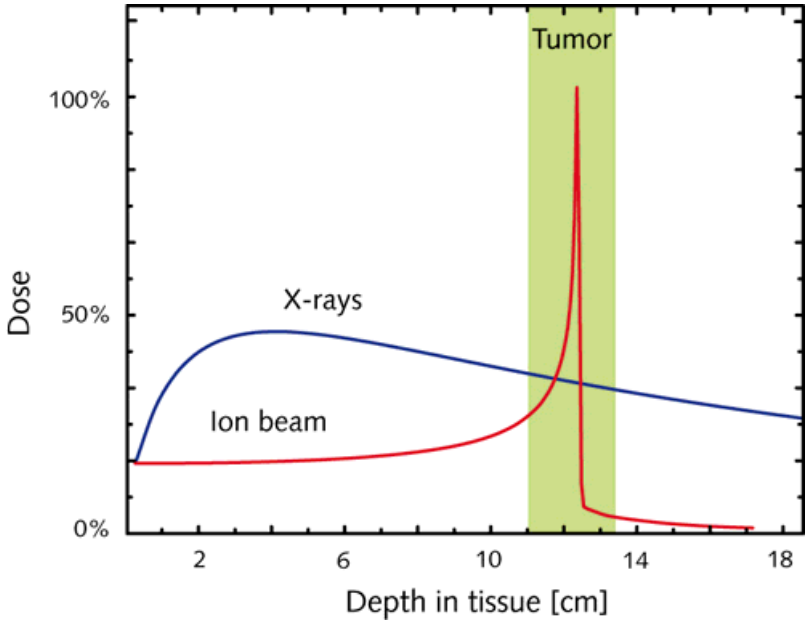

Figure 29: Dose distribution along the depth in patient tissues, comparison between Ion beam and X-rays [62]

This aspect is the most important revolutionary advantage of the Hadron therapy. In this way, regulating the emission energy of the ions, it is possible to set the peak of the dose released, precisely, in the tumor location. This procedure drastically reduces the energy deposited in the healthy tissues.
In the plot of Figure 29, that represents the behavior of the energy deposition with respect to the depth in the body of the patient, the peak of the ion beam is called "Bragg peak". This type of treatment is really precise and it is possible to control the penetration depth in order to treat also more extensive tumors. In order to produce the ion beam, it is impossible to accelerate the hadrons with a LINAC because they are too heavy. The facilities used in the Hadron Therapy field are circular accelerators and synchrotrons.
A more detailed description of the hadron therapy facilities is present in the following sections of this work.

The first idea to use particles to treat some deep-sealed cancers was initially proposed in the 1940s, after the Second World War. The first facility that was able to perform an ion beam treatment was developed by the Lawrence Berkeley Laboratory, Uppsala University and Harvard Cyclotron in the 1950s. The first exemplares of facilities were able only to produce ion beams with low-energy particles. For this reason, they were capable only to penetrate a few millimeters in the tissues and they could treat some ocular cancers. For example, prostate cancer requests a proton beam around 160 MeV, this means that these primordial facilities are not sufficient to treat this type of cancer.
In the 1980s/1990s and in the first decade of the 2000s, the number of Hadron Ther-

apy centers has increased and the accelerators facilities were improved. In 2014, only in the USA, the Proton Therapy centers were 14 and 39 in the rest of the world. In Figure 30, it is possible to appreciate the trend of the number of particle therapy facilities in the world.

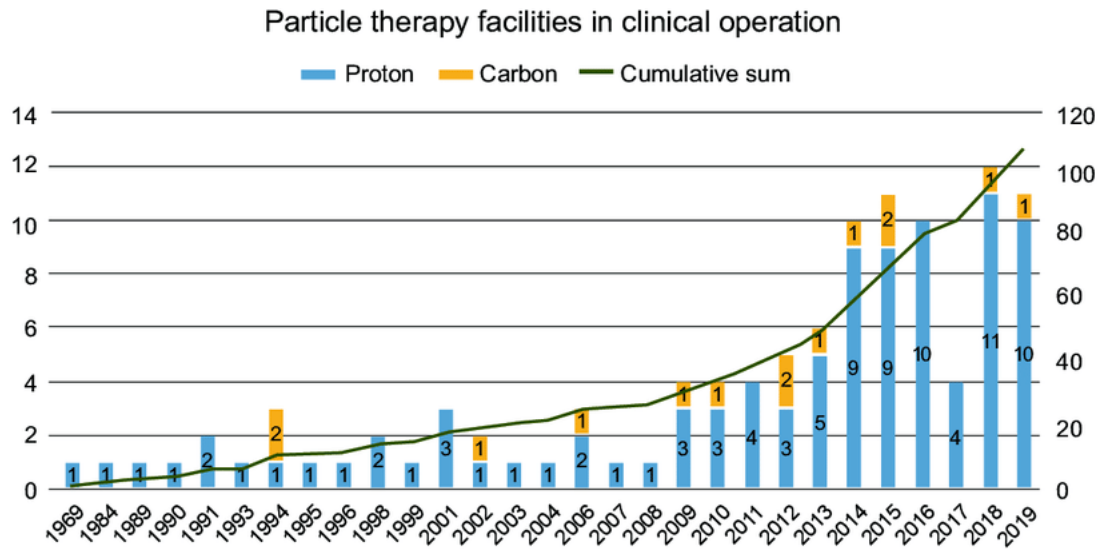

Figure 30: Particle therapy facilities in clinical operation[29]

Actually, the ion beam reaches the same penetration depth of the conventional radiotherapy. Proton Therapy, that is actually the most developed strategy, is suitable to treat a lot of cancer forms as:

- Radio-resistant tumours
- Limbs and Spinal cancers
- Paediatric solid tumours
- Pelvic tumours
- Chest tumours
- Tumours of the brain
- Head and neck cancers

5.2 Hadrontherapy

Hadrontherapy is currently the most promising form of external radiotherapy for the treatment of particularly resistant tumors. It is widely used, for example, to treat tumors that are resistant to X-rays treatment.
As previously explained, the most important improvement with respect to conventional external radiotherapy is the behavior of the deposited energy along the path of the particles in the tissues. The photons release its energy along the entire path, from the skin surface to the cancer mass, causing damage to the healthy cells. The hadrons release the maximum part of their energy at the end of the path, permitting a very precise treatment and the minimization of the damages to the healthy tissues. Considering the plot of the dose deposited with respect to the penetration depth for the hadrons, at a precise value of depth in the tissue, there is a peak of deposited dose that is called "Bragg peak". One of the most important purposes of the planning of the therapy is to set the Bragg peak position in correspondence with the position of the cancer mass.
If the cancer is extended, there is the necessity to move the position of the peak in order to deposit energy on the whole cancer mass. This procedure is defined as Spread-Out Bragg Peak (SOBP). In order to do this, there are two possibilities. The first option consists of regulating the energy level of the emitted particles in order to set the peak position in the right place. This approach is technically difficult because it requests the modification of the acceleration phase during the particle beam generation. The second strategy is based on the insertion of a wedge, that presents a composition similar to the body of the patient, between the source and the patient. In this way, it is possible to control the penetration depth of the beam and the Bragg peak position moving the wedge. This tool is usually made of water. In Figure 31, it is possible to see on the plot of the dose the movement of the Bragg peak to cover the wall cancer mass.

An important step to perform, before the particle treatment, is the localization of the tumor. In order to individuate the real position and dimension of the cancer, it is possible to subject the patient to different imaging strategies: MRI (Magnetic Resonance Imaging), CT (Computed Tomography) and PET (Positron Emission Tomography).
Generally speaking, the hadrons are composite subatomic particles and they are divided into two main categories: baryons and mesons. Hadrons are composed of two or more quarks held by the strong interaction. The baryons are composed of an odd number of quarks and mesons are composed of an even number of quarks. The baryons are characterized by a spin with a module of $\frac{1}{2}$, while mesons are characterized by integer values of spin. Two examples of hadrons, that are well known, are protons and neutrons. In Figure 32, it is possible to see a schematic representation of the mesons and baryons structure.

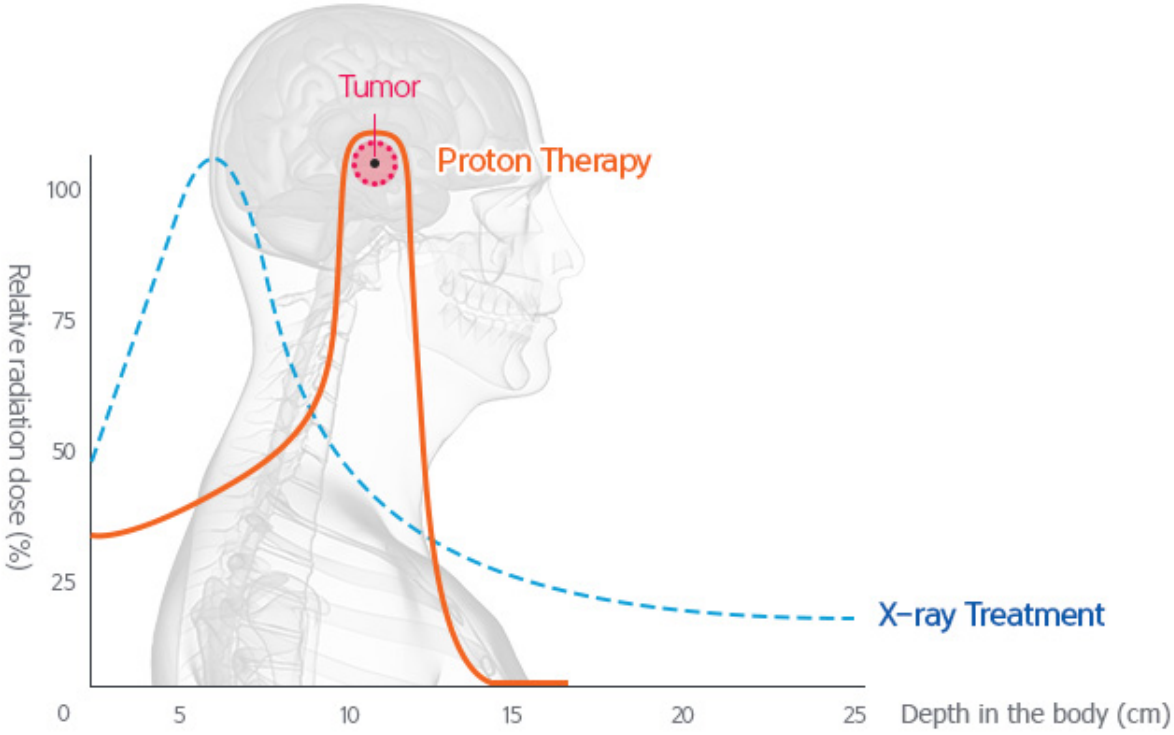

Figure 31: The plot of the dose released in case of extended cancer[57]

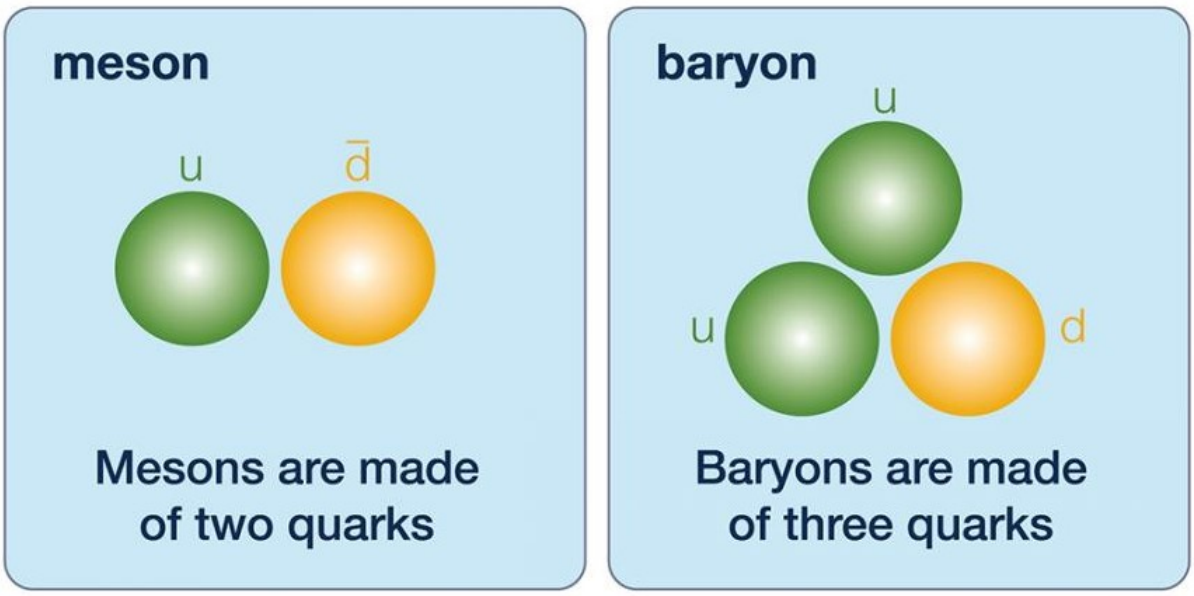

Figure 32: Mesons and Baryons graphical representation[90]

5.3 Particle accelerators

In order to reach the tumor cells with the protons beam, it is necessary to accelerate the particles. Higher is the depth of the cancer and higher is the energy of the particles that is necessary to set the Bragg peak in the right position.
The range of energies used in Proton therapy facilities is 70-250 MeV. For these high levels of energy, the LINACs are not sufficient because, in order to reach these values of energy, there would be a need for linear structures with lengths equal to several miles. Until now, the facilities, that are necessary to treat patients with the Proton therapy, are very expensive and this is the main aspect that slows down the diffusion of this type of therapy.
The two types of facility, that are used to perform Hadron Therapy, are the cyclotrons and the synchrotrons. The cyclotrons are used to accelerate only protons, while the synchrotrons are suitable to accelerate both protons and heavy ions, carbon ions for example. The trajectory shape of the particles is related to the principle of operation of the facilities: the particles in the cyclotron have a spiral trajectory while, in the synchrotron, the trajectory is circular.
The cyclotron was invented by Ernest Lawrence in 1932. The idea was to compact the accelerator structure giving the possibility to reach higher values of energy. The cyclotron, as it is shown in the Figure 33, is composed of two semi-circular D-shape electrodes and two magnetic coils.

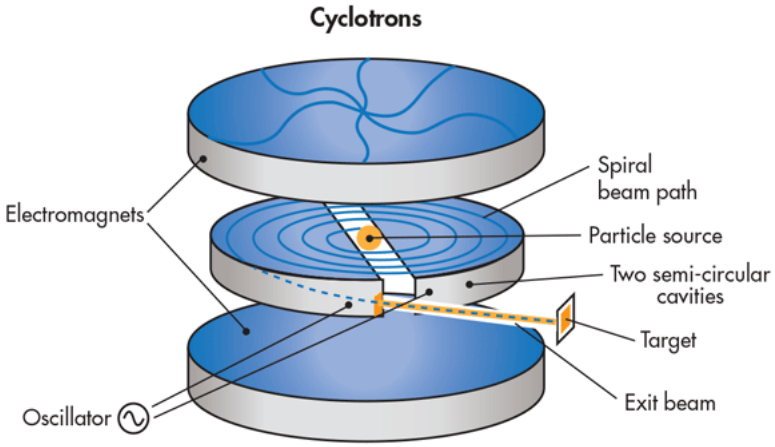

Figure 33: Scheme of a cyclotron facility[54]

The two D-shape electrodes generate an oscillating electric field between them and the two magnetic coils impose a magnetic field that is perpendicular to the plane of the electrodes. Considering to generate the particle to be accelerated in the center of the cyclotron, it is subjected to the two fields: the magnetic field and the oscillating

electric one.
The magnetic field is different to zero in the entire plane of the electrodes, the oscillating electric field is equal to zero in the electrodes and different to zero in the gap between them. The particle, as in the LINAC case, is accelerated between the two electrodes thanks to the differential potential generated between the two plates.
An electromagnetic field generates, on a moving particle, a Lorentz force equal to

$$F = q(E + v \wedge B)$$

In the electrodes, the electric field is equal to zero, so the force is only generated by the magnetic field. The Lorentz force imposes a circular path to the particle. When the particle reaches the gap between the electrodes, it is accelerated, so its velocity increases.
Considering a generic circular motion, the radius of curvature is directly proportional to the velocity of the body. This means that, at each passage of the particle in the gap, the radius of the circular motion increases.
Considering the circular path imposed by the magnetic field and the increasing of the radius due to the acceleration in the gap, the resulting trajectory of the particle is a spiral path, as it is clearly represented in Figure 34.

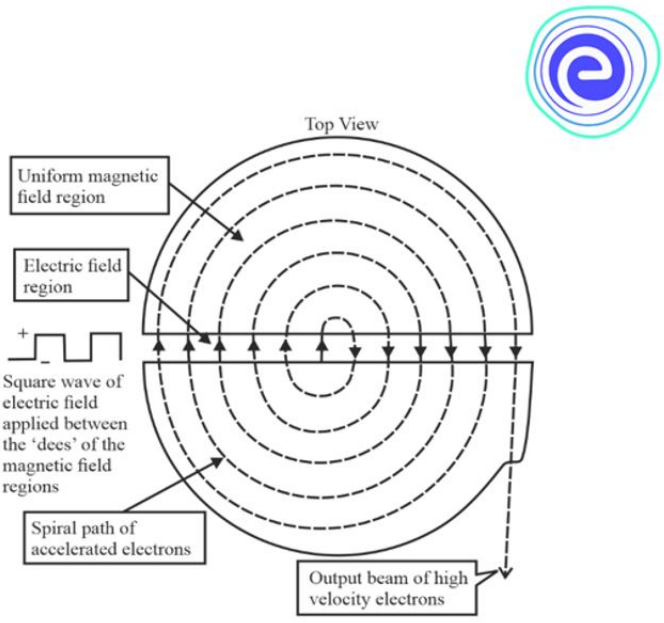

Figure 34: Trajectory of the particle in the cyclotron[45]

The target is positioned at the end of the spiral on the external side. In the cyclotron operation, the frequency of the electric field and the frequency of the particle rotation must be equal.
Considering the Lorentz force equation and the centripetal force on the particle

$$\frac{mv^2}{r} = B \cdot q \cdot v$$

m is the mass of the particle, v is its velocity, r is the radius of the circular motion, B is the magnitude of the magnetic field and q is the charge of the particle.

Dividing both sides by velocity and mass

$$\frac{v}{r} = \frac{Bq}{m} = \omega$$

ω is the angular velocity of the circular motion. It is necessary to remember that the frequency of the circular motion is equal to

$$f = \frac{\omega}{2\pi}$$

It is possible to conclude that

$$f = \frac{Bq}{2m\pi}$$

From this last equation, it is possible to conclude that the frequency of rotation is not dependent on the radius of the circular motion, so the frequency of the electric field could be constant. This approach is valid for non-relativistic particles. If the velocity of the particle is near the speed of the light, this treatment is not valid and an alternative theory, with some corrections, is necessary. In the case of relativistic particles, the frequency of the motion is not constant and it is necessary to change the frequency of the oscillating electric field.
There are two possible strategies to maintain the cyclotron frequency equal to the frequency of the circular motion: changing the frequency of the electric field, following the particle gyro-frequency, or varying the magnetic field. The facilities that respect the frequency equality, varying the electric field frequency, are called synchrocyclotrons. Those that vary the magnetic field are called isochronous cyclotron.
The synchrotron was invented by Edwin McMillan in 1945. It is structured in a cyclic structure composed by accelerating sections and deflecting sections. As in the cyclotron facility, the magnetic field is used in order to curve the trajectory of the particle and the electric field is used to accelerate it. The action of the two fields is synchronized in order to obtain a steady operation that is capable of accelerating particles at high levels of energy. It is possible to see the structure of a synchrotron in Figure 35.

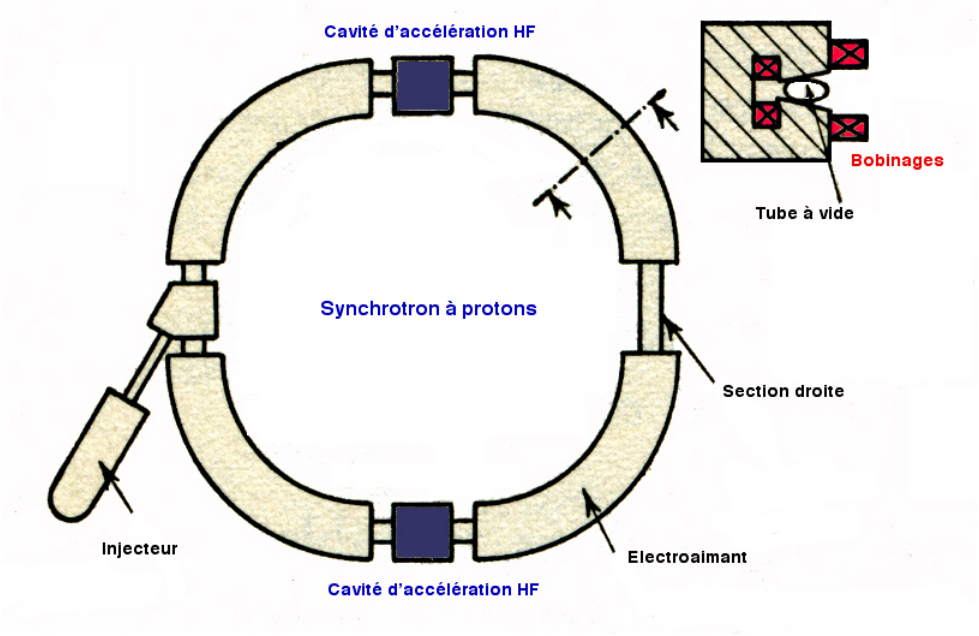

Figure 35: Schematic structure of a synchrotron[37]

The main principle, on which the synchrotron operation is based, is the phase stability: the synchronism between the electric field and the frequency of revolution of the particles is conserved. The circular structure of the synchrotron imposes a constant value of the radius. The frequency of the circular motion is equal to

$$\omega_c = \frac{v}{r}$$

Considering that the radius is constant and the velocity increases during the acceleration phase, the frequency of the synchrotron oscillation must increase. In order to follow the increase of the frequency of rotation, the magnetic field increases.
The synchrotron facility is composed of different parts that connect the particles generation to the patient. The first part is an ion source in which the particles are generated before the acceleration. Then the particles pass through two stages of linear accelerators that pre-accelerate the particles before the injection in the synchrotron structure. This step is necessary because the synchrotron is not able to manage zero-kinetic energy particles. After the pre-accelerating phase, the particles are injected in the circular structure of the synchrotron reaching, through the accelerating and deflections sections, the energy level requested. In the next step, the particles are injected in the treatment room beam lines that connect the output port of the synchrotron with the treatment room. At the end of the chain, the treatment room is the place in which the patient receives the dose of the particles. In Figure 36, it is possible to follow the whole path of the particles, from the source to the patient body.

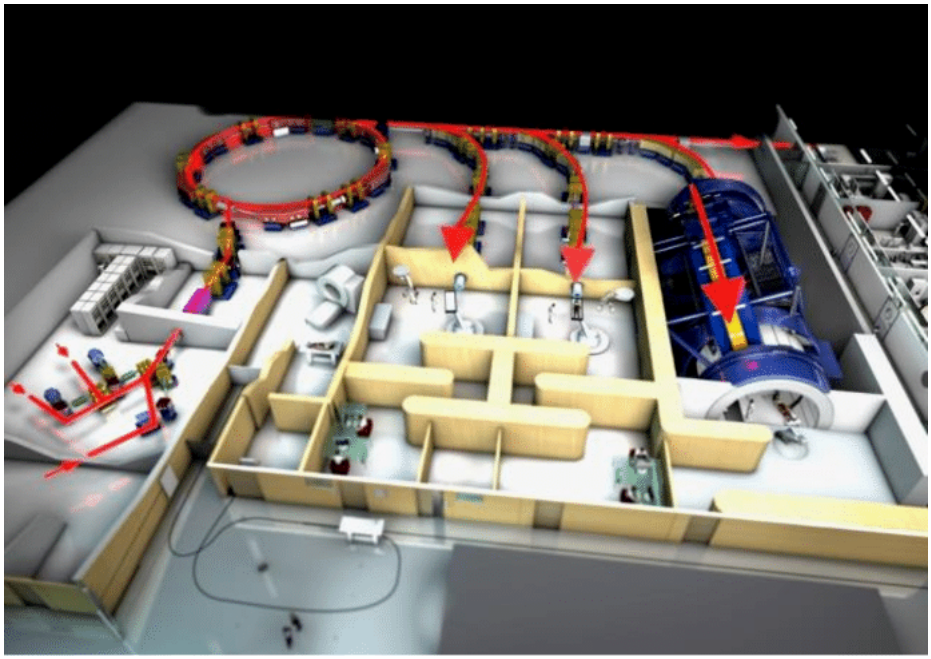

Figure 36: Path of the particles in the synchrotron facility[79]

Another type of accelerator used in Hadrontherapy, but that it is still not widespread, is the Cyclinac. It is a hybrid structure between a LINAC and a Cyclotron. The relativistic acceleration is performed in a LINAC structure after a non-relativistic acceleration section performed with a cyclotron. The main advantage of this solution is the lower cost and the low power consumption. Figure 37 shows the simplified representation of the structure of the Cyclinac.

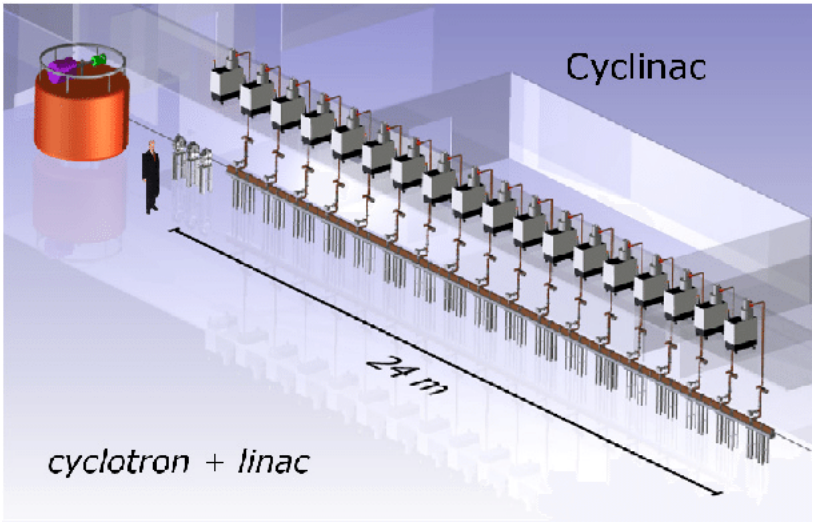

Figure 37: Structure of the Cyclinac[87]

5.4 Treatment planning

5.4.1 Introduction to RTP

The RTP (Radiotherapy Treatment Planning) is a very important phase of the external radiotherapy treatment of a patient. It represents the step in which the radiotherapist plans the characteristics of the external beam to set during the whole serie of therapy sessions. It is important to underline that RTP is a customized process performed for each patient. The main purpose of the RTP is to understand how to set the particle accelerators in order to obtain the prescribed dose distribution in the tissues of the patient. RTP is fundamental in order to design the field of the external treatment delivering high dose to the malignant cells and reducing as much as possible the dose to the healthy cells. This approach allows to reduce the side-effects of the Radiation Therapy and to increase the effectiveness of the treatment. The input data of the RTP is represented by an imaging of the tumor position. The main types of imaging strategies used are the Computed Tomography (CT), the Magnetic Resonance Imaging (MRI) and Positron Emission Tomography (PET). The CT is usually used as primary imaging in order to localize the tumor mass and the MRI is used as secondary imaging to highlight the soft tissues. The use of PET, up to now, is still not widespread. The first RTPs were performed manually on 2D x-rays images. In the 1970s, the first computerized RTP was performed. Currently, the RTP provides a 3D dose distribution and the tumor is characterized as a target volume.
The workflow, on which the treatment planning is based, starts from the positioning and immobilization of the patient and then with acquisition of the image of the tumor, a CT image for example. At this point, the contouring of the tumor mass is performed defining some characteristic volumes. After the contouring, the beam setting and the dose prescription are defined and the simulation of the treatment starts after the whole evaluation of the plan. After the end of the simulation, a phase of verification and validation is necessary in order to check the goodness of the results before performing the real Radiotherapy Treatment. In Figure 38, it is possible to see the whole scheme of a course of Radiotherapy. The parts related to the RTP are highlighted in red.

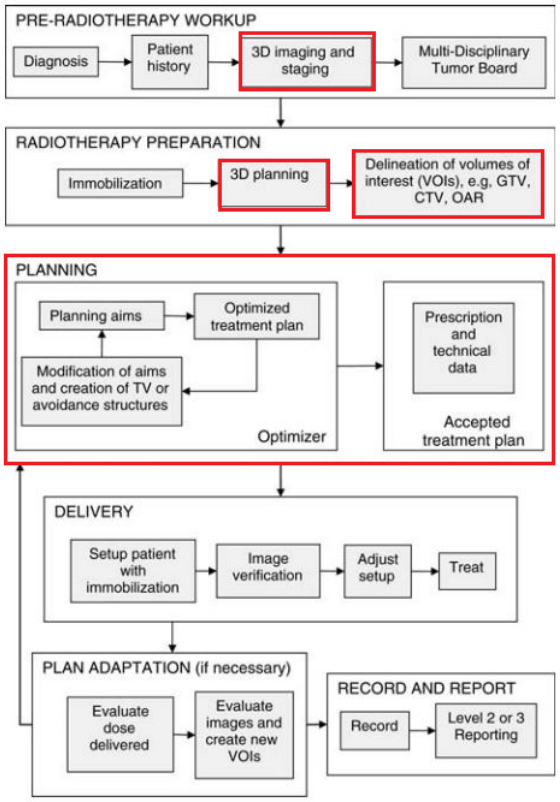

Figure 38: Scheme of the course of Radiotherapy[61]

5.4.2 Computed Tomography

The Computed Tomography (CT) was invented in 1971 and, originally, it was limited only to axial imaging of the body of the patient. The development of this imaging technique allows, currently, to obtain a 3D whole body imaging of a patient. Considering a z-axis passing through the body of the patient from the head to the feet, as it is shown in Figure 39, CT consists of a scan along the z-axis.
The main elements of a CT device are the X-rays tube, the X-rays detectors, a digital computer to process the data measured by the detectors and a system for the visualization in greyscale.
The patient is placed in a gantry surrounded by a rotating ring composed of X-rays sources and detectors. The CT device rotates around the patient generating hundreds of 2D conventional X-rays images. A whole CT is composed of around 200-400 conventional images. For this reason, a whole CT must be prescribed by the Radiologist only if it is strictly necessary because the patient receives a non-negligible absorbed radiation dose. The hundreds of images of the slices are processed by a computer that reconstructs the 3D image. A schematic representation of a CT device (tomograph) and its components is available in Figures 40 and 41.

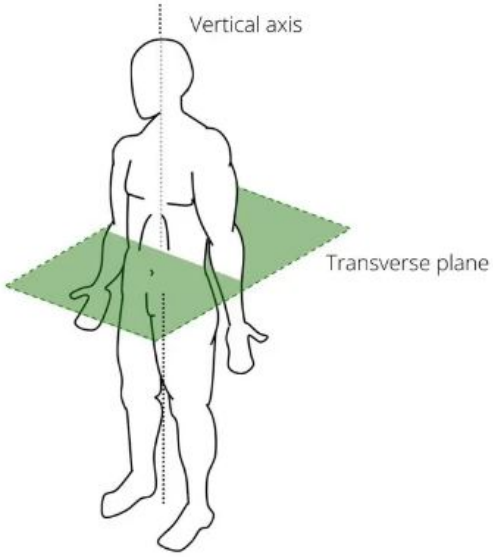

Figure 39: Reference axis of the body of the patient[39]

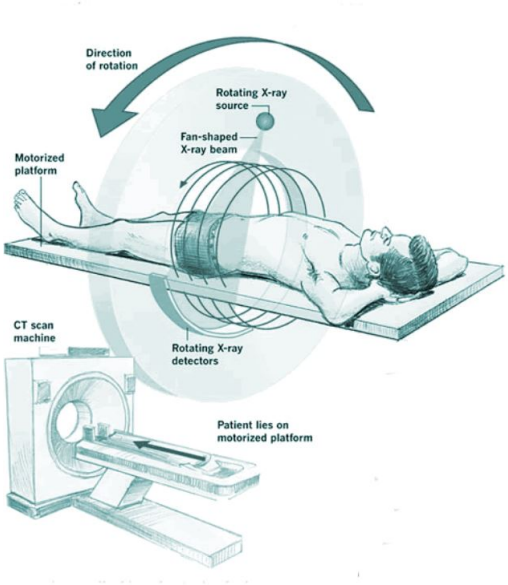

Figure 40: Schematic representation of the components of a Tomograph[43]

A source of X-rays generates a beam that hits the body of the patient with a beam of intensity I_0. After the interaction of the beam with the tissues, the intensity of the beam is attenuated and equal to $I(x)$. The intensity of the attenuated beam depends on the geometrical dimensions and characteristics of the crossed tissues. The attenuated beam hits an X-rays detector that converts its magnitude into amplified electrical pulses in order to estimate it and provide the information to the computer.

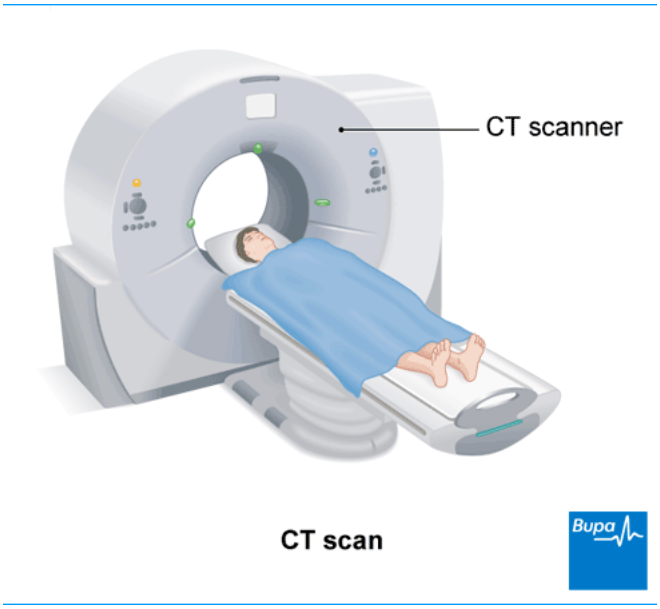

Figure 41: Graphical representation of a Tomograph[40]

The operation of the CT facility is based on the Lambert-Beer's Law. A more detailed description of this law is available in section 1.4 of this work.

$$I(x) = I(0)e^{-\mu x}$$

If the attenuation coefficient is a function of x, the general form is

$$I(x) = I(0)e^{\int_0^L -\mu(x)dx}$$

In order to solve this equation, the domain is discretized in subdomains, called "voxels", and knowing the magnitude of the unperturbed incident beam and detecting the magnitude of the attenuated one, it is possible to estimate the attenuation coefficient of the crossed tissues.
In reality, the mathematical method to solve the last integral equation is not so easy. It is possible to try to modify the last equation in order to estimate the linear attenuation coefficient.

$$ln(\tfrac{I(0)}{I(x)}) = \int_0^L \mu(x)dx$$

In this form, it is possible to know the integral quantity of on the whole domain, but it is necessary to obtain its distribution.

The following description does not claim to provide a complete and exhaustive explanation of the mathematical methods applied, but only to give a qualitative idea of the approach adopted. A detailed description of the solution of the previous equation is beyond the scope of this work.
The domain, as previously described, is discretized in subdomains and each of them is irradiated. In order to irradiate each subdomain, the scanner rotates around each of them.
Considering two systems of reference: the patient one that is fixed and the scanner one that is movable, these two systems are in relative movement and there is an angle between them. The scansion is performed along one direction in order to cover the whole target. Once the target is fully covered along that direction, the angle has changed and the detection is repeated along the new direction.
This approach generates a set of linear equations, but given that a lot of measurements are performed, in this type of problem the number of equations is larger than the number of unknowns. In this case, the system is not solvable performing the standard back-substitution method and alternative approaches are necessary. Two methods are suitable to solve this problem: the Least Squares Method (LSM) and the Fourier Transform Method (FTM). In the real applications, the FTMs are more suitable than the LSMs because the number of measurements is very large.
At this point, an explicit form of μ, as a function of I_0 and $I(x)$ is obtained. Following this procedure, a matrix of the linear attenuation coefficients is obtained. The value of this coefficient in each voxel permits reconstructing the internal structure of the crossed body. Each type of tissue is characterized by a range of values of the linear attenuation coefficient.
For example, bones are easily recognisable because they are characterized by very large values of coefficient, muscle tissues have small values of the coefficient and air presents a coefficient equal to zero.
If there is the need to highlight some types of tissues, it is possible to perform the CT introducing a contrast agent in the body of the patient. This procedure allows to increase the contrast of some parts of the body in order to improve the visualization. The contrast agent is used to highlight, for example, veins, arteries and lymph nodes.
Each voxel has a mean attenuation coefficient and the detail of the CT depends on the level of refinement performed. In order to process the matrix of mean attenuation coefficients, it is adopted a particular scale, the "Hounsfield scale". It was invented by Sir. Godfrey Hounsfield. This scale is based on the Hounsfield units (HU) that are defined as follows.

$$HU_{mat} = \frac{\mu_{mat} - \mu_{H_20}}{\mu_{H_20}} \cdot 1000$$

As it is clear from the last equation, the linear attenuation coefficient of the water is used as a reference value and the HU of the water is equal to zero. The HU scale starts from values of -1000 for the air and reaches values of around 2000-3000 for bones and high density tissues. An example of interpretation of a CT image in terms

of Hounsfield units is available in Figure 42.
The CT images must be univocally interpreted by the radiologists and the oncologists. For this reason, an international standard definition of the imaging characteristics is necessary. This standard procedure is called DICOM (Digital Imaging COmmunications in Medicine). It is an international standard for medical images and it defines the formats for medical images that can be exchanged through specialists. DICOM imposes some data and quality levels that are necessary for clinical use. These constraints must be respected by all devices. DICOM standard is implemented in almost every radiology imaging device and from 1993, it presents a fully digital workflow procedure.

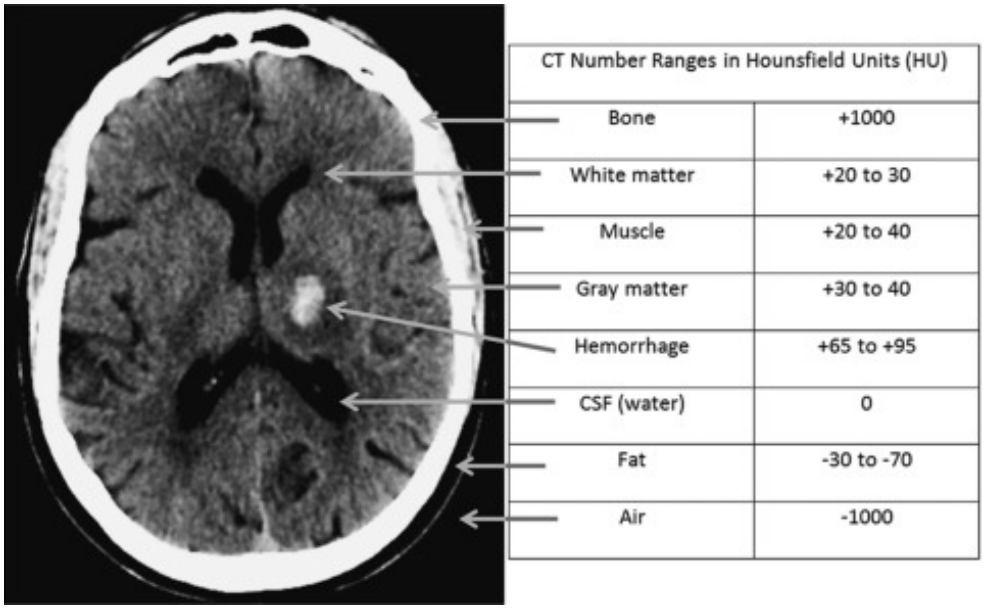

Figure 42: Example of the interpretation of a CT in terms of Hounsfield units[5]

5.4.3 Contouring and volume definitions

The procedure of definition of the volume of the target is a key-step of the Radiotherapy Treatment Planning and it is described in the published reports by ICRU (International Commission on Radiation Units and measurements [61]). The approach is based on the definitions of different volumes with increasing sizes, starting from the volume described by the CT image. This procedure is called "Contouring".

The first step is to define a preliminary volume to describe the tumor mass. The first volume is the gross visible extent of the tumor mass and it is called GTV (Gross Target Volume). The GTV is defined basically starting from the image of the tumor mass obtained from the CT, MRI or PET.

The second step is based on the definition of a tissue volume that contains the GTV and the subclinical microscopic malignant disease around the gross volume that are necessary to treat. This second volume is called Clinical Target Volume (CTV).
At this point, a third volume is defined in order to compensate for expected physiological movements and variations in size, shape and position of the CTV. This volume is defined as Internal Target Volume (ITV).
The next volume is a geometrical concept set for the treatment, in order to select the characteristics of the beam and consider eventual variations or uncertainties. This volume is defined to ensure that the prescribed dose is delivered in the CTV. This volume is defined as Planning Target Volume (PTV) and it is the tool used in order to compensate for the uncertainties related to the treatment planning. To compensate for the uncertainties means that some small changes of the condition of the patient, during the sessions of treatment, do not compromise the whole plan.
At this point, it is necessary to underline that GTV and CTV are oncological concepts based on the CT image. The ITV and the PTV are, instead, geometrical concepts that are defined in order to reach an effective and robust treatment planning.
After the definition of the PTV, it is possible to define the tissue volume that is planned to receive at least the dose prescribed by the radiation oncologist. This volume is called Treated Volume (TV).
The last concentric volume defined is the tissue volume that receives a significant dose respect to the normal tolerance for tissues, it is called Irradiated Volume (IV).
A very important volume to define during the contouring is the Organ At Risk volume (OAR). It represents a volume that describes an organ whose radiation sensitivity is such that the dose received during the treatment is significant.
In Figure 43, a graphical description of the volumes is reported.

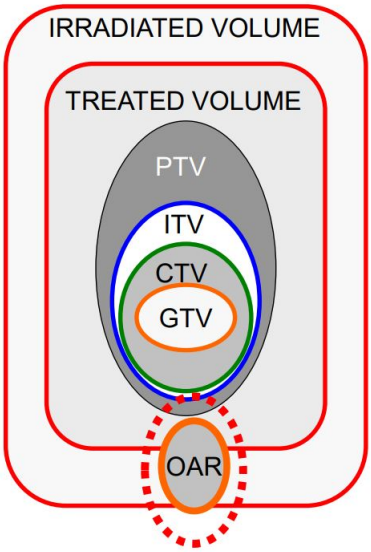

Figure 43: Scheme of the volumes during the contouring phase[23]

5.4.4 Simulation of the treatment, inverse and forward planning

There are two possible strategies to perform the planning of the real Radiation Therapy. One is called "forward planning" and the other is called "inverse planning". In Figure 44, a scheme of the two different approaches is shown.

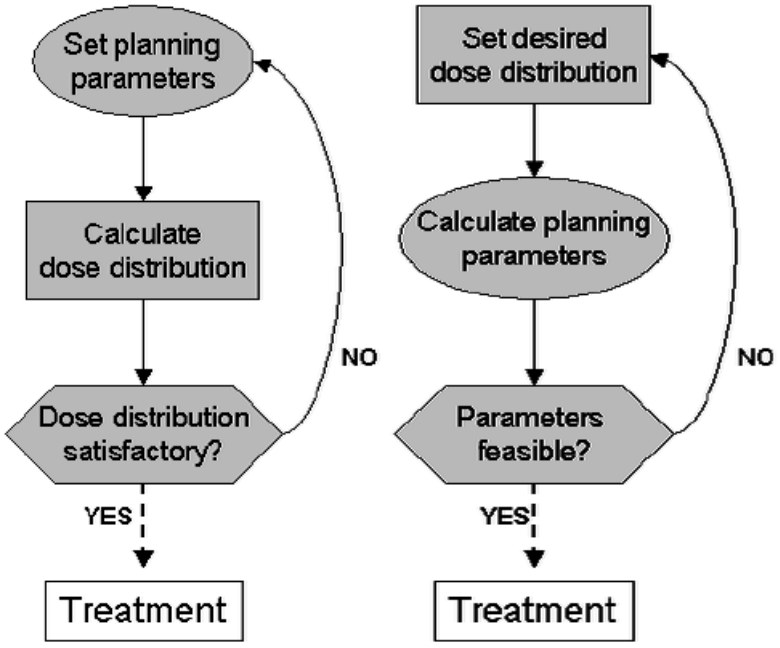

Figure 44: Schemes of the forward planning approach (on the left) and the inverse planning (on the right)[98]

The forward approaches are based on predictive methods that could be analytical or statistical. An example of statistical based forward method is a Monte Carlo simulation. The forward analytical methods are based on the discretization of the target and on the model of the beam transport in terms of WEPL. This way to treat the physics problem is the same adopted in the inverse approach and it is better described below. For now, it is enough to underline that the forward analytical methods, in general, do not treat the physics of the problem faithfully but perform the calculation of the transport in WEPL.
The main characteristic of the forward approaches is that the input data of the model are the setting characteristics of the external beam and the CT image of the patient. The model performs the simulation providing the dose distribution in the tissues of the patient. The Monte Carlo approach to the forward problem is usually more reliable because, unlike the analytical methods, it is based on the real physics of the transport phenomenon. Obviously, Monte Carlo methods for forward planning require more computational effort than analytical methods.

The inverse planning is based on the opposite approach: the input data of the simulation are the prescribed dose distribution in the patient and the CT image of the patient. This approach is a very quick analytical method, but it is not accurate in all cases. It represents a key role in a fast and efficient clinical workflow because provides the characteristics to set the treatment session in order to obtain the dose distribution imposed. The inverse planning method starts from the discretization of the tumor mass in subdomains called "voxels" and the first input data is the magnitude of the deposition of energy prescribed in each voxel. The method, starting from the dose distribution that the Radiotherapist wants to obtain in the tissues of the patient, "inversely" calculates the energy of the particles and the intensity of the beam. This method is based on the irradiation of the volume of the target with a large number of beams, called "Pencil Beams"(PBs).
The first step is to map the target into a set of parallel homogenous iso-energy slabs, in order to set the energies of the beams necessary to reach the depth of each slab. At this point, each beam is transported through the target and the related deposited dose is calculated with analytical equations for each voxel. In order to regulate the magnitude of each beam, the weight of each PB is set in order to obtain the dose distribution that it is requested. This step is also called "weight optimization". The inverse planning method works in terms of "Water Equivalent Path Length" (WEPL) relating to the density of the tissues. It redefines the CT image in terms of WEPL exploiting pre-computed dose curves constructed experimentally in water samples.

A brief description of the mathematical method is reported below.

The input of the inverse planning simulation is the ideal dose distribution that the Radiotherapist wants to obtain.

$$\bar{d^{id}} = ideal \quad dose \quad distribution \in \Re^I$$

$$I = number \quad of \quad voxels$$

At this point, the beams are defined in a dose matrix.

$$[D] = dose \quad matrix \in \Re^{I \times J}$$

$$J = number \quad of \quad beams$$

It is necessary to assign to each beam a weighting factor.

$$\bar{w} = weighting \quad factors \in \Re^J$$

The main problem is defined in the matrix form as follows.

$$\bar{d^{id}} = [D]\bar{w}$$

This problem must be solved for $\bar{w}$, but it is mathematically impossible.

The optimization approach is based, generally speaking, on the addition of an error term that must be minimized.

$$\bar{d^{id}} = [D]\bar{w} + \epsilon$$

There are a lot of possible optimization methods to minimize the error ϵ. The description of these methods is beyond the purpose of this work.
The inverse planning method presents some limitations. For example, the transport of the pencil beams and the range of them depends only on the tissues crossed along the central axis of the voxel. This aspect is a limit because this approach is completely insensitive to lateral inhomogeneities. This is the most important key point that justify an inaccurate estimation of the dose distribution in case of complex geometries and heterogeneous domains.
The forward and inverse analytical methods share the same discretization approach based on voxels and the analysis of the physics in terms of WEPL. These methods are really optimized and fast, but results are not precise.
The forward methods are used in order to check the effective dose behavior in the patient tissues starting from the facility setting evaluated with the inverse planning. A very interesting procedure is to perform the inverse planning simulation, that is faster with respect to the Monte Carlo model, and after obtaining the characteristics of the external particle beam, to perform the Monte Carlo forward simulation setting the beam as imposed by the inverse planning simulation. In this way, the statistical forward approach works as a double-check strategy to verify if the prescribed setting of the beam allows to obtain the desired dose distribution.
Obviously, the fact that the Monte Carlo simulation is based on the real physics of the problem makes this method much more effective than the analytical forward one for checking the dose distribution.

5.5 Benchmarking of the Monte Carlo simulation

In section 3.8 of this work, the benchmarking of a Monte Carlo model is described. The Monte Carlo model used in this work is based on a C++ script developed using the package tool Geant4. This package is briefly presented in section 4.
In order to check the validity of the Monte Carlo simulation, two analyses are performed. The manipulation of data is completely performed using Matlab. The

comparison of data, in this case, is performed referring to the peak position, in order to focus the attention on the point with the maximum release of energy.
Firstly, the C++ model developed by "I-See s.r.l." and implemented in the web tool is taken as reference. This Monte Carlo script simulates the transport phenomenon of a beam of protons in the matter. The preliminary purpose is to perform simulations for different levels of energy of the beam comparing the results of two versions of Geant4. The two versions are 'Geant4-v10.3.3' and 'Geant4v11.0.3'. It is necessary to remember that a beam of protons releases its energy to matter mainly in the last part of the path. This characteristic is well described, as previously said, by the presence of a peak in the dose-depth plot. The comparison of the results of the two Geant4 versions is performed comparing the behavior of the Bragg peaks.

The simulations are performed generating 100000 random events.

The energy range considered is between 50 MeV and 250 MeV, performing each simulation increasing 10 MeV at each step.

The results of the comparison are shown in Figure 45.

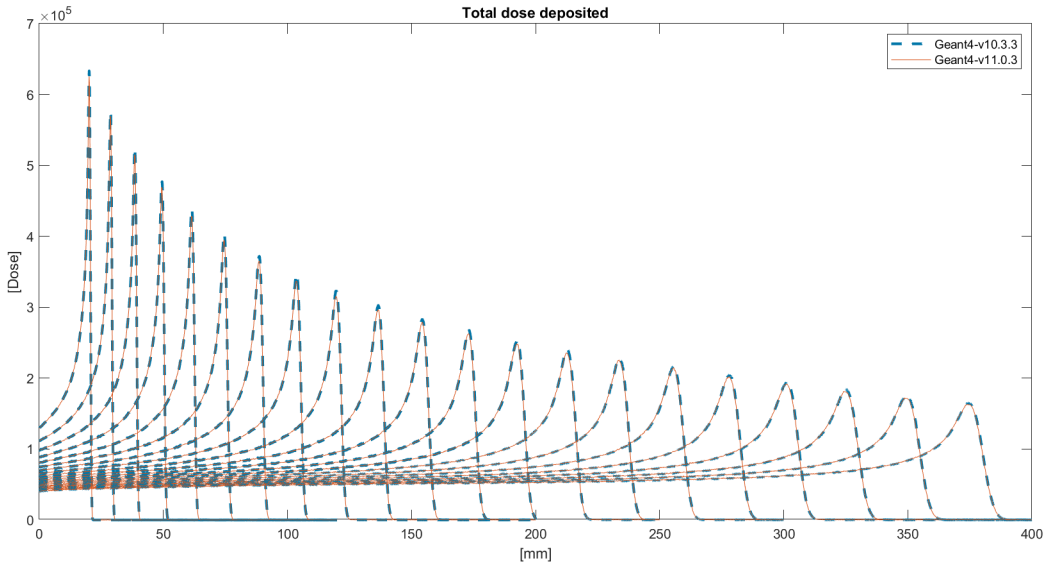

Figure 45: Comparison of the Bragg's peaks of two versions of Geant4

The blue dashed line represents the results obtained with the older version of Geant4 and the orange continous line represents the ones related to the newer version. It is possible to see clearly that the difference between the two versions is negligible.
Considering, as an example, the beam of 140 MeV, the peak obtained by the new version is slightly lower than the old version. The discrepancy between the peaks is represented in Figure 46 and the relative difference between the values of the dose is of the order of 2%. In particular, the new version of Geant4 has a 2 percent lower peak than the older version.

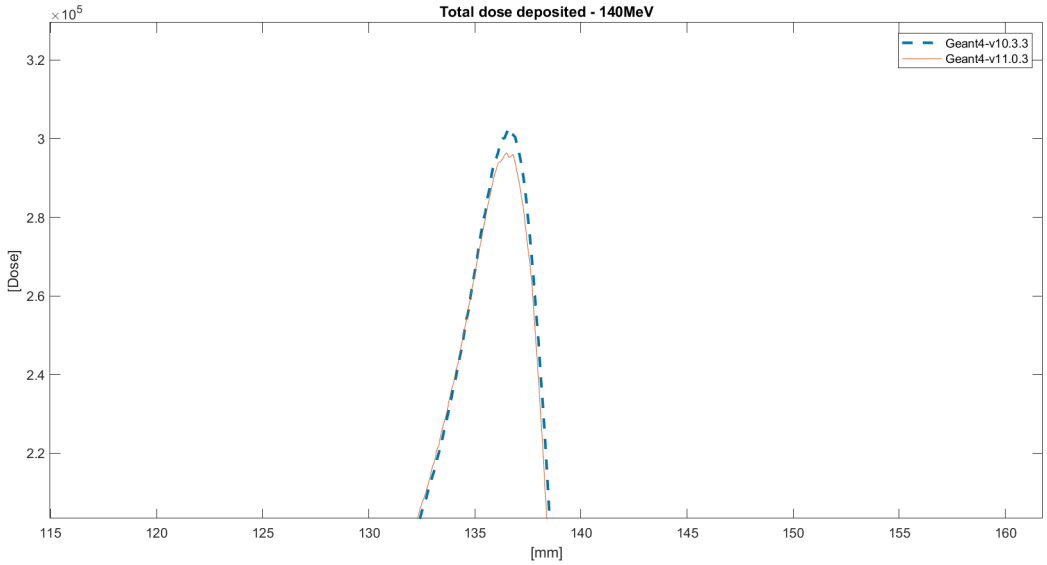

Figure 46: Example of the discrepancy of the Bragg's peaks for the different Geant4 versions

At this point, the second step is the benchmarking of the Monte Carlo model.

In order to validate the simulation, experimental results measured by CNAO in Pavia are taken as reference. The results of the experimental measures performed in the accelerator facility are shown in Figure 47.

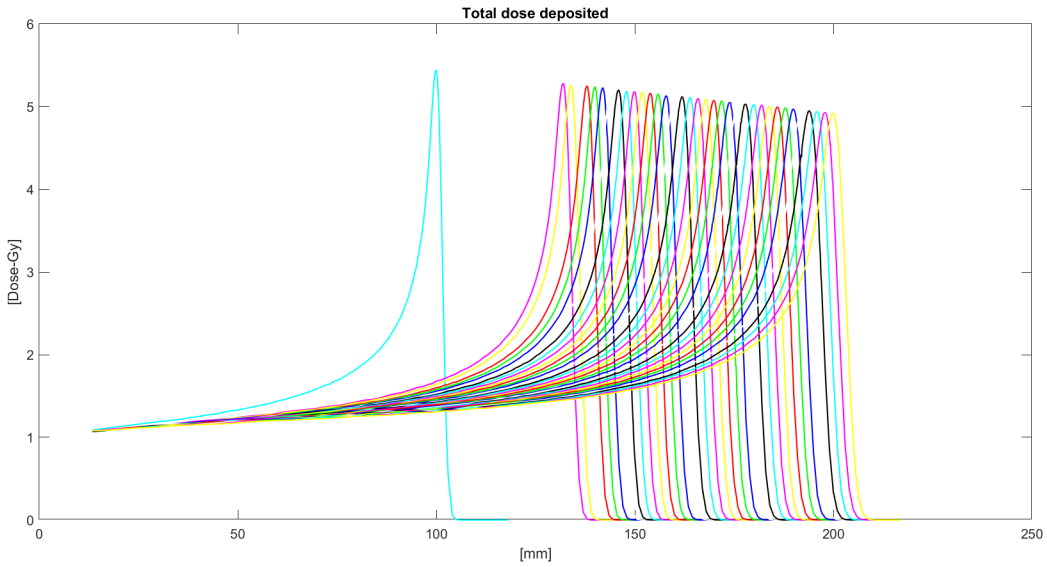

Figure 47: Experimental results of a proton beam transport at different levels of energy in the CNAO facility

The data used to perform the benchmarking are those related to a beam of protons

generated in the synchrotron facility at three different levels of energy: 118 MeV, 160 MeV and 173 MeV.
As explained in section 3.8, the values of the dose are normalized to the maximum value. In this way, the comparison is independent of the number of particles generated in the Monte Carlo simulation and in the experimental experience.

In Figure 48, the results of the comparison between the relative doses of the experimental data and those obtained by the Monte Carlo simulation are shown.

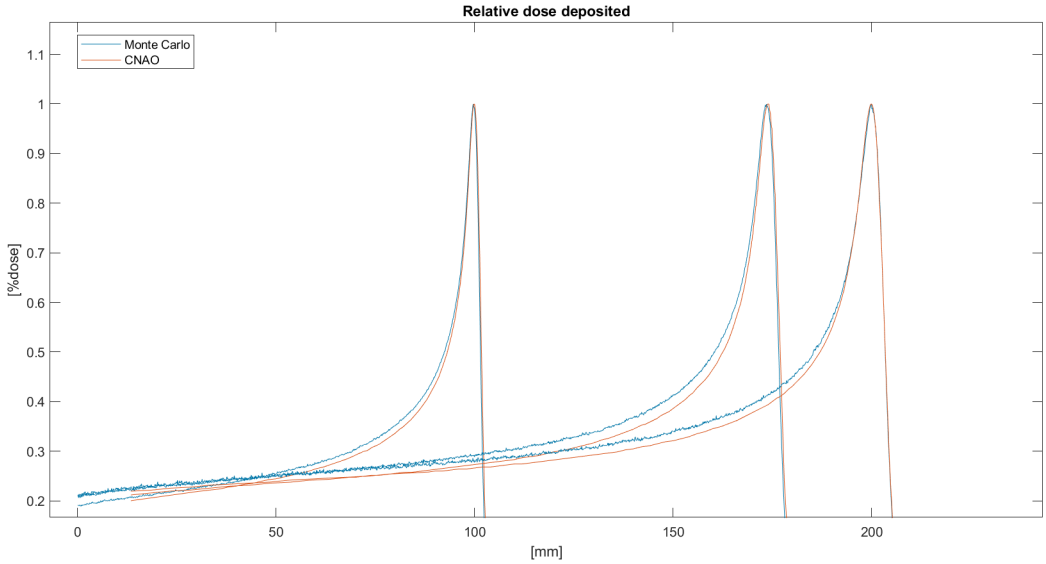

Figure 48: Plot of comparison of the experimental and simulation results of different levels of energy proton beams transport

In the previous plot, it is possible to notice that the positions of the peaks are slightly different. In the 173 MeV case, the difference between the positions of the two peaks is negligible. In the 160 MeV case, the peak obtained by the Monte Carlo simulation is at 173.6 mm and the one obtained in the synchrotron facility is located at 173.9 mm. In the 118 MeV case, the peak obtained by the Monte Carlo simulation is at 99.7 mm and the one obtained in the synchrotron facility is located at 99.9 mm. The difference is of the order of tenths of a millimeter and corresponds to a relative difference of about 0.5 percent.

In Figure 49, 50 and 51 it is possible to see the zoom of the difference between the peaks for the three different levels of energy.

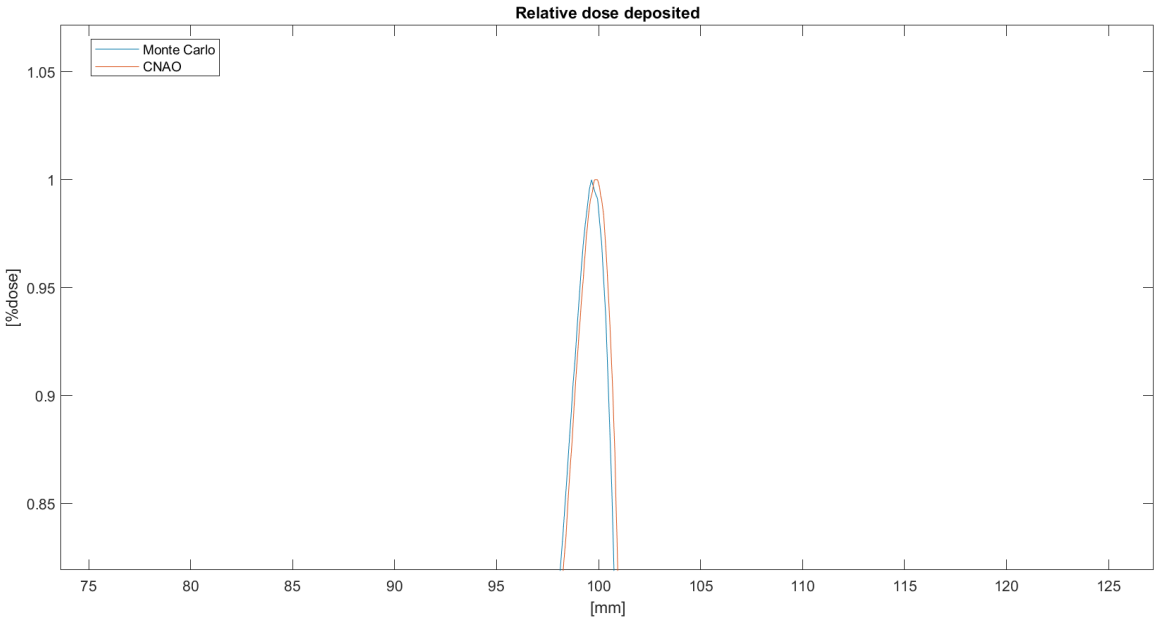

Figure 49: Zoom of the difference between the peaks - 118 MeV

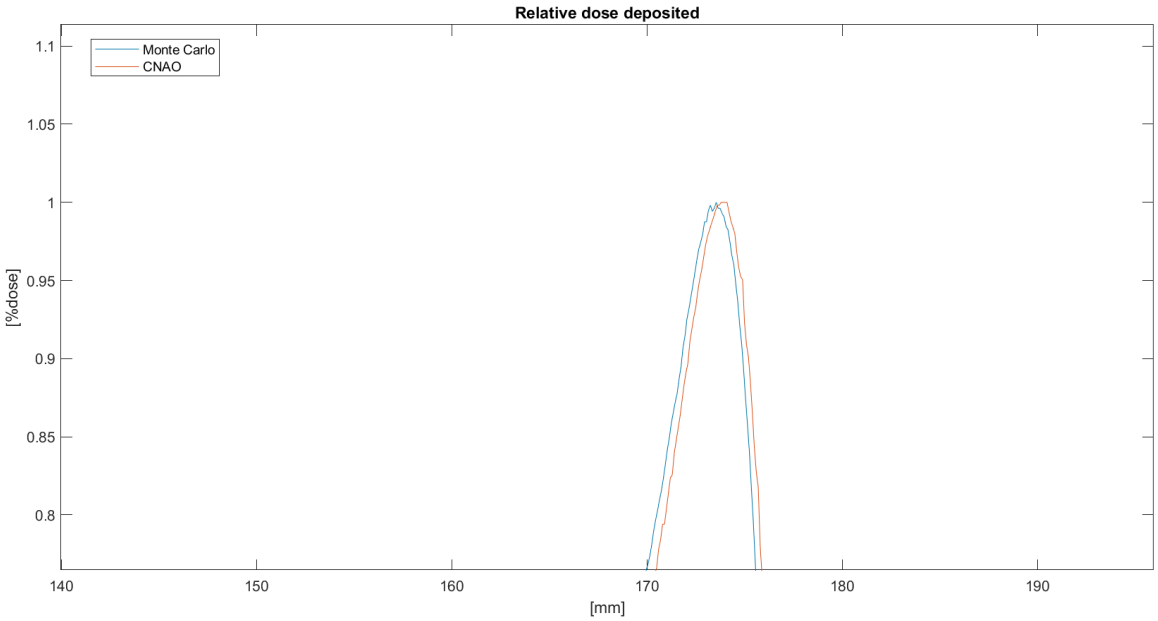

Figure 50: Zoom of the difference between the peaks - 160 MeV

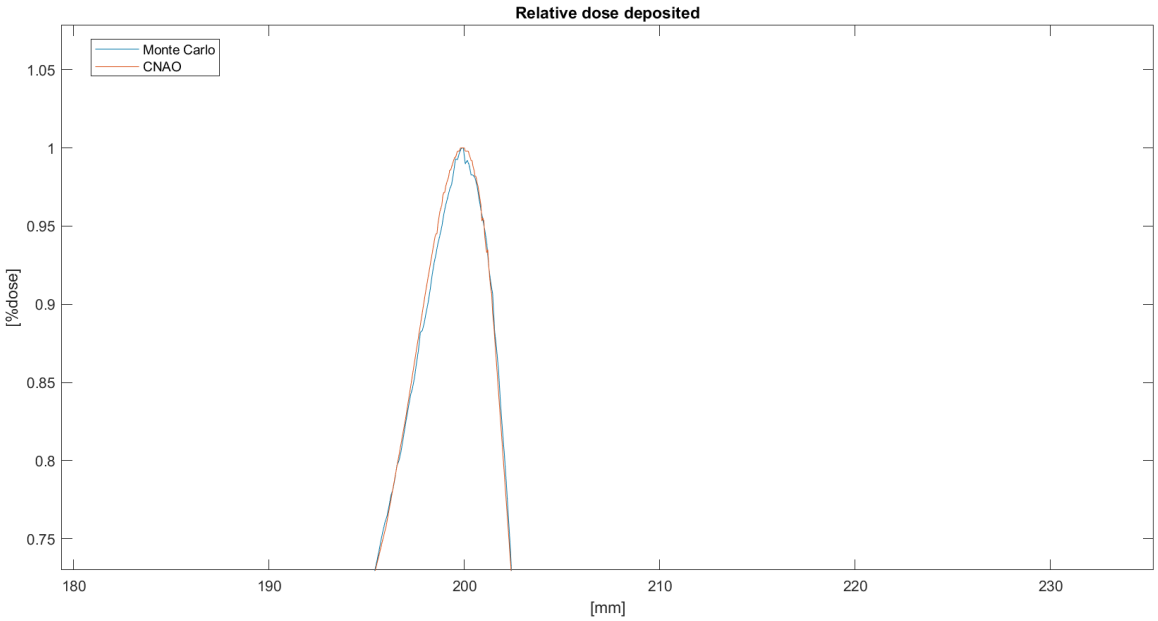

Figure 51: Zoom of the difference between the peaks - 173 MeV

Considering that the difference between the peaks is less than a millimeter for all the three cases, for the purposes of this work, it is possible to conclude that the Monte Carlo model on which the web tool is based results validated.
It is important to highlight that, in these cases, in which the model is used for clinical planning, the attention is focused on the peak position. The peak is the most important aspect to consider because shows the behavior of the dose delivery in correspondence of the target.

6 Robustness analysis

6.1 Introduction to Robustness

The simulation performed during a RTP has, as its main target, the prediction of the dose distribution in the tissues of the patient. The results given by the simulation are affected and influenced by some uncertainties. Proton Therapy is sensitive to changes in anatomical structure and the uncertainties could cause some not negligible deviations from the prescribed dose distribution. The risks related to this phenomena are to release an insufficient dose to the tumor cells or to over irradiate the OARs.
The variations are mainly of two types: intra-variations and inter-variations. The intra-variations are, for example, the respiratory motion or the gastrointestinal movement during the treatment. The inter-variations are setup errors of the treatment or shape change of tumor or organs.
Some examples of these uncertainties are the patient geometry, the approximations on the physic problem and the prediction of biological effects. The strategy, widely used to manage the uncertainties, is to define, as previously described, the PTV. It represents a geometrical concept that it is useful to set margins. This is the conventional method to take into account errors in dose distribution, but this approach, which was developed for the conventional Radiotherapy, is not sufficient for Proton Therapy applications. In Proton Therapy, the very precise and narrow action of the protons beam requests advanced methods to manage uncertainties.
The more recent solution to manage the uncertainties in the treatment planning is to implement some mathematical methods in order to obtain "Robust Treatment Planning" algorithms. The word "robust" means a plan in which the uncertainties introduced lead to an acceptable perturbation in the dose distribution.
The uncertainties of the planning could derive from the phase of the target volume definition or for example from the dose prescription.
Generally speaking, the uncertainties, in a RTP, are divided in two categories: the biological uncertainties and the physics ones. The physics uncertainties are those related to the prediction of the physical dose distribution delivered. The biological ones are related to the uncertainties on the estimation of the effects of the dose on the cells. This aspect is evaluated using the concept of Relative Biological Effectiveness (RBE). An RBE model is implemented to manage the biological effects, but these types of models are dependent on the LET distribution, characteristics of the tissues and the dose. These input data are affected by uncertainties that cause deviation during the evaluation of the biological effects.
The implementation of a Robust Treatment Planning permits to maintain a stable result of the dose distribution in the tissues of the patient also in case of variations and uncertainties in the input data of the simulation.

In Figure 52, it is possible to appreciate the different effect of the uncertainties (perturbed scenario) in case of the conventional model and in case of a Robust Treatment Planning.

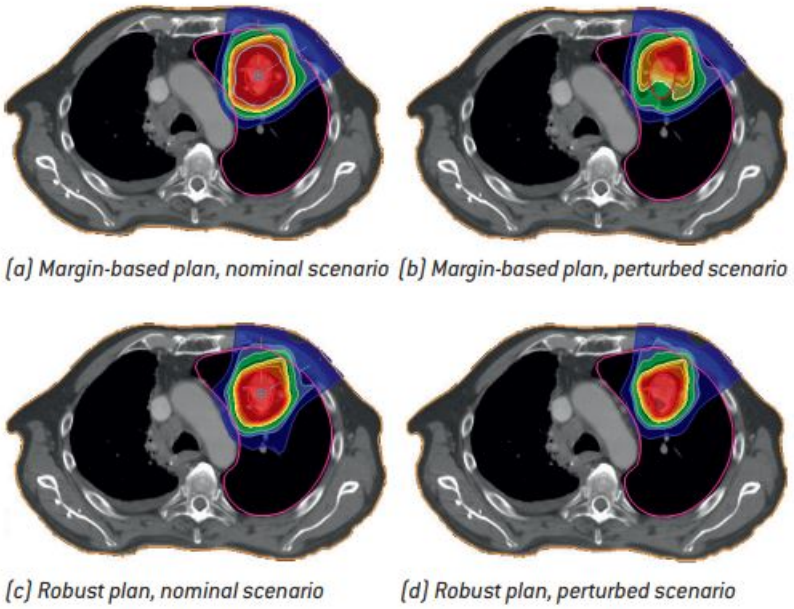

Figure 52: Comparison between a robust plan and a conventional plane in case of a perturbed scenario[83]

In the conventional model, the perturbation causes a not negligible deviation of the dose distribution, risking to over irradiate healthy tissues. In the robust case, the distribution of the dose remains stable.

6.2 Analysis of the Robustness

6.2.1 Introduction

The aim of this work is to analyze the behavior of a Treatment Planning System introducing uncertainties in the input of the model. The TPS used is structured in two sections and permits to perform the inverse model simulation and the forward Monte Carlo one. Initially, the attention is focused mainly on the analytical methods because they are widely used in clinical planning.
The TPS user receives as input two data: the CT of the patient case and the contouring file of the PTV and the organs. In order to produce regulated and

comparable results, both of these input data are implemented in DICOM. The CT is loaded as a series of DICOM images (.dcm) that represent the slices that are necessary to visualize the target and the organs of interest.

In Figure 53 and Figure 54, an example of CT slices and of the contouring file are reported. For the CT figure, only some exemplifying slices are reported. A whole CT is composed of tens or hundreds slices according to the specific case. For the contouring figure, the image shown is that one obtained by the contouring phase, that information is then converted in DICOM.

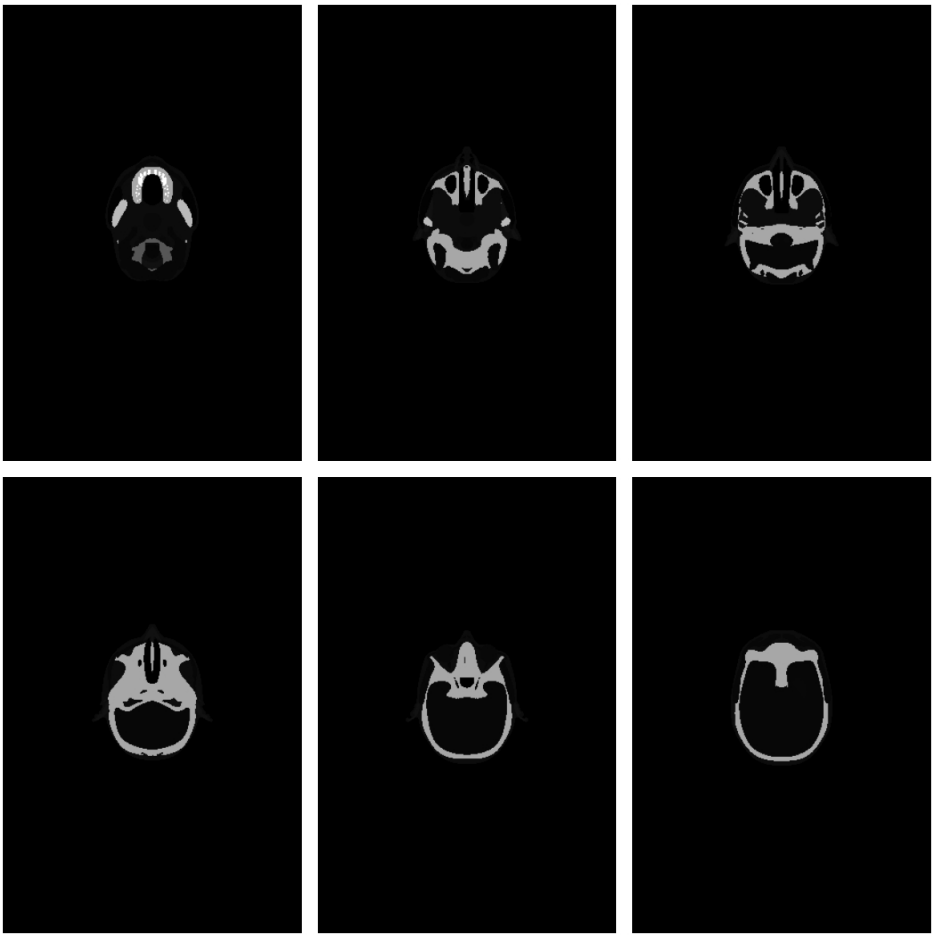

Figure 53: Example of CT input for TPS

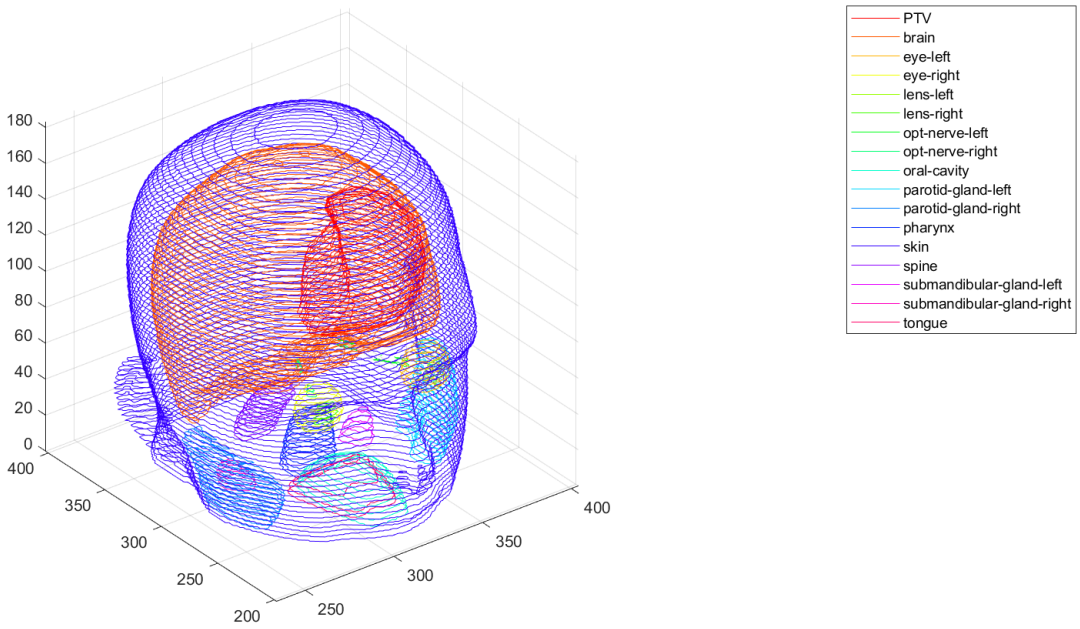

Figure 54: Example of contouring input for TPS

In this analysis, the patient case is developed starting from a "virtual patient" 3D model. In reality the contouring procedure is performed by the medical physicist, starting from the real CT of the patient. The creation of the patient case from a virtual 3D model allows one to obtain a clearer CT with respect to the real ones and to have the contouring of the PTV and of the organs already constructed. The 3D patient model permits to have the correct contouring of all the organs in the body. This choice does not compromise the validity of the robustness analysis.
The uncertainties are introduced in the CT given as an input. Each slice of the CT is discretized in voxels according to the resolution that it is necessary to obtain.
The information of each voxel is converted from greyscale to Hounsfield units (HUs). The creation of the DICOM images of the slices is performed starting from the matrix of the Hounsfield numbers in which the greyscale slice is converted. The DICOM slices, once implemented on the TPS, are converted in terms of electron density that is the form suitable for the simulation algorithms.
The purpose of this work is to introduce an uncertainty on the HUs in order to focus the attention on the variation on the dose distribution that this perturbation causes. During the compilation of the HUs matrix, the values are perturbed by 20%. The comparison with respect to the unperturbed case is performed with respect to an overshoot scenario, in which the perturbation is positive, and respect an undershoot scenario, in which the perturbation is negative.
In the overshoot scenario, the HUs are incremented, this means that the tissues are denser than the reference scenario. The perturbation expected in the dose distribution is the presence of some under-irradiated points, because the dose release is less effective for dense tissues. In case of overshoot of the HUs, the CT image appears

darker than the reference one.
In the undershoot scenario the HUs are decreased, so the tissues are less dense than the unperturbed scenario. The perturbation expected, in this case, in the dose distribution, is the presence of hot-spots in which the dose deposited is larger than the required one. In case of undershooting of the HUs, the CT image appears brighter than the reference one.
The main target of the analysis is to estimate the perturbation of the dose distribution that the uncertainty on the HUs causes. If the results of each scenario are very similar the TPS is robust, in the opposite case, it is necessary to understand how to make the model more reliable. The main purpose is to use the forward methods to verify the effect of the uncertainties.

The tools and the applications used in this analysis are described in the following section.

6.2.2 TPS characteristics

The applications and the tools used in this work are developed by I-See s.r.l..
The CT is generated by the web application "Virtual Patient 3D" that is based on an anthropomorphic virtual phantom (Figure 55). The Virtual Patient is a web interface where it is possible to navigate through the body of a virtual patient and it permits to position a tumor mass, defining its dimension and orientation. It is also possible to model the cancer mass in a 3D software developer, like "Blender", for example, and import it in the web tool. Once positioned the target mass, the Virtual Patient allows to generate and download the CT images set of the case study of interest. An example of tumor mass positioned in the Virtual Patient is presented in Figure 56.
The simulation tool used in this work is another web application developed by I-See s.r.l., "4 See Plan". This web tool receives as an input the CT images and the contouring file in DICOM and it allows to perform the simulation of the Radiotherapy treatment. 4 See Plan gives the possibility to simulate the same case study both with PB algorithms and Monte Carlo model.
The inverse planning algorithm (Fast Optimization) implemented on 4 See Plan, in addition to the inputs described above (CT and contouring), receives, by the user, information on the prescribed total dose to the target, the rotation of the couche, the rotation of the gantry and the number of fractions of dose releases.
Fast optimization gives as output the dose matrix and the Dose Volume Histograms (DVH) for each organ. DVHs could be of two types: cumulative DVHs and differential DHVs. In this work, the DVHs considered are cumulative. A DVH plot shows on x-axis the dose and on y-axis the percentage of the volume of the tissue that receives a certain value of dose. DVH represents a very useful 2D tool to estimate the 3D dose release in the tissues of the patient during a Radiotherapy Treatment Planning. Each organ taken into account during a RTP has its DVH. The attention

Figure 55: Anthropomorphic virtual phantom [46]

is usually mainly focused on the DVH of the PTV and of the Organs At Risk (OAR). In order to understand better the meaning of a DVH, it could be useful to suppose that an OAR, for example the brain, must receive at most a prescribed cumulative dose imposed by the medical physicist. An example of dose constraint is that at most 40% of the brain (OAR) can receive 30 Gy. At the end of the simulation of a RTP, it is possible to choose the corresponding curve and check if the prescribed condition is satisfied.
In Figure 57, an example of DVH is shown.

The Monte Carlo model, instead, in addition to the input described above, receives the field defined in the Fast Optimization phase. In 4 See Plan, in order to run the Monte Carlo simulation, it is mandatory to perform before a Fast Optimization process. The Monte Carlo gives as output the profile depth of the beam and the dose distribution in the tissues of the patient.
The analytical forward method is not available from the 4SeePlan interface, but it is externally implemented in a script developed by I See s.r.l..
The images generated by the Virtual Patient are not ready to load on 4SeePlan. The CT slices must be manipulated in order to be in the right format for the simulation

Figure 56: Example of tumor positioning [46]

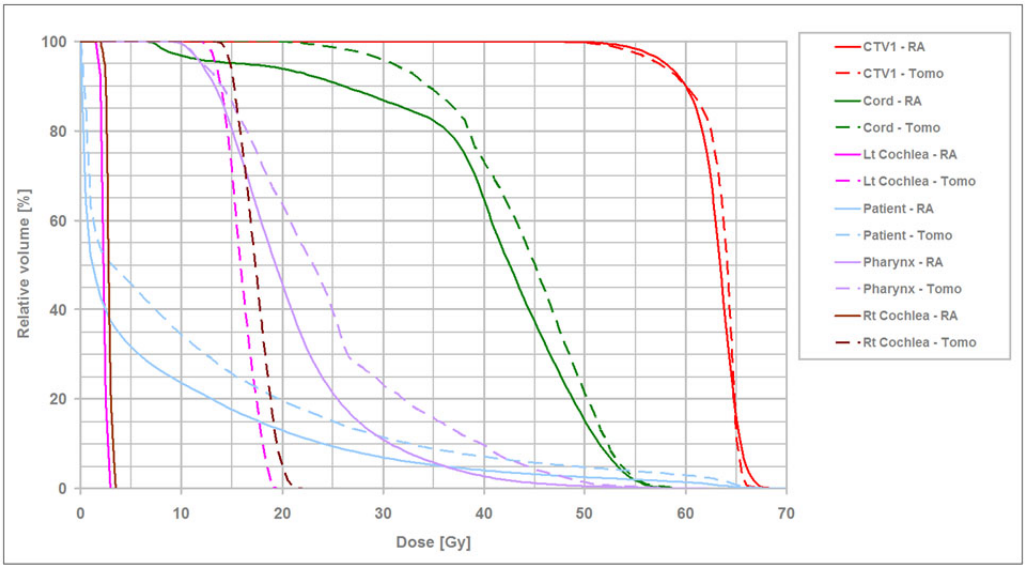

Figure 57: Example of DVH [8]

and the contouring must be performed. All the following steps are performed with Matlab scripts developed by I-See s.r.l. .
As described previously, the Virtual Patient generates the slices of the CT for each organ. The first step is to composite all the slices in greyscale images and generate the matrix with the HUs. This procedure is implemented in the script 'compositing.m'. At this point, using the HUs matrix, a set of DICOM images is generated and this set will be one of the two inputs for 4SeePlan. Starting, as in the previous

step, from the slices generated by the Virtual Patient, the contouring is performed and then it is converted in DICOM format. At this point, the two inputs necessary for 4SeePlan are ready.
For brevity, the description of the steps between the Virtual Patient and 4SeePlan is not detailed. Some specific documents produced by I-See s.r.l. are available to understand each step.

In Figure 58, a scheme of the workflow followed is shown.

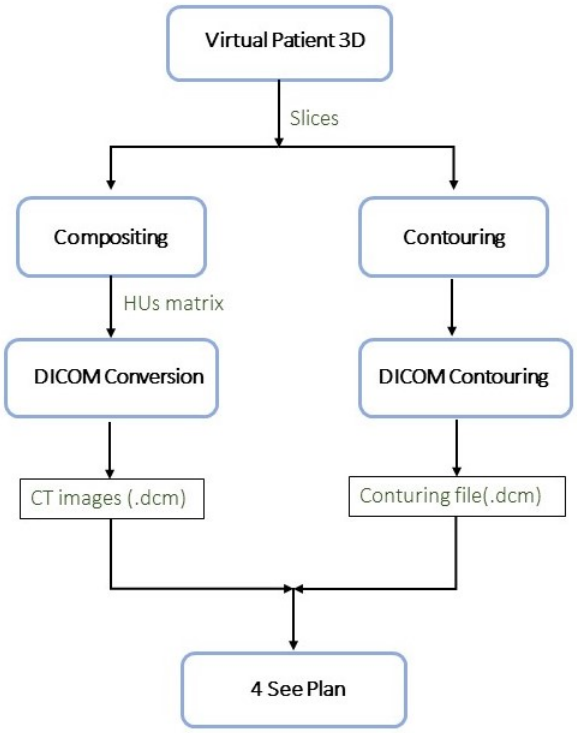

Figure 58: Workflow from VP3D to 4SP

The introduction of the uncertainties on HUs described in the previous section is performed during the compositing phase.

6.2.3 Case study

The target used in the simulation is a centrally located brain tumor. The cancer mass is positioned in the Virtual Patient frame. The target of the case study is modeled by I-See s.r.l. using the 3D CAD tool "Blender". In the tumor positioning section of the Virtual Patient, it is only possible to model ellipsoidal targets. In order to obtain more complex geometries, it is necessary to use a 3D CAD software

and then import the model in the Virtual Patient.
In Figure 59, Figure 60 and Figure 61, it is possible to see the shape and the position of the target chosen for this analysis.

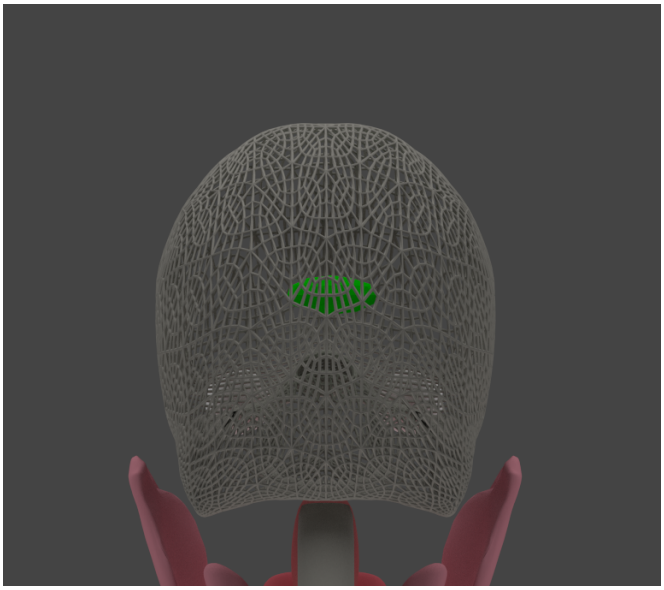

Figure 59: Rear view of the target[46]

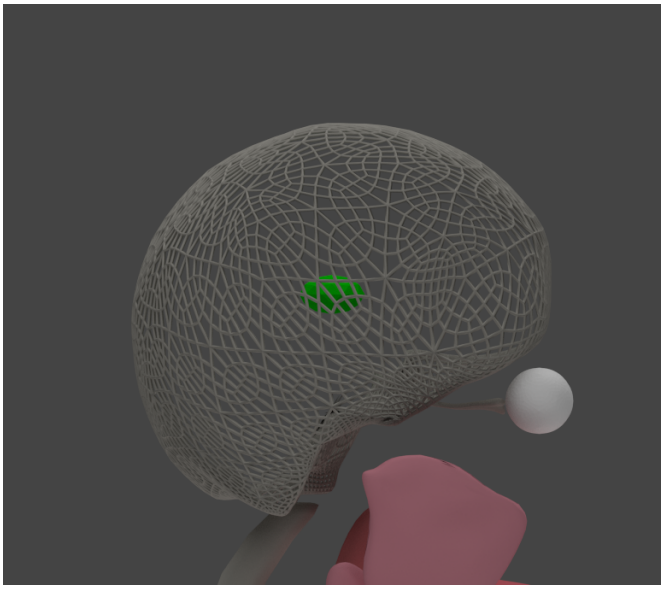

Figure 60: Lateral view of the target[46]

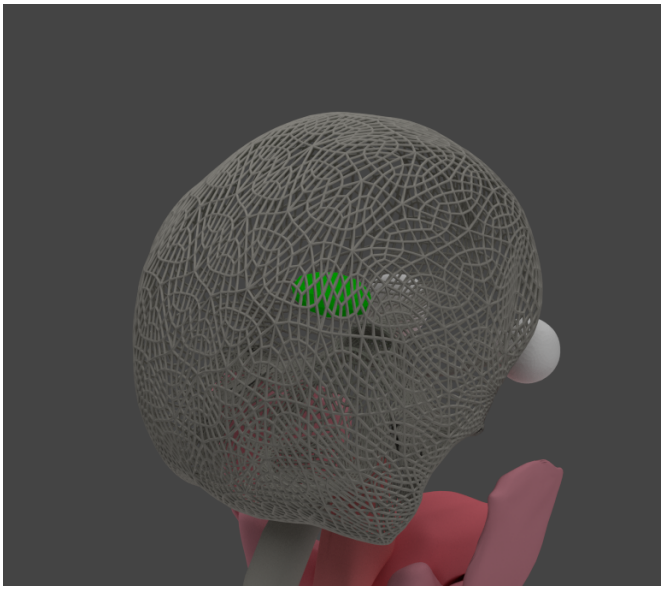

Figure 61: Isometric view of the target[46]

The grey grid represents the brain and the green mass represents the target.
Once the target is chosen, it is necessary to perform the sectioning. After checking the correctness of the target definition, it is mandatory to set the number of slices in which to section the target. For this analysis, the mass is sectioned into 20 slices. At this point, the slices generated are the equivalent of the CT images created with a Tomograph in reality. It is possible to download the slices from the Virtual Patient and to perform the post-processing of the CT described in the previous section.
The dose requested in the target is 5 Gy and the treatment is performed imposing the zero value to the angle of the couch and the angle of the gantry.
In Figure 62, the section of the target and PTV considered in this work is shown.

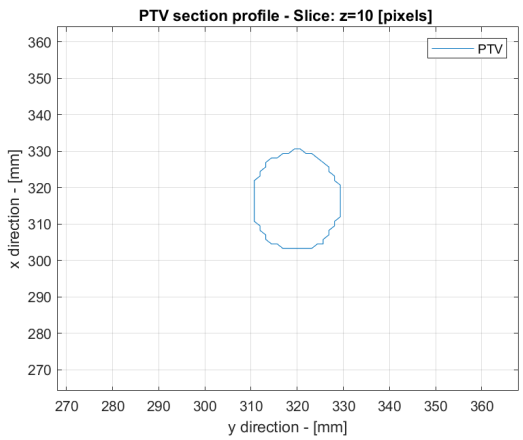

Figure 62: Section of Target and PTV

6.2.4 Workflow

The purpose of this section is to present the logical steps followed during this work, in order to make easier the interpretation of the results.
It is crucial to remember that the inverse planning is used to set the therapy facility in order to obtain the right dose distribution in the target. It is important to understand the effect of the introduction of uncertainties on the dose behavior starting from the inverse plan.
The inverse method generates a file that lists the Pencil Beams that are necessary to obtain the prescribed dose distribution. Each beam is characterized by position, fluence, energy and deflection. The first target of this work is to perform four inverse simulations with different CT files keeping constant the contouring and the dose value.

The four cases are:

- Unperturbed CT
- 20% Undershoot CT
- 20% Overshoot CT
- Uniform CT (HU = const = 1000)

The uniform case is composed by the head of the Virtual Patient in which the HUs are constant to 1000. This case is used only an extreme case for the comparison. The purpose of this part is to focus the attention on the energy of the beams, estimated by the inverse planning, in order to monitor the sensitivity of the method.
At this point, the second step is to use the analytical forward method to verify how the perturbation introduced influences the dose distribution.
The inverse method is not suitable to evaluate the effect of the perturbation because the driver of this approach is the desired dose value in the target. Varying the CT characteristic, the dose distribution will be the desired anyway. For this reason, in order to highlight the variation in the dose distribution caused by the perturbation introduced, forward methods are necessary. The analytical forward method receives as input the CT and the beam file generated by the unperturbed inverse plan.

The analytical forward model is applied to two cases:

- 20% Overshoot CT
- 20% Undershoot CT

In both cases, the beam file used as an input is that related to the unperturbed inverse plan. In this way, it is possible to estimate the effects of the uncertainties

that could appear after the preliminary plan.
The last step of this work is to introduce the Monte Carlo method as a check of the effects of the perturbations in the CT. The procedure followed is the same of the analytical forward approach.

For the Monte Carlo method, three simulations are performed:

- Unperturbed CT
- 20% Overshoot CT
- 20% Undershoot CT

Also in this case, the beam file given as an input to the Monte Carlo algorithm is the one related to the unperturbed inverse plan.

Finally, following this workflow, it is assumed to perform an inverse plan on a patient and set up the facility following the plan. At this point, it is assumed that the patient presents some uncertainties during the various treatment sessions. The objective is to highlight how, starting from the initial setup, the uncertainties introduced compromise the dose distribution. In order to do this, the results of the two forward methods are compared: the analytical and the Monte Carlo model.
An uncertainty of 20% on the HUs may appear, on a preliminary analysis, a decidedly excessive perturbation of the CT. Actually, the choice is justified by the fact that the HUs, both in analytical and statistical models, are converted into density values through the interpolation of the values of a calibration curve. A 20% perturbation of the HUs corresponds to a lower uncertainty, as a percentage, of the density values.
In Figure 63 and Figure 64, calibration curves used in this work are shown.

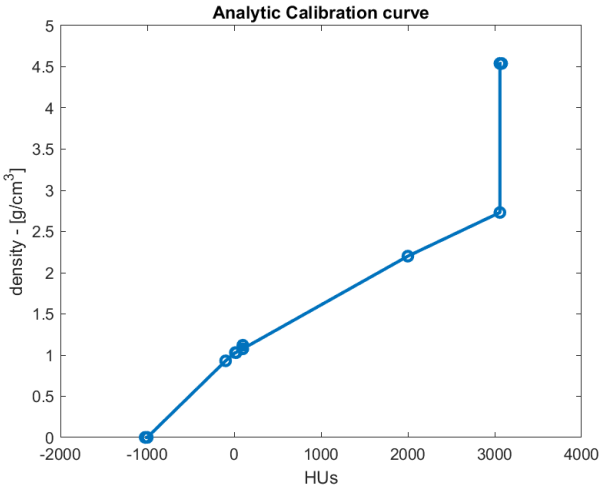

Figure 63: Calibration curve used in the Analytical method

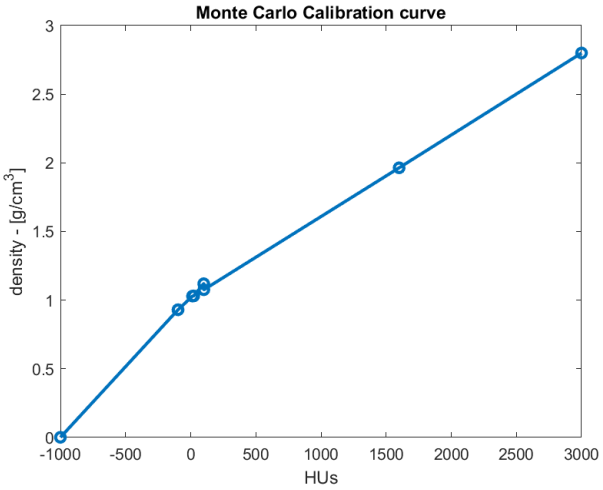

Figure 64: Calibration curve used in the Monte Carlo method

Considering, as an example, the calibration curve used in the analytical method and the value of HU of the bone structures (HU=1000), it is useful to estimate the 20% of perturbation how impacts on the density.

Performing the interpolation on the curve

$$HU_{std} = 1000 \rightarrow \rho_{std} = 1.61[g/cm^3]$$

Introducing the perturbations

$$HU_{under} = HU_{std} - (HU_{std} \cdot 0.2) = 800$$

$$HU_{over} = HU_{std} + (HU_{std} \cdot 0.2) = 1200$$

Interpolating these values on the curve

$$HU_{under} = 800 \rightarrow \rho_{under} = 1.49[g/cm^3]$$

$$HU_{over} = 1200 \rightarrow \rho_{over} = 1.73[g/cm^3]$$

The Undershoot perturbation corresponds, in terms of density, to an uncertainty of 8%. The Overshoot perturbation corresponds to an uncertainty of 7.5%. This means that 20% of uncertainty on HUs corresponds, as a percentage, to less then half perturbation in terms of density.

6.3 Results

6.3.1 Introduction

In order to understand the results obtained in this work, it is necessary to specify that all the results considered in this section are related to the same position. The position chosen is defined calculating the half of the whole dimension of the CT in all of the three directions. In this way, the position is exactly in the centre of the domain.

In Figure 65, it is possible to see the position of the two axis of sectioning. In Figure 66, the CT slice considered in this work is shown.

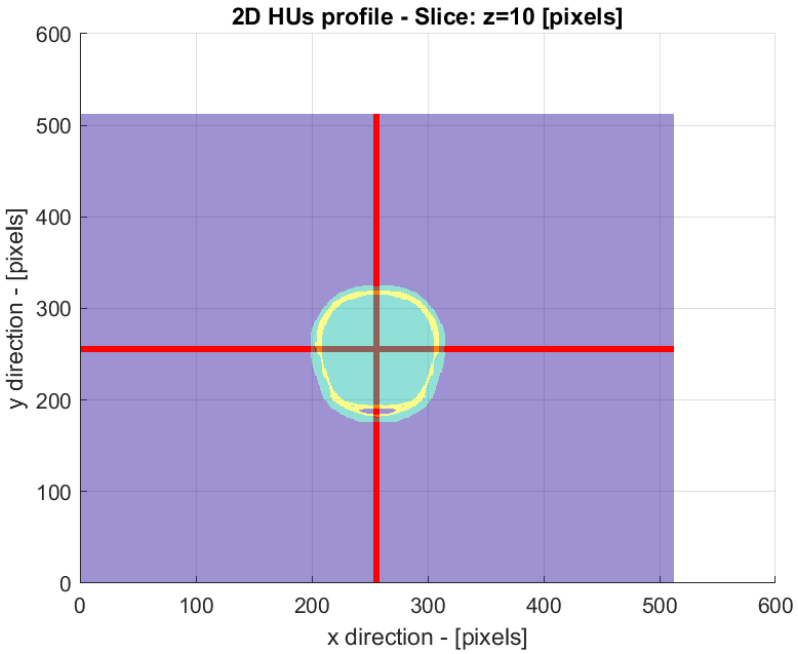

Figure 65: Position of the axis of sectioning

Another important aspect, that is necessary to underline, is that the dimensions of the dose matrix obtained with the analytical and statistical method are different. The inverse and forward analytical method consider only the part of the CT in which is the body of the patient is present. In this case, the domain is discretized in pixels: 59 along x, 66 along y and 19 along z. The Monte Carlo model works on the whole CT and for this reason the domain is discretized according the resolution imposed during the aquisition. In this case, the domain in the CT is discretized in 512 pixels along x, 512 along y and 20 along z. Taking into account this different resolution between the models, it will be necessary to perform some adjustments

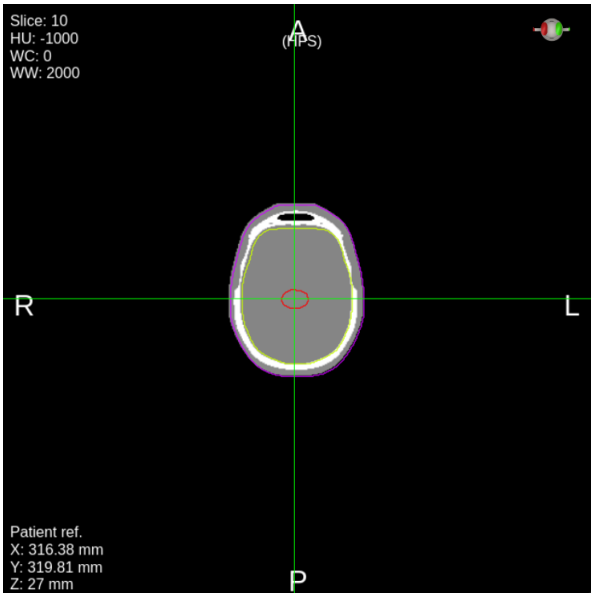

Figure 66: CT slice of reference[46]

and translations in order to obtain a correct comparison.
In order to consider, during the comparison, the same positions in the two methods, it is necessary to select the right slice along x,y and z. Considering the Monte Carlo model results, it is sufficient to select the slice 256 along x and y and the slice 10 along z. Considering, instead, the analytical model results, the comparison is effective selecting the slice 29 along x, the slice 33 along y and the slice 9 along z. In x and y direction, the choice is driven by the purpose to select the position in the centre of the domain. In z direction, the slice is the ninth because the domain of analytical method is translated upward by 2cm. Obviously, the different resolution requests some approximations in the choice of the position in the two different domains.

In Figure 67, it is possible to appreciate the two different domains. The red one is the limited one related to the analytic methods and the blue is the one related to the Monte Carlo model.
In addition to the different domain size for the two computational methods, the resolution of the two domains is also different. The Monte Carlo model domain is discretized with pixels of 1.24 [mm] along x and y, while the pixels along z are 3 [mm]. The domain of the analytical model is discretized with 3 [mm] pixels along all three directions. The different resolution of the results will be very evident in the dose distribution plots.

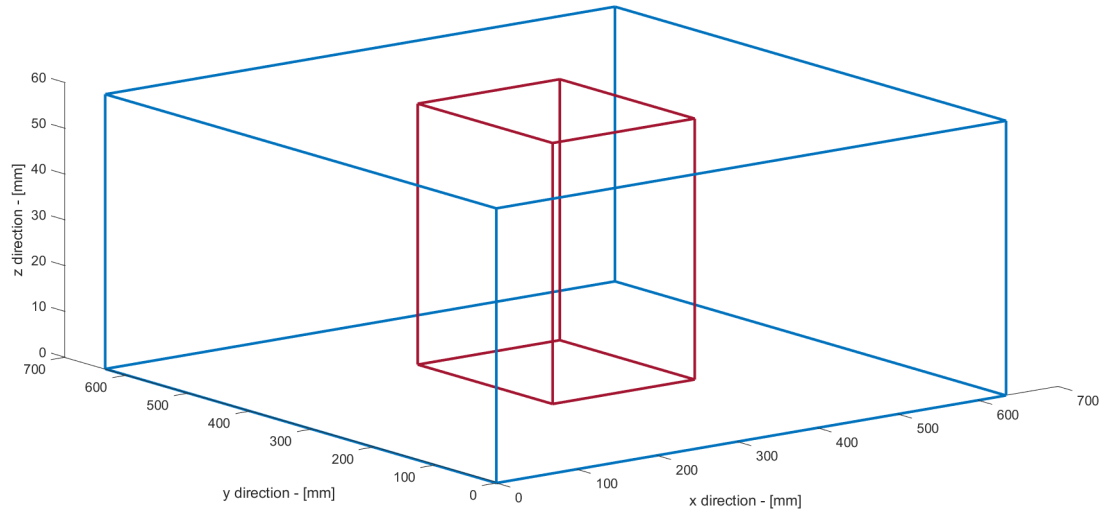

Figure 67: Representation of the two different domains

6.3.2 Hounsfield units profile

The first target is to verify the correct introduction of the perturbation in the HUs matrix of the CT. In order to do this, it is necessary to verify the behavior of the HUs in the CT projecting the profile along an x and a y axis. The position that is chosen is that indicated in the introduction of this section. The CT cases considered, as previously described, are four.
Firstly, in Figure 68, it is possible to see the HUs profile along the x direction.
The behavior of the uniform case is constant and linear as it was predictable. The others three plots are consistent with the perturbation introduced. The two symmetrical peaks are related to the walls of the skull. The two peaks reach values of HU equal to 1000 that is the value typical of the bone structures. The symmetry of the plot is consistent with the position of the projection axis and with the fact that along the frontal plane the anatomy of the human head is symmetrical. The step that is present in the central part of the plot is related to the presence of the target. The uncertainty on the HUs is introduced also on the tumor mass, but , due to the scaling of the plot, in this figure the perturbation introduced is not evident.
In Figure 69, the y projection is shown. The comments are the same made for the previous plot. In this case, the plot is not symmetrical, as it was predictable. The human head is not symmetrical along the sagittal plan. As in the previous plot, the central step indicates the target and the peaks, with HUs equal to 1000, are related to bone structures. An aspect that is important to underline is the presence, on the left of the plot, of a drop to -1000. That section is related to the frontal part of the head of the virtual patient and in that position there are paranasal sinuses. These structures are empty bone cavities and for this reason in all cases considered,with

the exception of the uniform case, the HUs are imposed equal to -1000. Remember that this value is the characteristic one of the air.

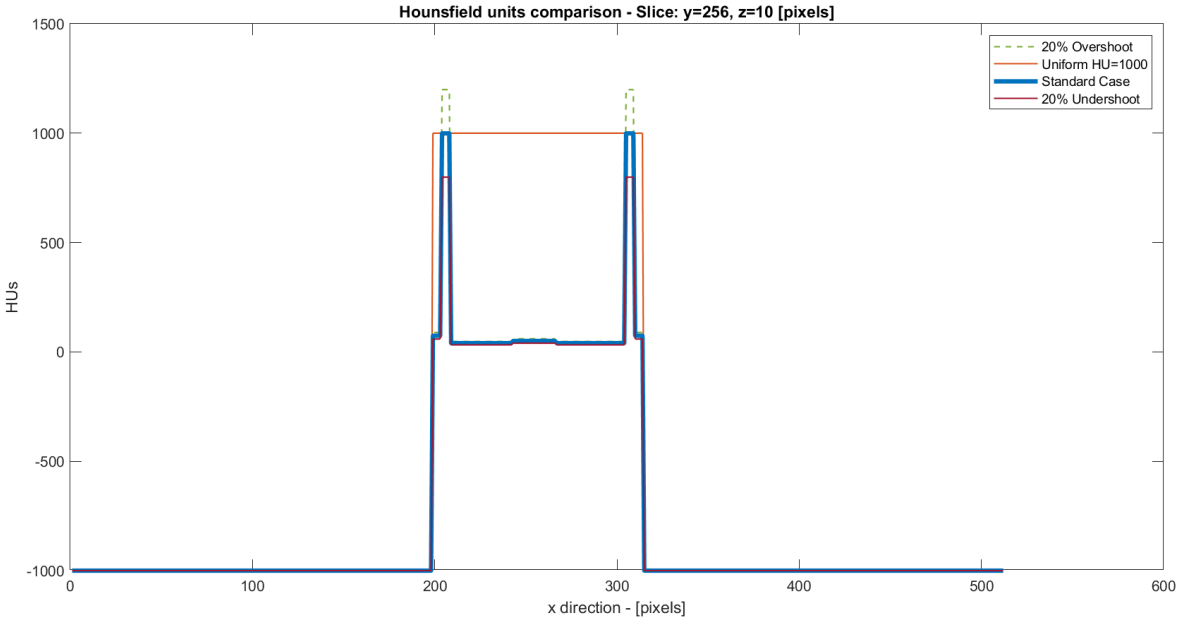

Figure 68: Projection along x of HUs profile

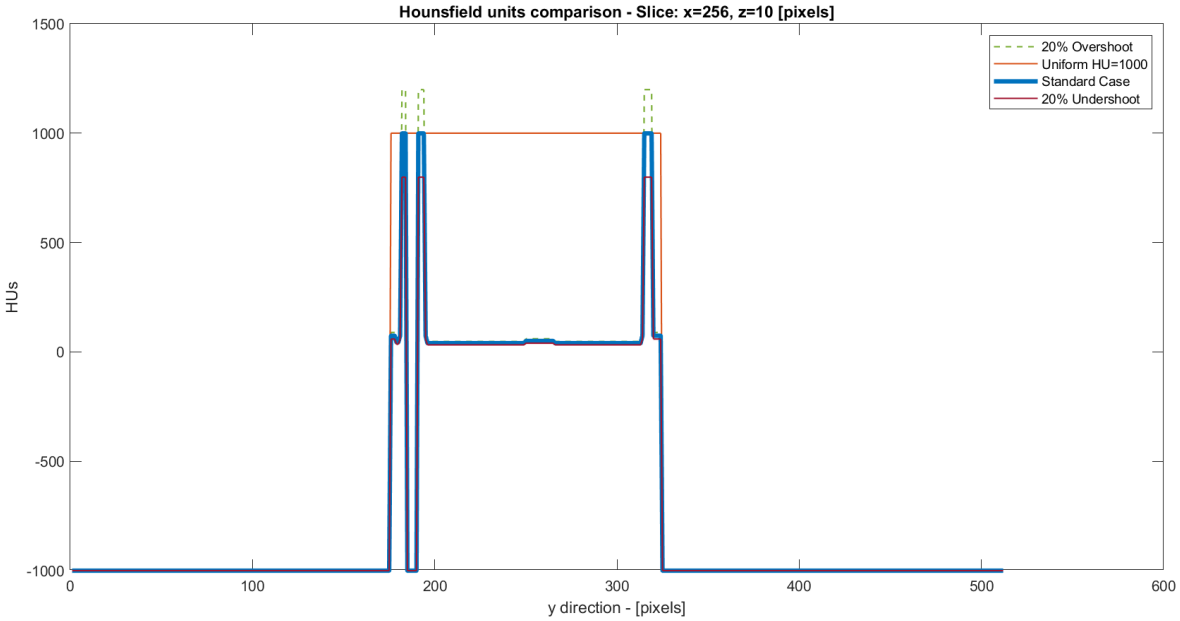

Figure 69: Projection along y of HUs profile

Finally, in Figure 70, it is possible to appreciate the 3D behaviour of the HUs in the unperturbed Computed Tomography. The green part represents the bone of the skull, the blue part represents the skin around the skull and it is possible to appreciate, also in this 3D view, the detail of the paranasal sinuses. The purple color indicates the HU value of -1000.

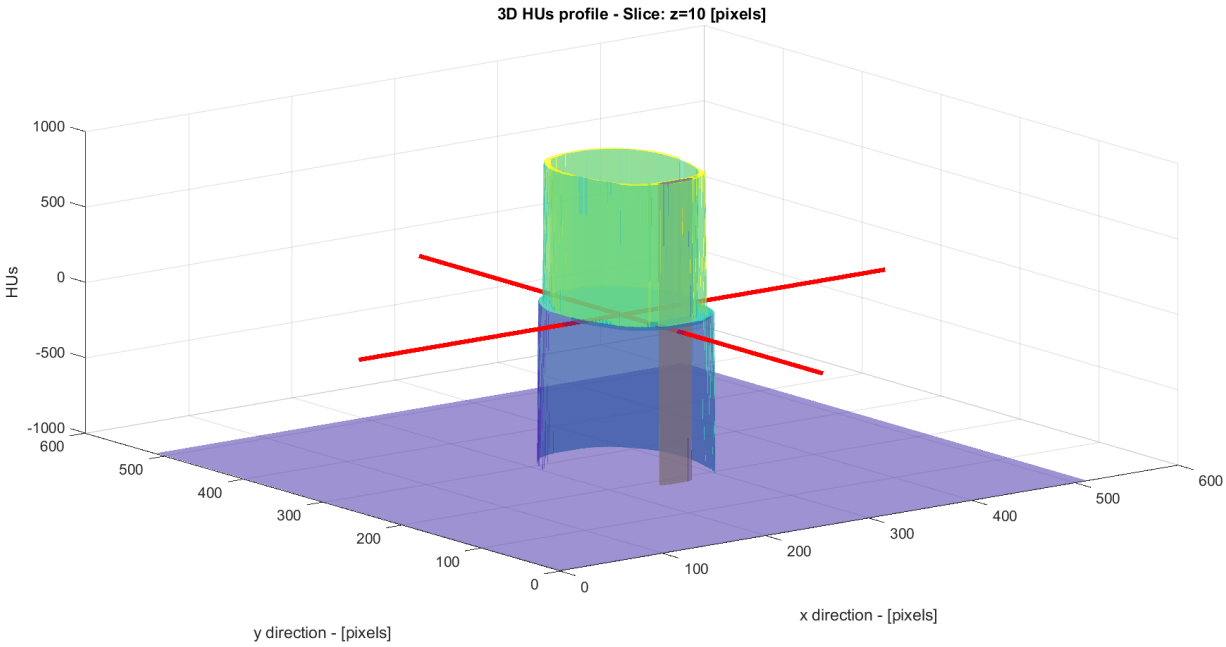

Figure 70: 3D plot of HUs profile

The red lines are the graphical reference for the previous x and y projection.

6.3.3 Inverse plans

Once checked that the perturbation introduced in the HU profile is effective, it is useful to monitor the results of the inverse plans. As previously described, this step of the analysis is based on four CT cases.
Remembering that inverse plan receives as an input the DICOM files and the value of the prescribed dose in the target, an useful aspect to monitor is the beam file given as an output at the end of the inverse plan. The beam file is characterized by the parameters of the beams that are necessary to obtain the prescribed behavior of the dose. In particular, the beam file reports the position, the orientation, the fluence, the energy and the deflection of each particle beam. Defining the Energy Range of each case as the gap between the minimum and the maximum energy value

of the beams, it is possible to perform a qualitative estimation of the effect of the perturbation.

In Figure 71, it is possible to see the Energy Range of each case.

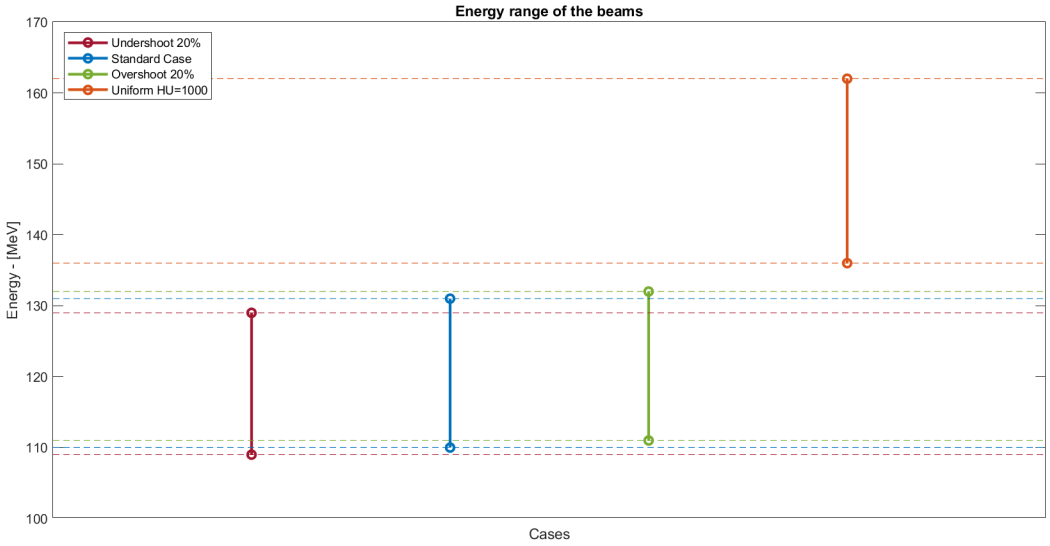

Figure 71: Comparison of the energy ranges for the four CT cases

Considering the plot in Figure 71, the Uniform case, the orange line, presents the highest energy range. This results is physically consistent because, in order to deposit the same dose value in a denser domain, it is necessary to generate beams with high energies.
Considering the other three cases, the Energy Ranges are consistent with the perturbation introduced in the CT cases. For the same reason explained previously in the Uniform case, the Overshoot case presents an Energy Range higher than the Standard one. The Undershoot case presents a lower Energy Range, respect the Standard one, because the tissues are less dense and lower energies of the beams are necessary in order to deposit the same dose distribution in the target.
From this qualitative plot, it is possible to notice that the Undershoot perturbation influences, more than the Overshoot one, the energy range respect the Standard case, in particular comparing the maximum value of energy.

6.3.4 Forward analytical simulations

The forward approach is used as a post-planning check method in order to verify if the beams, computed by the inverse method, are correct to obtain the desired dose distribution. The main drawback of the analytical forward method is the aspect that it is based on the same analytical and discretization approach used in the

inverse plan. This means that, if no perturbation is introduced, the results of the two analytical methods are equivalent. The dose distribution obtained in the inverse plan with the Standard CT case is equal to the one obtained from the analytical forward method.

In order to visualize the shape of the 3D dose distribution in a Proton Therapy Treatment Planning System, in Figure 72, the dose distribution for the Standard case is shown.

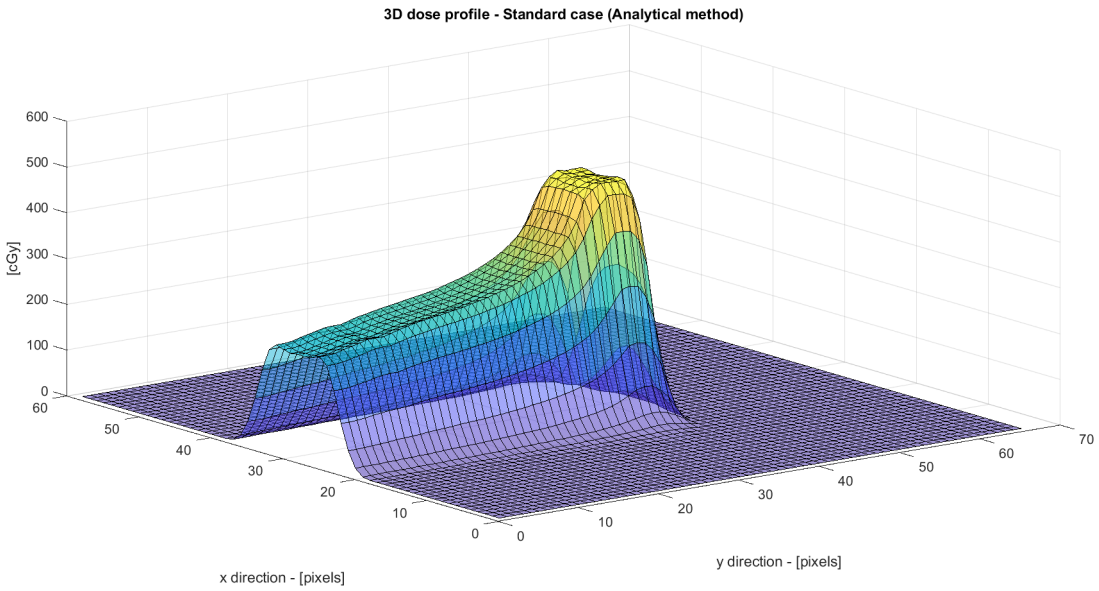

Figure 72: 3D dose distribution of the analytical methods in the domain

In the yellow part, it is possible to notice that, in correspondence with the target, the dose curve presents the characteristic Spread-Out Bragg Peak (SOBP).
Returning to the analytical forward approach, it could be used, in this case, decoupling the input data. This method receives as an input, as described above, the CT and the beam file produced by the inverse plan. It is possible to decouple the input data giving to the forward method, as an input, the perturbed CT cases and the beam file obtained from the Standard inverse plan. In this way, it is possible to simulate the situation in which the plan is performed in nominal conditions, but during the treatment sessions some uncertainties are introduced. This approach allows to compare the dose distribution of the nominal scenario with the one obtained in the two perturbed conditions: the Undershoot and the Overshoot cases.
It is crucial to repeat and underline that, in both cases, the beam file is related to the nominal scenario and this approach is the same followed for the Monte Carlo simulations.
In order to perform the comparison, the dose curve is sectioned along x and y axis. The section is performed in the middle of the 3D domain. For example, sectioning

along y, it is possible to appreciate the peak and its spreading in correspondence of the target.
In Figure 73, the dose curve is plotted together with the HUs profile in the same section.

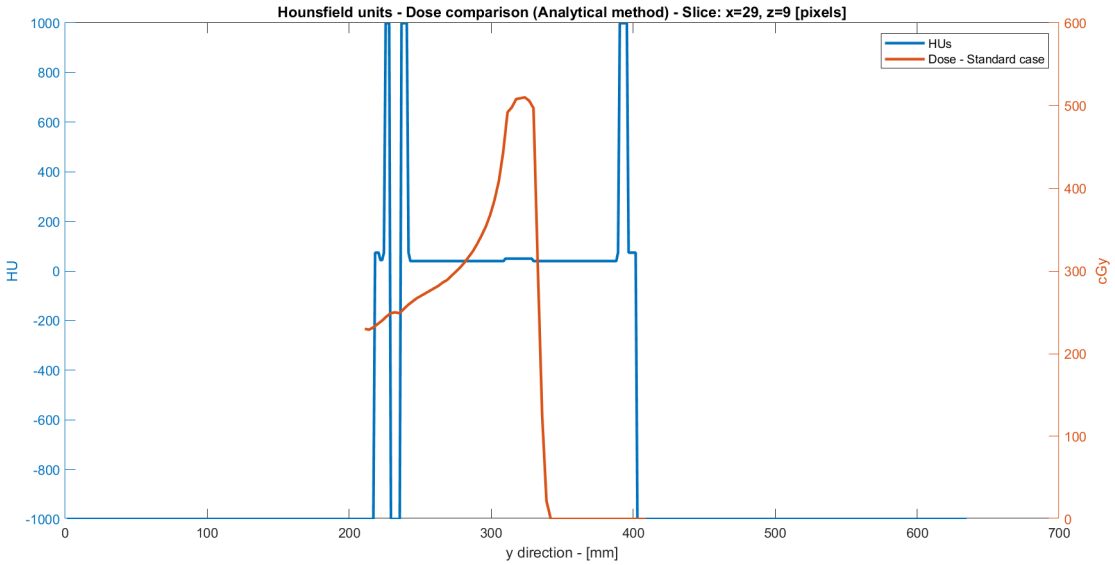

Figure 73: HUs profile and dose curve plot in nominal scenario

It is possible to notice the spreading of the peak in correspondence of the step in the HUs profile caused by the presence of the tumor mass.

In Figure 74 and Figure 75, it is possible to see the comparison between the Undershoot case and the Standard case in the two sections.
Starting from the dose profile along y (Figure 74), the SOBP is evident in correspondence of the target for both curves. The maximum value reached by the Undershoot curve is is higher than that of the standard case of 10 cGy. The range of the dose plot for the Undershoot case is shifted forward of around 1.8 [mm]. This result is consistent with the perturbation introduced, because the tissues, in the Undershoot case, are less dense and the peak reaches higher depths.
Considering the dose profile along x (Figure 75), the resulting plot could be counterintuitive, because the curve of the Undershoot case is lower than the nominal scenario one. This results is justified by the fact that the section is performed in a point in which the Undershoot curve is farther from the peak than the Standard one. The black dashed line in the y projection indicates the reference position for the x projection.

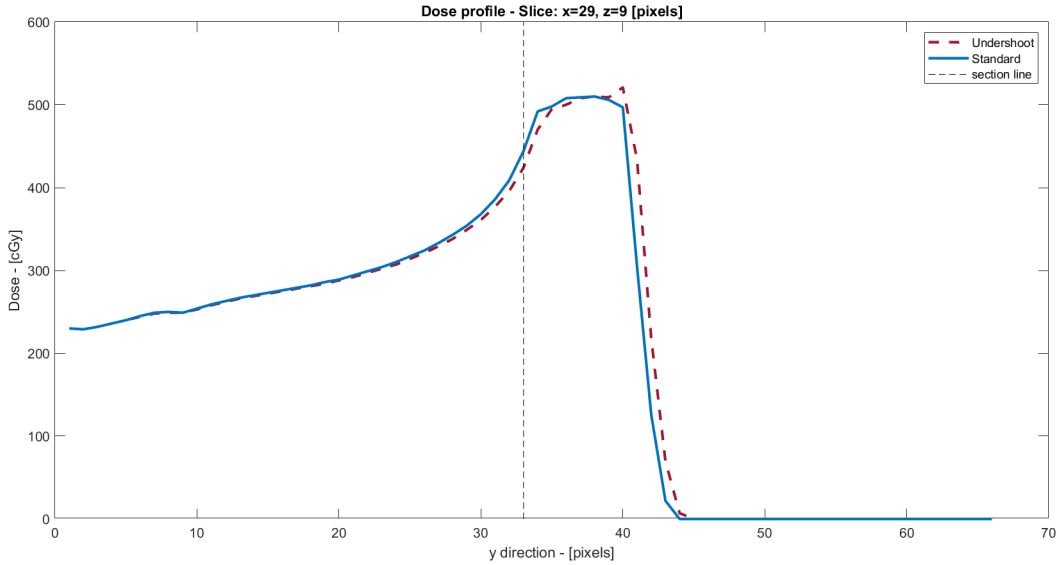

Figure 74: Undershoot and Standard case comparison of dose curve along y

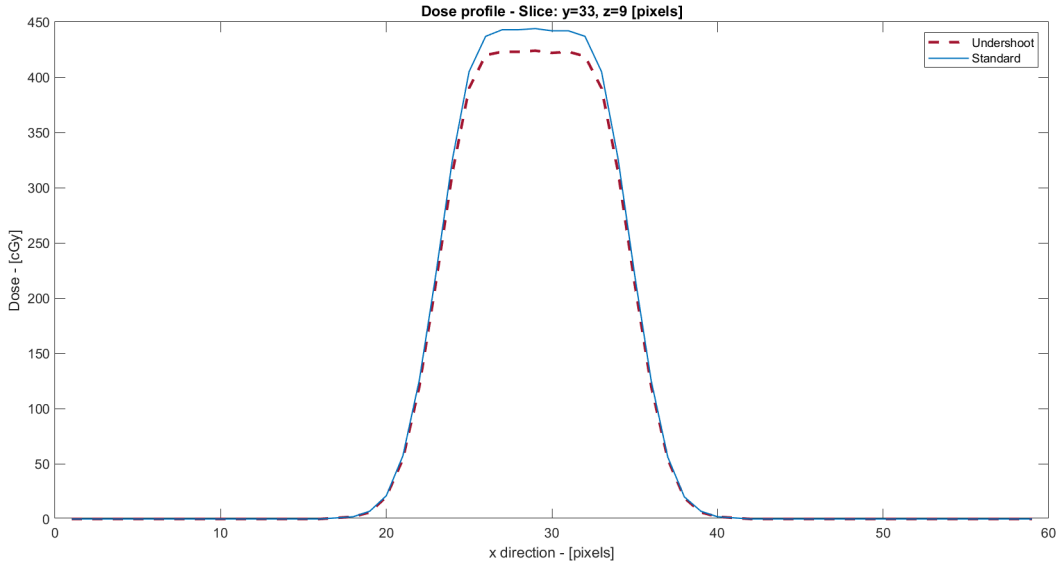

Figure 75: Undershoot and Standard case comparison of dose curve along x

Passing to the Overshoot case, in Figure 76 and Figure 77, it is possible to see the same comparison performed for the Undershoot scenario.

Also in this case, the result is consistent with the perturbation introduced. Tissues are denser than the Standard CT case and, for this reason, the peak is shifted backward of about 1.4 [mm]. The curves reach the same maximum value of dose. Considering Figure 77, the comments made previously for the Undershoot case are also valid in this case.

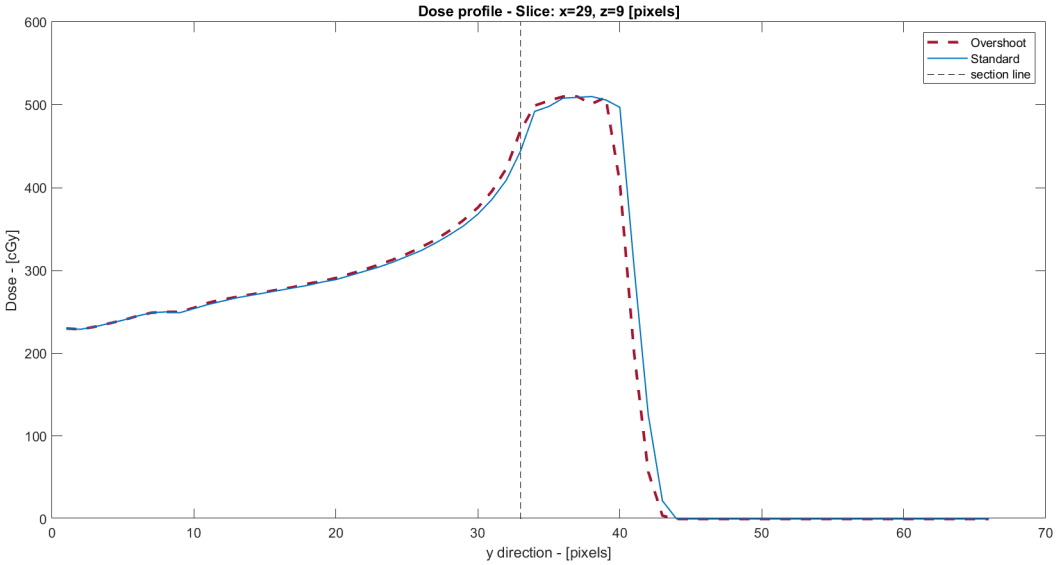

Figure 76: Overshoot and Standard case comparison of dose curve along y

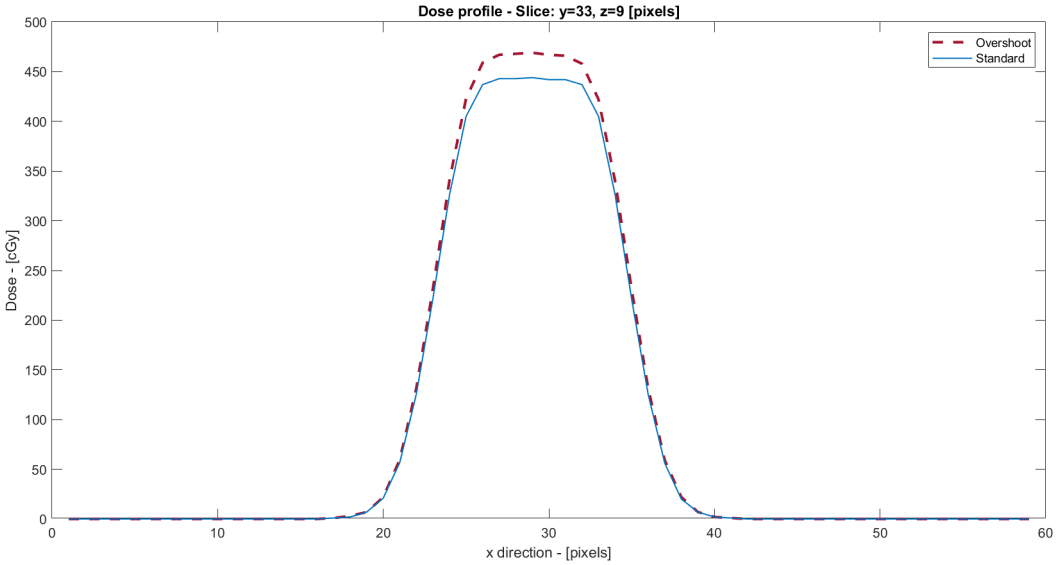

Figure 77: Overshoot and Standard case comparison of dose curve along x

The vertical dashed black line, that is reported in the y-projection plot, also in this case, is only a reference of the position of the relative x-projection.

At this point, it is very interesting focusing the attention on the 2D dose distribution in the slice of interest. In all 2D dose distribution plots shown in this work, the blue line indicates the PTV.

Starting from the x-y plot of the nominal scenario, in Figure 78, it is possible to see the 2D section of the dose behavior in the Standard CT case.

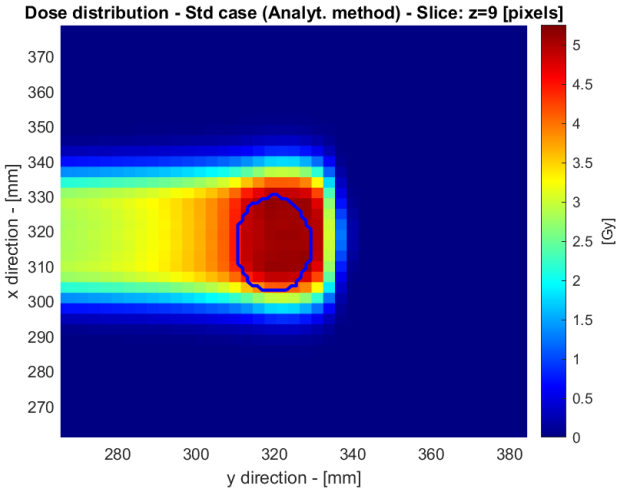

Figure 78: 2D plot Dose behavior for the Standard case

From this plot, it is clear that the target is well centered by the particles beam and the dose deposition is consistent with the desired value. It is possibe to conclude that the PTV is well covered according to the value of dose prescribed by the treatment. Now, it is necessary to move the attention on the dose distribution in the perturbed CT cases. In Figure 79 and Figure 80, are reported, respectively the dose behavior of the Undershoot case and the Overshoot one.

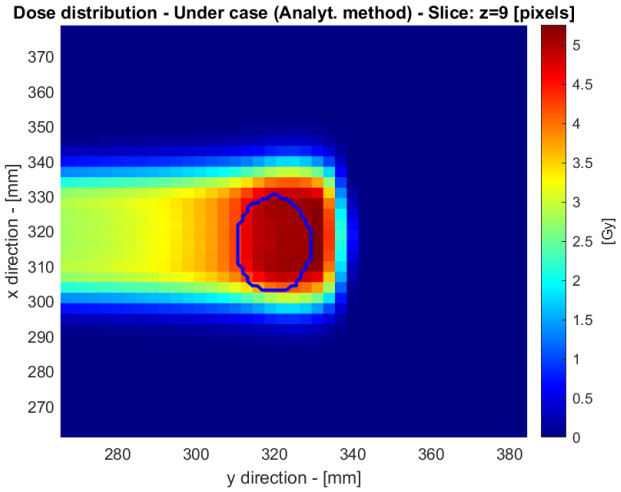

Figure 79: 2D plot dose behavior for the Undershoot case

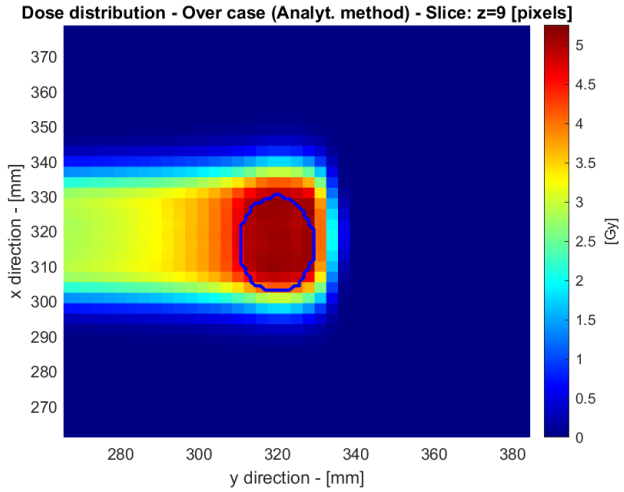

Figure 80: 2D plot dose behavior for the Overshoot case

Starting from the Undershoot plot, it is evident that the beam field is shifted beyond the PTV and this result is consistent with the physical uncertainty introduced. Considering, viceversa, the Overshoot plot, the dose field is shifted backward respect the PTV position. Also in this case, the result was predictable because the shift is caused by the density increase of the tissues crossed by the particle beam. An effective way to highlight the effect of the perturbation is plotting the punctual difference for each perturbed scenario.
In Figure 81, the difference between the Undershoot CT case and the nominal one is reported.

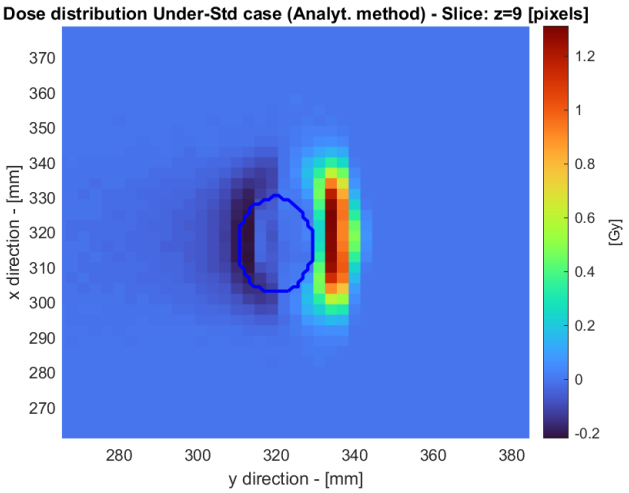

Figure 81: 2D plot dose difference between the Undershoot case field and the Standard one

From this plot, it is evident that there is an over irradiated area beyond the PTV. This aspect could be a problem: it is related to the irradiation of healthy tissues. It is important to monitor this effect spending particular attention to the presence of any OARs. Considering the PTV, there is a light under irradiation on the left side in the order of tenths of a Gray. As it is clear, this under irradiated area is caused by the forward shifted of the dose field.

In Figure 82, the difference between the Standard CT case and the Overshoot one is reported.

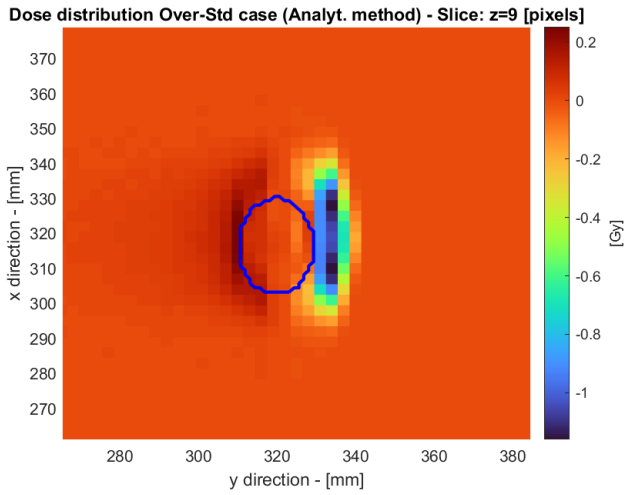

Figure 82: 2D plot dose difference between the Standard case field and the Overshoot one

The comments made for the previous plot are valid also in this case. In this case, the shift of the dose field is backward. This aspect causes an under irradiated zone beyond the target and a slight under irradiation in the PTV.
From a clinical point of view, it is possible to conclude that, the analytical forward method highlights an over irradiation on the PTV in the Undershoot scenario. This area receives a dose deposition that could cause some damages to healthy tissues. Excluding this over irradiation, the perturbation of the dose deposition behaviour in the PTV, for both perturbed cases, is very limited and in the order of tenths of a Gray.

6.3.5 Monte Carlo simulations

In this section, the same workflow analysis adopted for the forward analytical method results is followed for the Monte Carlo ones.
As a first key-point, it is important to remember that the quality of the Monte Carlo

model results is strictly related to the number of events on which the inference analysis is based.
For all the Monte Carlo simulations the number of events adopted is equal to $3 \cdot 10^6$.
In order to visualize the 3D behaviour of the dose profile in a Monte Carlo simulation, in Figure 83, the 3D dose profile of the Standard CT case is shown.

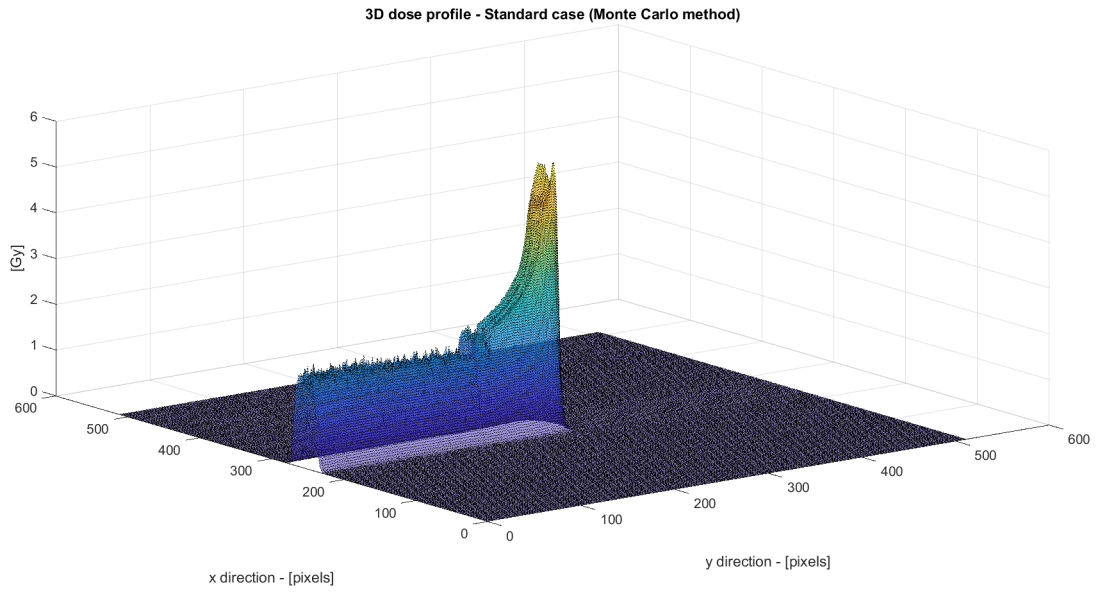

Figure 83: 3D dose distribution of the Monte Carlo method in the domain

Comparing the same result obtained with the analytical method, it is possible to qualitatively notice the different characteristics of the plot. In the Monte Carlo model results, the behaviour is quite irregular and jagged, this aspect respects the statistical and predictive nature of the Monte Carlo simulations. Also in this case, the SOBP in correspondence of the target is evident.
At this point, it is necessary to perform some sections of the 3D plot in order to highlight some interesting aspects. The first point to investigate is the position of the dose plot respect to the HUs profile.
In Figure 84, this comparison is shown considering the projection along the y direction.

The dose plot is related to the Standard CT case. It is possible to notice that the SOBP is located in correspondence of the step in the HU plot. This means that the plan is corrected set in order to deposit the relevant part of the dose in correspondence of the target. Another very important aspect to notice is how the variation of HU, in correspondence of the paranasal sinus, influences the physical transport of the particle beam.

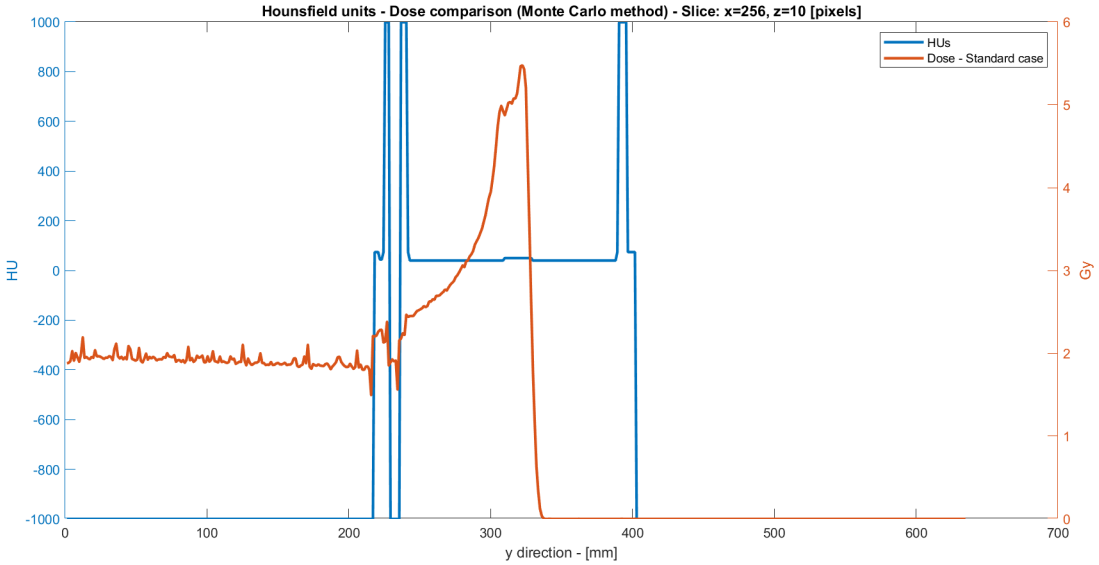

Figure 84: HUs profile and dose curve plot in nominal scenario (Monte Carlo)

In Figure 85 and Figure 86, it is possible to see, respectively, the y-projection dose behaviour and the x-projection one comparing the Standard CT case and the Undershoot one.

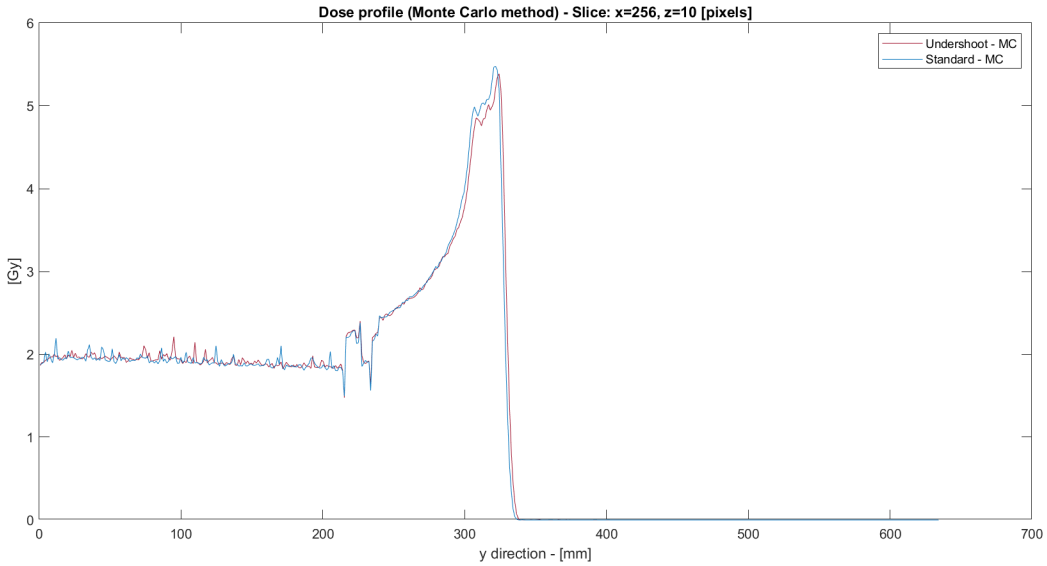

Figure 85: Undershoot and Standard case comparison of dose curve along y (Monte Carlo)

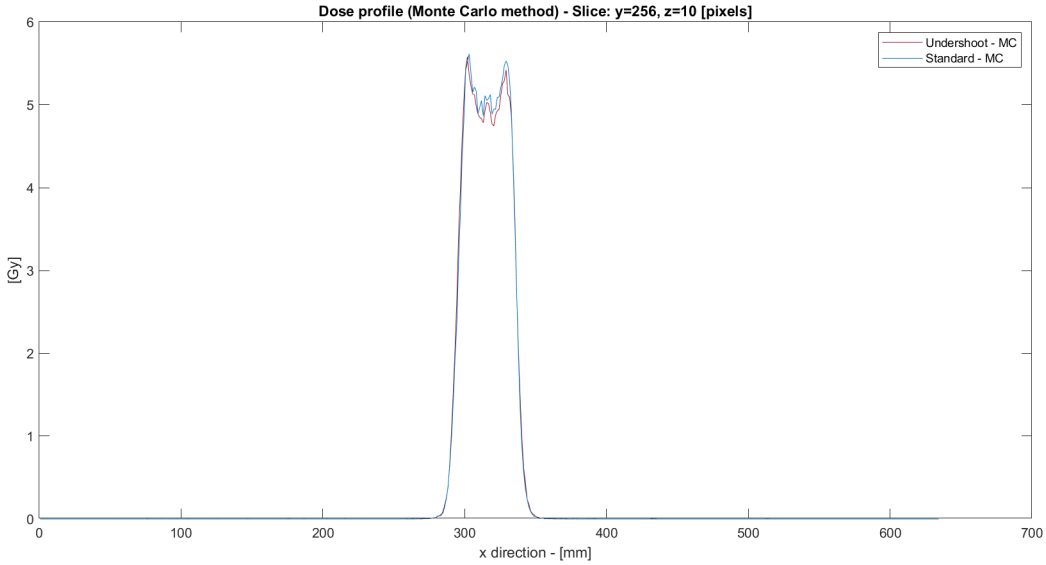

Figure 86: Undershoot and Standard case comparison of dose curve along x (Monte Carlo)

Qualitative comments, made for the analytical forward method, are valid also in this case. From a quantitative point of view, the peak of the Undershoot case is shifted of 1.8 [mm] and the maximum value of dose is lower than less that a tenth of a Gray. The comments for the x-projection plot are the same made for the analytical forward model results.

In Figure 87 and Figure 88, the y-projection of the dose profile and the x-projection one are shown, comparing the Standard CT case and the Overshoot case.
Results are consistent with the perturbation introduced. From a qualitative point of view, the comments made in the previous sections are also valid here. Quantitatively, the peak of the Overshoot plot is backward shifted of 1.9 [mm] and the maximum value of dose is lower than less than a tenth of a Gray.

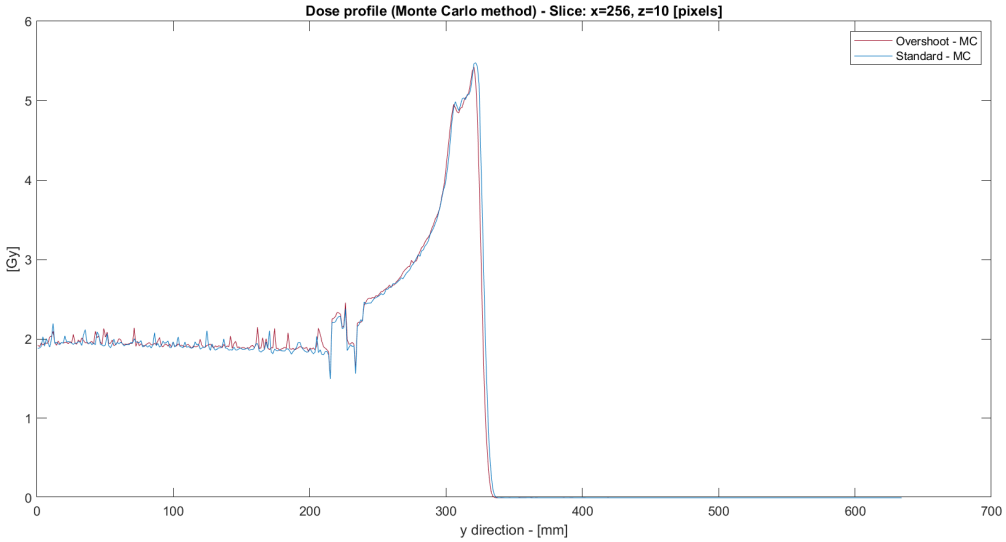

Figure 87: Overshoot and Standard case comparison of dose curve along y (Monte Carlo)

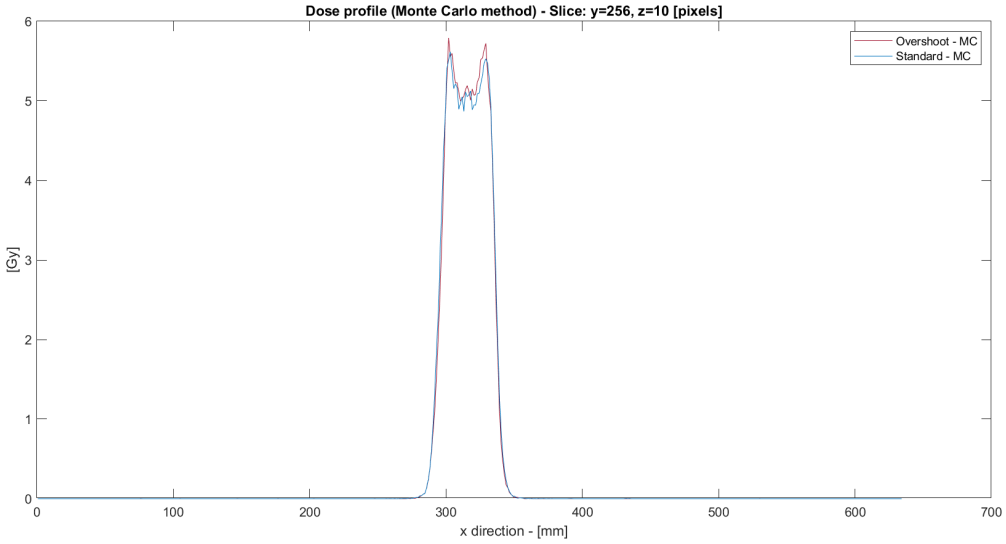

Figure 88: Overshoot and Standard case comparison of dose curve along x (Monte Carlo)

At this point, as for the forward analytical method results, it is useful to focus the attention on x-y dose behaviour in the slice taken as a reference in this work.
In Figure 89, the 2D dose distribution in the Standard scenario is shown.

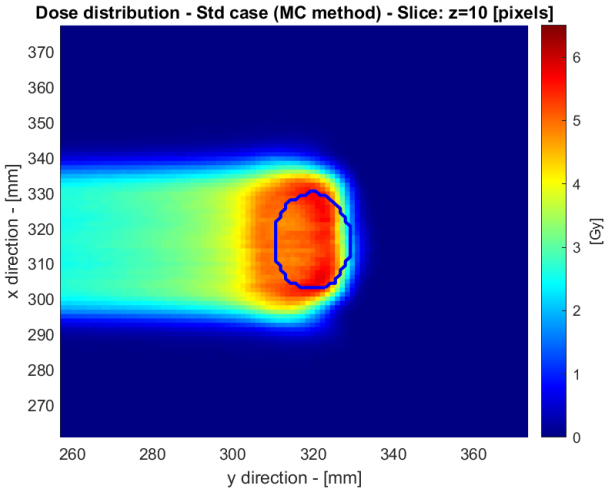

Figure 89: 2D plot Dose behavior for the Standard case (Monte Carlo)

This plot highlights that the PTV is not completely covered and it could be necessary to correct the characteristics of the beams obtained as the result of the inverse plan.

In Figure 90 and Figure 91, the 2D dose plots, respectively, of the Undershoot case and the Overshoot one are shown.

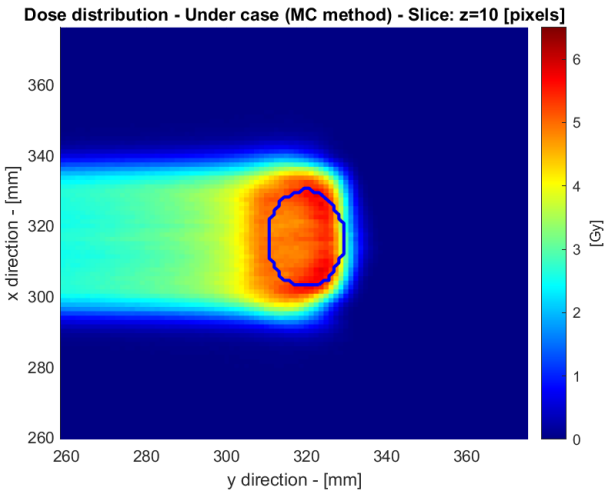

Figure 90: 2D plot dose behavior for the Undershoot case (Monte Carlo)

In the Undershoot case distribution plot, the dose deposition profile is shifted forward and this translation corrects the bad coverage noticed in the nominal scenario plot. Considering, instead, the Overshoot case distribution plot, the dose profile is shifted backward respect to the PTV and this aspect accentuates the uncoverage of the PTV.

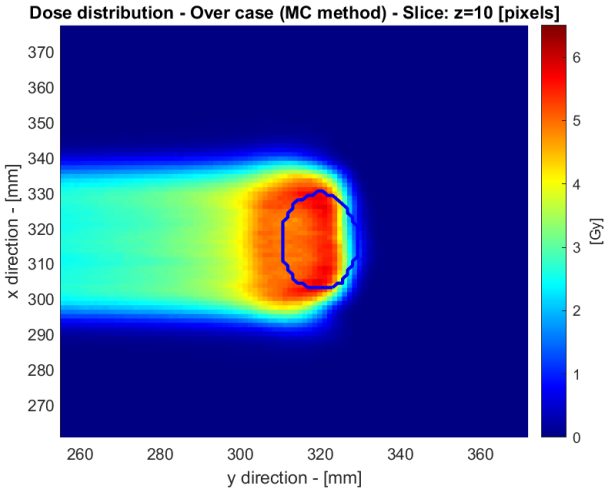

Figure 91: 2D plot dose behavior for the Overshoot case (Monte Carlo)

In order to perform a more quantitative analysis of the perturbation introduction effect, as made for the forward analytical method, it is useful to perform the punctual difference of the previous plots. In Figure 92, the difference between the Undershoot case 2D dose plot and the Standard case one is shown.

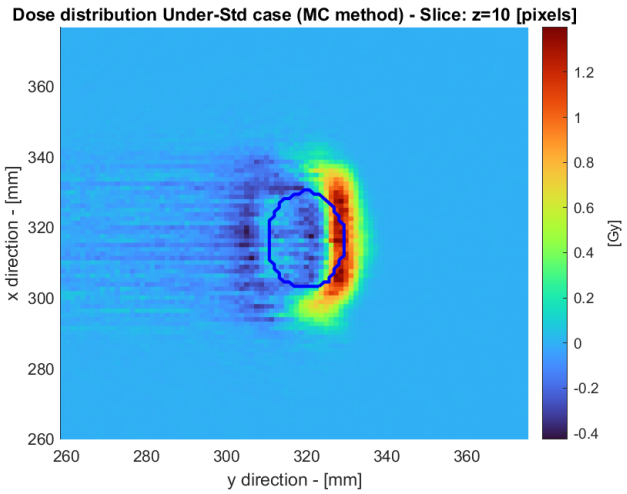

Figure 92: 2D plot dose difference between the Undershoot case field and the Standard one (Monte Carlo)

This plot shows that the part of the PTV that is not well covered in the Standard scenario is partly compensated, in the Undershoot one, by the forward shift. An important point to underline is the presence, out of the PTV, of an over irradiated area. Also in this case, this aspect could be a clinical problem because it could be related to a dose delivery on healthy tissues.

In Figure 93, the difference between the Standard case 2D dose plot and the Overshoot case one is shown.

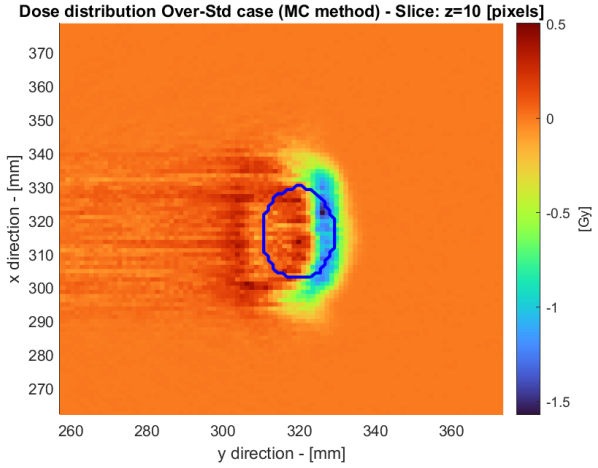

Figure 93: 2D plot dose difference between the Standard case field and the Overshoot one (Monte Carlo)

From this plot, it is possible to notice that the under irradiated part of the PTV, present in the Standard scenario, is extended. This effect is related to the backward shift of the dose distribution plot. The under irradiated part is also present out of the PTV, but this aspect is not relevant for clinical purposes.
It is possible to conclude that the Monte Carlo model highlights that, also without any perturbation in the CT characteristics, the inverse plan causes a not completely correct coverage of the PTV.

6.3.6 Analytical and Monte Carlo comparison

One of the targets of this work is to compare the sensitivity respect uncertainties of the two forward approaches. It is necessary to remember that the two methods are based on completely different mathematical approach. In this analysis, both methods receive, as an input, the beam file obtained from the inverse plan and the CT of each perturbed case.
The analytical model is an optimized correction-based algorithm developed with Pencil Beams method. The dose distribution is calculated thanks to dose kernels that are estimated starting from the absorbed dose of a homogeneous medium, such as water. The approach is the same followed in the inverse planning, but in the opposite direction. This method is very fast, but it gives an ideal behaviour of the results because is based on kernels calculated in a homogeneous medium. The inhomogeneity correction is only performed in the longitudinal direction. The correction does not consider lateral scatter. This aspect causes errors in dose distribution calculation in heterogeneous domains. The one-dimensional density correction is the

main reason for its speed.
The Monte Carlo simulation is considered the most accurate method for estimating dose distribution during a treatment plan. It models the real physics phenomenon of transport by simulating the interaction of a large number of particles in the computational domain. Obviously, the result of a Monte Carlo model is realistic and predictive of the actual dose behaviour, but its quality is strictly related to the correctness of the statistical information of the physical phenomenon.
It is necessary to remember that the two models have different computational domain resolution. The mesh of the Monte Carlo model is finer than the analytical one.
In all the curves considered in the comparison, the analytical method presents results that are always smoother and more regular than those of Monte Carlo model. This aspect is closely linked to the nature of the two calculation methods. The analytical method works only with longitudinal discontinuities by converting the domain in terms of Water Equivalent Path Length (WEPL). The Monte Carlo method, on the other hand, simulates real transport phenomenon of particles in matter. It is possible to say that the statistical method results are more realistic while those of the analytical model are idealized and less accurate.
The comparison between the results of the analytical simulation and the Monte Carlo one is performed respecting the order in which the results are presented.

The first plot to consider is the one relating to the comparison between the dose curve along y and the HUs profile (Figure 73 and Figure 84). The preliminary aspect to underline is the maximum value of the dose plots. The maximum value of the analytical model dose profile is equal to 5.1 [Gy] while the Monte Carlo one is equal to 5.5 [Gy]. The Monte Carlo algorithm result shows an over-irradiation, with respect to the prescribed dose (5 [Gy]), greater than that calculated by the analytical method.
The second aspect to note is that, in correspondence of the paranasal sinuses, the analytical model is almost unaffected by density discontinuities. The Monte Carlo model, on the other hand, in that point, shows a great sensitivity to the variation of density of the material. This confirms, that the statistical approach models the physics of the problem more accurately than the analytical one. Both dose profile plots refer to the Standard CT case.
The comments on the translation of the peaks and their maximum value for the results of both models have already been performed in sections 6.3.4 and 6.3.5 of this work.

As regards the 2D distribution of the dose in the slice of reference, it is not possible to make a punctual comparison between the results of the two approaches due to the different resolution of the calculation domain. For this reason, it is necessary to make the comparison respect the dose value prescribed by the treatment. For this type of plots, it is useful to focus the attention only on the area delimited by the PTV profile.

Starting from the Undershoot case, in Figure 94 and Figure 95, the punctual differ-

ences of the dose distribution of the two methods and the prescribed dose value are shown.

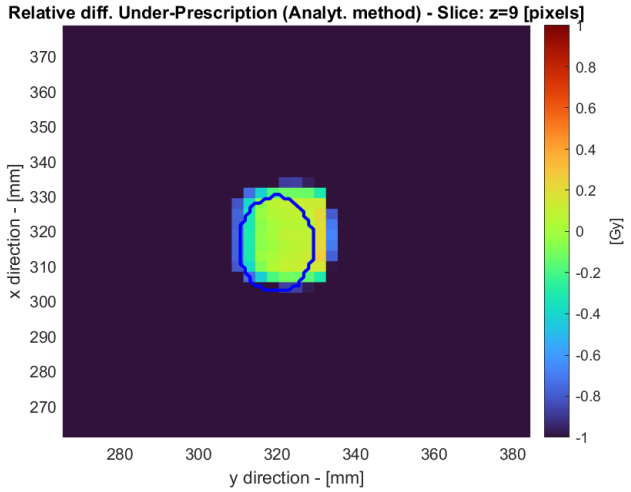

Figure 94: 2D plot dose difference between the Undershoot case field and the prescribed dose (Analytical)

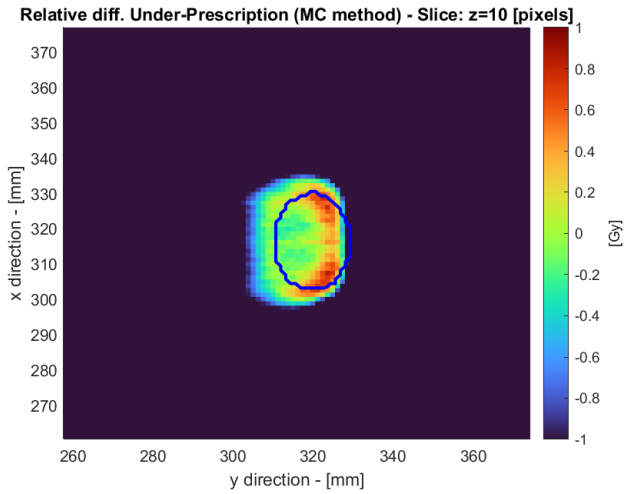

Figure 95: 2D plot dose difference between the Undershoot case field and the prescribed dose (Monte Carlo)

As mentioned earlier, the two direct methods estimate the magnitude of dose field shift due to perturbations differently. For example, the Monte Carlo model presents incomplete coverage of the PTV, already in the unperturbed scenario, that the analytical method does not show.
In this section, the target is not to focus on the PTV coverage, but mainly on the dose values in the PTV.

Starting from the Undershoot scenario, it is evident from Figure 94 that, within the PTV, there are no critical points of over-irradiation. In the lower left part, there is a limited area of under-irradiation, but mainly due to the translation described above.
On the other hand, considering Figure 95, the Monte Carlo model results show a large area, in the right part of the PTV, where the deposited dose is one Gray higher than the prescribed dose. This aspect, which is not predicted by the analytical method, could represent a critical aspect from the clinical point of view.
In Figure 96 and Figure 97, the same plots presented previously for the Undershoot case are shown for the Overshoot one.

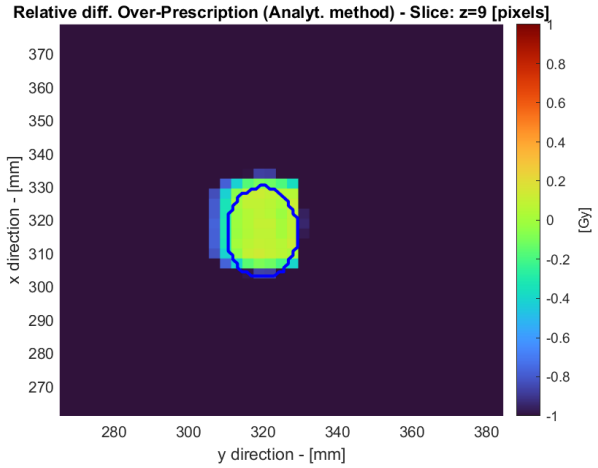

Figure 96: 2D plot dose difference between the Overshoot case field and the prescribed dose (Analytical)

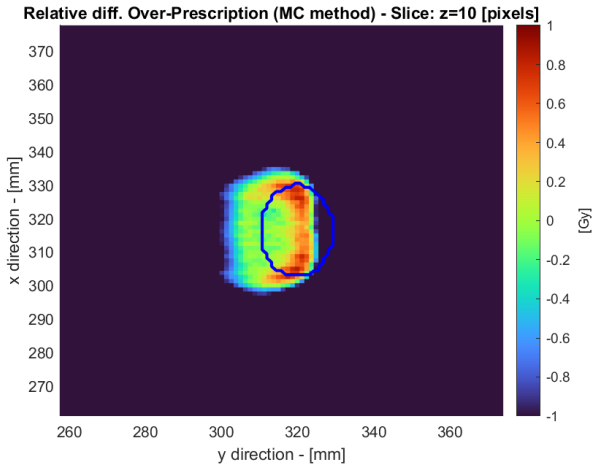

Figure 97: 2D plot dose difference between the Overshoot case field and the prescribed dose (Monte Carlo)

In this case, it results evident how the analytical model underestimates the extension of the under-irradiated area of the PTV due to the backward shift.
Considering, as for the previous plot, the dose values, also in this case, the Monte Carlo model results highlight an area in which the dose value is one Gray higher than the prescribed dose. The analytical simulation does not present this area.
The presence of this area of over-radiation, in Monte Carlo simulations, appears to be independent of the introduced perturbation. In both perturbed cases, it is present a zone, in the right side of the PTV, where the dose values are greater than the prescribed dose by about one unit. To test this hypothesis, the point difference with the value of 5 [Gy] can also be performed for the Monte Carlo simulation with the Standard CT. The result is shown in Figure 98.

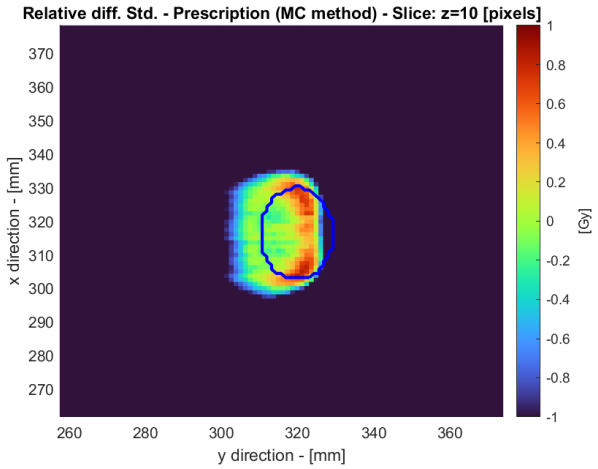

Figure 98: 2D plot dose difference between the Standard case field and the prescribed dose (Monte Carlo)

This plot confirms that the presence of the area in which there is an over-irradiation of 1 [Gy] is independent of the perturbations introduced. This means that the Monte Carlo simulation highlights an over-irradiation of about 20 percent compared with the prescription.

6.3.7 DVHs analysis

In section 6.2.2 of this work, an output data of the TPS is described, DVHs. The Dose Value Histograms are widely used in clinical evaluation because they provide integrated and quickly assessable information on dose release in the PTV and in the various Organs At Risk (OAR). In this analysis, PTV and brain DVHs are considered.

In Figure 99, the comparison between the PTV DVH evaluated with the inverse analytical method and the one evaluated with the Monte Carlo simulation is shown. Both curves are relative to the Standard CT case.

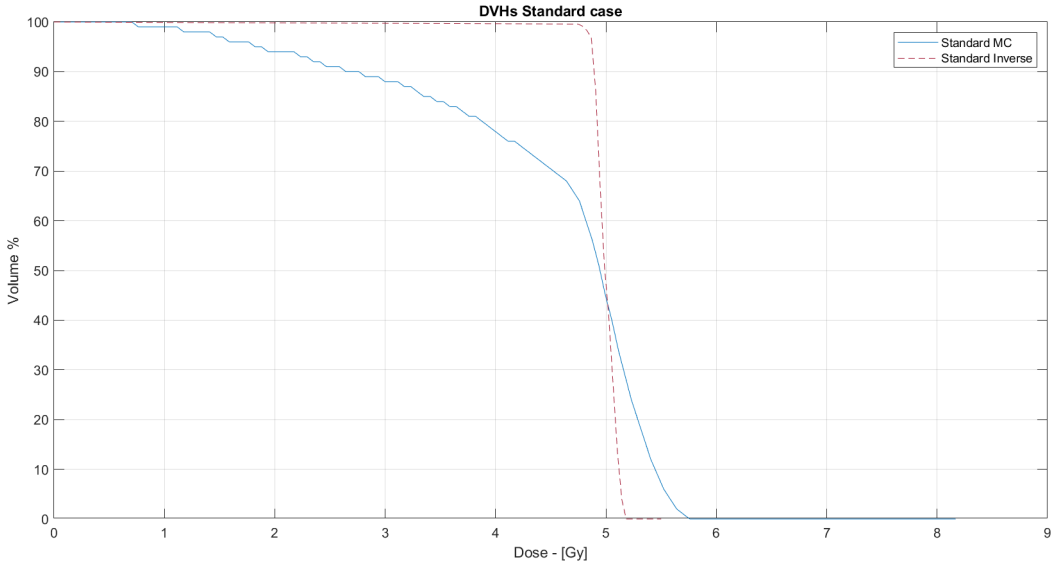

Figure 99: PTV DVHs comparison of Monte Carlo model and Analytical method (Standard scenario)

This plot shows that the analytical method presents an ideal behaviour for a PTV, because almost the 100 % of the PTV receives the prescribed dose of 5 [Gy]. Monte Carlo plot, instead, presents a behaviour consistent with 2D dose distribution plot obtained.
In Figure 89 in section 6.3.5, the dose distribution plot shows an under irradiated part of the PTV.

Introducing perturbations in the CT, also DVHs behaviour is influenced.
In Figure 100, the DVHs of the Monte Carlo simulations for the three CT scenarios are shown. Also in this case, the contour considered is the PTV.
From this plot, it is clear that, as was predictable, the Overshoot perturbation increases the under irradiation of the PTV and the Undershoot one reduces it. These results are consistent with the 2D dose plot in section 6.3.5 and they are consistent with the physical perturbations introduced.
Focusing the attention on the brain DVH, it is possible to evaluate the effects of the plan on a healthy tissue.
In Figure 101, the comparison between the Standard case results of the Monte Carlo and the Inverse method is shown.

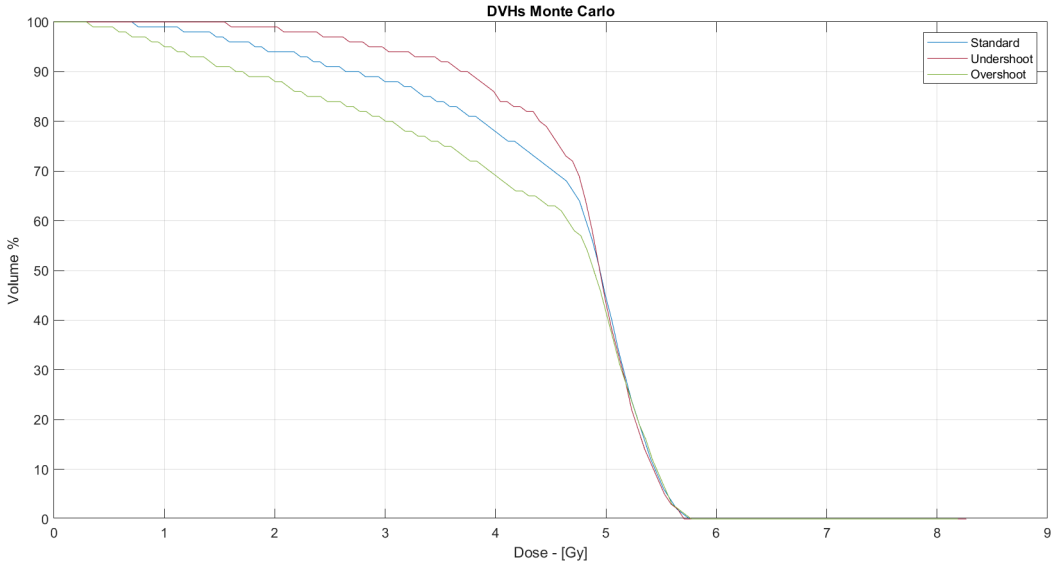

Figure 100: PTV DVHs comparison of Monte Carlo model for the three CT scenarios

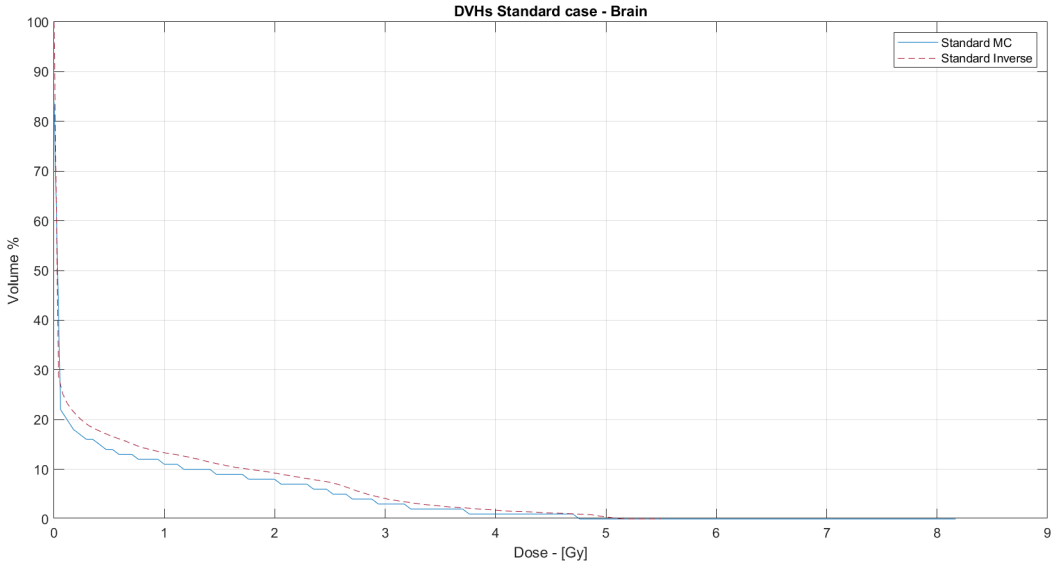

Figure 101: Brain DVHs comparison of Monte Carlo model and Inverse method (Standard scenario)

The Monte Carlo model results and the analytical ones are very similar, but the Monte Carlo plot is slightly lower that the analytical one.
Considering the perturbed cases simulated with Monte Carlo simulations, from Figure 102, it is clear that there are no variations regarding the DVH of the brain.

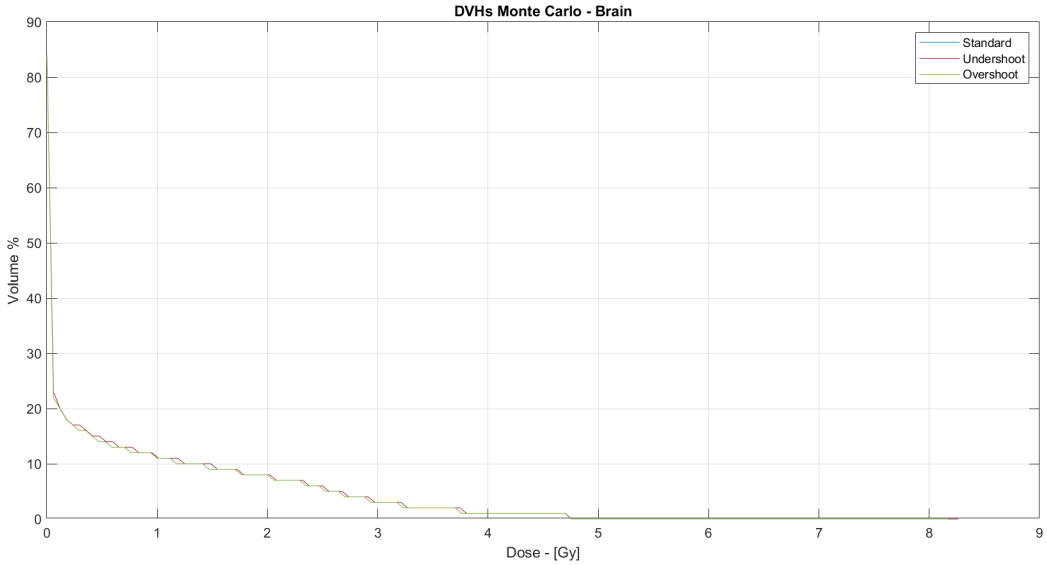

Figure 102: Brain DVHs comparison of Monte Carlo model for the three CT scenarios

6.3.8 PTV coverage

In this section, the purpose is to perform a quantitative analysis of the correct coverage of the PTV in each simulation case. The simulations considered are those performed with direct methods: unperturbed CT, Undershoot one and Overshoot one.
The main target is to confirm or not the qualitative coverage of the PTV evaluated in the 2D plots. The estimation of the PTV coverage is performed writing a Matlab script.
For each case, the slice of reference is selected from the dose 3D matrix. In this way, it is possible to focus the attention on the 2D dose distribution. The script constructs a geometrical shape from the contour of the PTV and, screening each pixel of the slice selected, it checks, with the function 'inShape', whether the pixel is within the PTV or not. Once the point is verified to be within the PTV, the next check is made to see if the dose value, in that pixel, is greater than or equal to the 80 percent of the prescribed dose value (4 [Gy]). In this way, the percentage of pixels sufficiently irradiated can be calculated.
It is necessary to underline that, in this case, the values, greater than the prescribed one, are not of interest. This analysis is performed, for the cases listed above, for both direct simulation methods. Obviously, the estimation performed for Monte Carlo models is more accurate than the one calculated with the analytical simulations. This aspect is due to the different resolution of the domains.
Results of these analysis are presented in Table 5.

Simulation case	Percentage of PTV coverage
Standard Analytical method	93.5%
Undershoot Analytical method	82.6%
Overshoot Analytical method	93.5%
Standard Monte Carlo method	92.6%
Undershoot Monte Carlo method	96.3%
Overshoot Monte Carlo method	88.6%

Table 5: Percentage of PTV coverage for simulation cases

Values reported in the previous table must be compared with the qualitative behaviour shown in sections 6.3.4 and 6.3.5 of this work. Values computed confirm the coverage of the PTV qualitatively evaluated form the 2D dose plots.
For convenience, a set of images of the relevant 2D plots is given below.

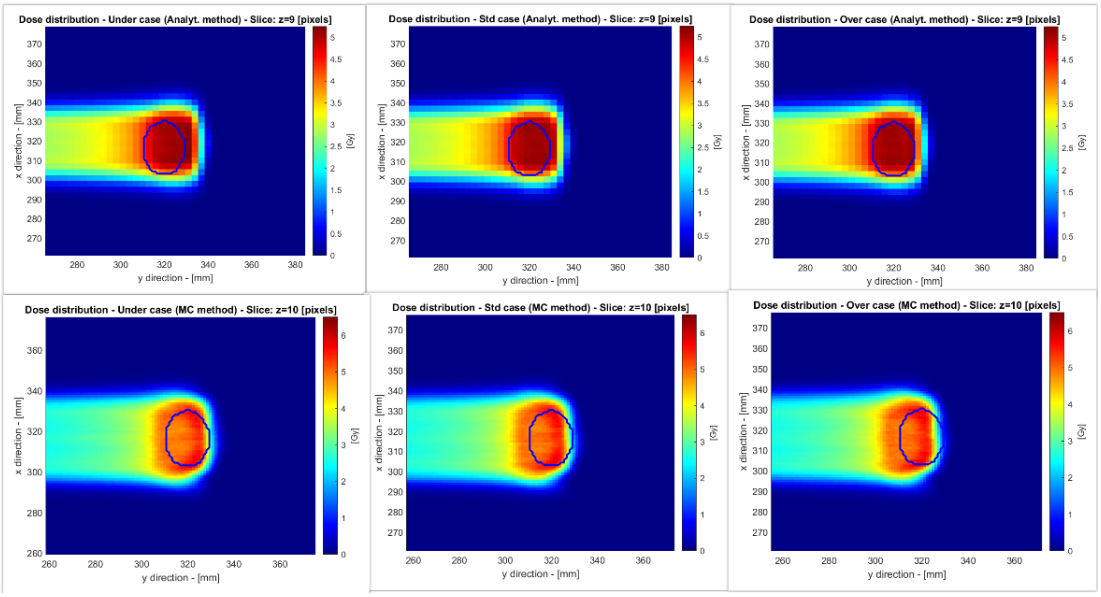

Figure 103: 2D dose plots resume

7 Importance of replanning

The prescribed dose distribution is estimated by medical staff. After the contouring phase of the CT, the specialist evaluates the correct value of dose to deposit in the PTV. Usually, the plan prescription is also composed of a maximum or minimum volumetric percentage of each affected organ relative to a dose value that must be received. Maximum volume percentage limits are imposed for OARs. For example, less than 30% of the volume of the Organ At Risk must receive a certain dose value. However, minimum volume percentage limits are defined for PTV. For example, during a treatment, at least 95% of the PTV volume should receive the prescribed dose value.

These limits are set to obtain, in the same treatment plan, the two most important goals of a Radiotherapy treatment: deposit the right dose in the tumor mass, limiting the irradiation of healthy tissues as much as possible. The balance between these two objectives is a very complex evaluation to calculate. The balance between costs and benefits of treatment is a specific aspect for each patient and for each different condition that only specialized medical personnel can evaluate.
It is important to notice that the volumetric constraints are expressed following the graphical structure of the DVHs. Obviously, limits are expressed consistently to DVHs in order to simplify the control of the correctness of a treatment plan. If the DVH, produced by an inverse plan or by a forward method used as a double check, does not satisfy the constraints imposed by the treatment prescription, replanning is necessary.

Causes of replanning:

- misalignment of the target
- significant changes in tumor volume
- underestimation of physiological movement, for example breathing movement
- bad acquisition during the imaging phase
- surgeries during the period of treatment sessions

In order to correct and take into account this type of perturbation of the patient condition, it is necessary to repeat the Computed Tomography. There are different studies that demonstrate the benefits of replanning during the treatment sessions.

For example, in Table 6, Quality of Life (QoL) indexes estimated from the patients experience are shown. These results are presented in the paper by Haihua Yang et al. [20]

Parameter	6 mo after therapy	12 mo after therapy
Global QoL (Non-Replanning)	63.95 ± 6.23	77.91 ± 12.45
Global QoL (Replanning)	73.35 ± 16.76	81.59 ± 19.64
Phys. funct. (Non-Replanning)	96.74 ± 7.47	97.83 ± 4.98
Phys. funct. (Replanning)	98.29 ± 4.36	99.07 ± 3.26

Table 6: Quality of Life for patients Replanning/Non-Replanning treatments[20]

These values are based on the replanning effect analysis on patients with Nasopharyngeal carcinoma.

Another very interesting result is that presented in the study by X. Zhou et al. [100]. Among various findings presented in this study, the behaviour of the Local-regional Recurrence Free Survival (LRFS) percentage is very explicative. This quantity is used to monitor the long term effects of Radiotherapy, in particular the recurrence of the disease from micrometastasis, for example.
In Figure 104, the comparison between the replanning based treatments and without replanning ones is shown. This study is performed for IMRT.

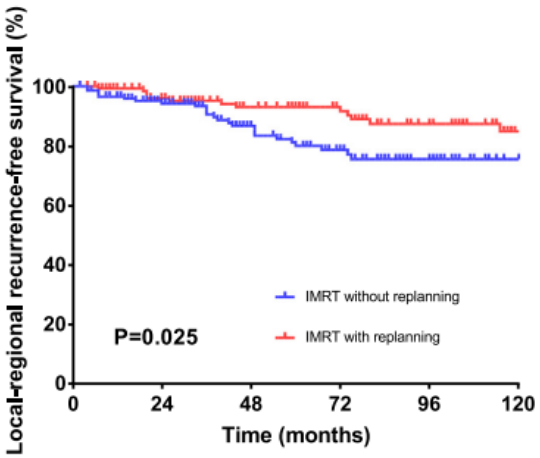

Figure 104: LRFS plots comparison between replanning and non-replanning treatments [100]

The plot shows that the replanning has beneficial effects on decreasing the onset of new long-term diseases. This improvement is related to a better irradiation of the target and a reduction of the energy release in healthy tissues.

8 Conclusions

Proton Therapy represents an expanding cancer treatment strategy. The advantages, compared to the conventional external radiotherapy, are considerable. For example, the amount of energy deposited in healthy tissues is very low and the irradiation is really precise. Currently, Proton Therapy is the most promising external treatment method with ionizing radiation. The development of this therapy strategy requires very advanced Treatment Planning Systems. Proton Therapy is sensitive to the physical and biological uncertainties that may occur in the patient. For this reason, it is necessary to have planning and control systems that are suitable to perform the simulation of the real treatment and that are robust respect to the perturbations that may occur in the patient.
The Inverse Planning method is the most efficient approach to obtain the characteristics of the particle beam necessary to irradiate the target in the correct manner. Introducing uncertainties on the density values, it became evident how, in order to obtain the desired dose distribution in each perturbed scenario, the inverse model sets the characteristics of the beams. The comparison of the Energy Ranges confirms the correctness of the introduction of perturbations. The scenario, in which the density of the tissues is increased, requests higher energies than in the Standard case. The scenario, in which the density of the tissues is decreased, requests lower energies than in the Standard case.
Analytical methods, generally speaking, are very fast and light as computational effort. For this reason, they are easily implemented in the clinical workflow, both as a forward approach and as an inverse one. It is important, however, to remember that analytical methods do not simulate the real physics of the problem and give an idealized and inaccurate solution of the dose distribution in the tissues of the patient. This limitation of the analytical methods is accentuated, for example, in cases where the particle beam passes through sections which present inhomogeneities. Considering the dose profiles along y, obtained by the two different forward methods, the behaviour of the two plots, in correspondence of the paranasal sinuses, is a confirmation. The dose profile of the analytical method was slightly affected by the density discontinuity, whereas the Monte Carlo model showed a markedly discontinuous trend at that point. The analytical model is almost insensitive to these large material variations. This is one of the reasons why an advanced and physically consistent tool to accurately simulate 3D dose distribution within the patient is necessary.
The Monte Carlo method is a valid alternative to the forward analytical method. It adopts a statistical approach that extrapolates the macroscopic results from a large number of experiments that are performed, at the microscopic level, by simulating the transport of each individual particle. This characteristic ensures that the real physics of the problem is modeled and that the quality of the results is strictly related to the number of events generated and the correct definition of the physical problem. The statistical approach presents, as its main limitation, the great compu-

tational effort it requires. For this reason, the implementation of the Monte Carlo models on GPU represents a very interesting field of development for both graphic unit manufacturers and researchers.
In this work, it is possible to conclude that the check, performed with the forward methods, represents a fundamental passage in the planning of a Proton Therapy treatment.
The analytical method shows a beam translation, due to the introduction of the perturbation in the CT, which consequently causes a translation of the dose distribution profile on the PTV. The translations are consistent with the physical uncertainties introduced. In the Overshoot case, the translation is backward, while, in the Undershoot case, the translation is forward. As regards the dose values within the PTV, the variation from the prescribed value is limited and in the order of tenths of a Gray.
Considering, instead, the results of the Monte Carlo simulations, it is possible to note that the translation of the dose profile is much more marked than that foreseen by the analytical method. The analytical method underestimates the translations due to the introduction of perturbations. In addition, it is interesting to note that, even in the unperturbed scenario, the Monte Carlo simulation shows, within the PTV, an area where the dose values exceed by 20% the dose prescribed by the treatment. Moreover, it highlights how the treatment plan, inversely obtained, does not irradiate the PTV perfectly. As mentioned above, these phenomena are independent of the introduction of uncertainties. This result is very interesting because it emphasizes that, even in the absence of perturbations, the Monte Carlo method represents a very useful tool to verify that the prescribed dose, used as input of the inverse planning, is actually obtained.
Considering PTV coverage, the Monte Carlo simulation highlights a lower percentage of irradiated area, in the Standard scenario, respect to the Analytical one. This result confirms that it is necessary to check the treatment plan with a physically consistent model, even without the introduction of uncertainties. As a further example, the Monte Carlo simulation shows how the forward shift, that it is present in the Undershoot case, partially compensates for the imperfect PTV coverage of the Standard case.
This work can be expanded in several directions. For example, it is possible to compare the two direct methods by improving the domain resolution of the analytical method to the same detail as the Monte Carlo model. In this way, it is possible to make a more accurate and punctual comparison for each voxel. The qualitative comparison, carried out in this work, could give more quantitative information regarding the over-irradiated zones.
The perturbation, introduced in the CT, is not realistic, but it is sufficient to preliminary investigate the answer of the planning systems. A possible further improvement, it is the introduction of a more realistic uncertainty. A possibility is the variation of the dimension and the position of the tumor mass. For example, a really interesting aspect to investigate is the effect of the pulmonary respiration in the treatment planning of a lung cancer.

References

[1] Neda Ranjbarnovin Zahra Khazaeipour Ali Arab Kheradmand. Postmastectomy locoregional recurrence and recurrence-free survival in breast cancer patients. *World Journal of Surgical Oncology*, 8:30, 2010.

[2] Joseph Y.Ting XiaodongWu Jeffrey A.Fiedler ChingchongYang Marcia L.Watzich ArnoldMarkoe. Dose-volume histograms for bladder and rectum. *International Journal of Radiation Oncology*, 38:1105–1111, 1997.

[3] N. Bodgi, L. & Foray. The nucleo-shuttling of the atm protein as a basis for a novel theory of radiation response: resolution of the linear-quadratic model. *International Journal of Radiation Biology*, 92:3, 2016.

[4] N. Bodgi L. Canet A. Pujo-Menjouet L. Lesne A. Victor J.-M. & Foray. Mathematical models of radiation action on living cells: From the target theory to the modern approaches. a historical and critical review. *Journal of Theoretical Biology*, 394:93, 2016.

[5] Michael J. Aminoff François Boller and Dick F. Swaab. *Handbook of Clinical Neurology*. Elsevier, 2003.

[6] Luther W. Brady and Theodore E. Yaeger. *Encyclopedia of Radiation Oncology*. Springer, 2013.

[7] D. J. Brenner. *The linear-quadratic model is an appropriate methodology for determining isoeffective doses at large doses per fraction*. Elsevier, 2008.

[8] https://en.wikipedia.org/w/index.php?curid=32800049 CC BY 3.0.

[9] Fortuna De Martino Stefania Clemente Christian Graeff Giuseppe Palma Laura Cella. Dose calculation algorithms for external radiation therapy: An overview for practitioners. *Applied sciences*, 11:6806, 2021.

[10] K.H. Leenhouts H.P. Chadwick. A molecular theory of cell survival. *Phys. Med. Biol.*, 13:78, 1973.

[11] Geant4 collaboration. *Book for application developers - Release 11.0*. CERN, 2021.

[12] Geant4 collaboration. *Introduction to Geant4 - Release 11.0*. CERN, 2021.

[13] Prof. Gianni Coppa. *Notes from lectures of the course Biomedical and industrial applications of radiation*. Politecnico di Torino, 2022.

[14] Bert J Perez-Ponce H El Bitar Z Jan S Boursier Y Vintache D Bonissent A Morel C Brasse D Visvikis D. Geant4-based monte carlo simulations on gpu for medical applications. *Physics in Medicine & Biology*, 58:16, 2013.

[15] Bruce A. Faddegon Jungwook Shin Carlos M. Castenada José Ramos-Méndez Inder K. Daftari. Experimental depth dose curves of a 67.5 mev proton beam for benchmarking and validation of monte carlo simulation. *Med. Phys.*, 42:7, 2015.

[16] Maarten Lambrecht Daniëlle B P Eekers Claire Alapetite Neil G Burnet Valentin Calugaru Ida E M Coremans Piero Fossati Morten Høyer Johannes A Langendijk Alejandra Méndez Romero Frank Paulsen Ana Perpar Laurette Renard Dirk de Ruysscher Beate Timmermann Pavel Vitek Damien C Weber Hiske L van der Weide Gillian A Whitfield Ruud Wiggenraad Erik Roelofs Petra Witt Nyström Esther G C Troost. Radiation dose constraints for organs at risk in neuro-oncology; the european particle therapy network consensus. *Radiother Oncol*, 128:26–36, 2018.

[17] S. Ballivet de Régloix O. Maurin A. Crambert S. Kourouma P. Clément Y. Pons. Chirurgia del seno frontale (tumori e traumi esclusi). *EMC Tecniche Chirurgiche - Chirurgia ORL e cervico facciale*, 24:1–15, 2020.

[18] Iwan Cornelius Susanna Guatelli Pauline Fournier Jeffrey C. Crosbie Manuel Sanchez del Rio Elke Brauer-Krisch Anatoly Rosenfelda Michael Lercha. Benchmarking and validation of a geant4–shadow monte carlo simulation for dose calculations in microbeam radiation therapy. *Journal of Synchrotron Radiation*, 21:518–528, 2014.

[19] MDCurtiland Deville. *Prostate Cancer (Second Edition)*. Elsevier, 2016.

[20] Haihua Yang Wei Hu Wei Wang Peifang Chen Weijun Ding and Wei Luo. Replanning during intensity modulated radiation therapy improved quality of life in patients with nasopharyngeal carcinoma. *Int J Radiation Oncol Biol Phys*, 85:47–54, 2013.

[21] Marcos d'Ávila Nunes. *Hadron Therapy Physics and Simulations*. Springer, 2013.

[22] Nadja Ebert and Michael Baumann. *Radiation Oncology*. Elsevier, 2019.

[23] IAEA Eduardo Rosenblatt. Defining target volumes and organs at risk: a common language. *Division of Human Health IAEA*.

[24] Stefan Andersson-Engels Erik Alerstam, Tomas Svensson. Parallel computing with graphics processing units for high-speed monte carlo simulation of photon migration. *Journal of Biomedical Optics*, 13:6, 2008.

[25] Xun Jia Xuejun Gu Yan Jiang Graves Michael Folkerts and Steve B.Jiang. Gpu-based fast monte carlo simulation for radiotherapy dose calculation. *Center for Advanced Radiotherapy Technologies and Department of Radiation Oncology, University of California San Diego*.

[26] Harald Paganetti Drosoula Giantsoudi. Relative biological effectiveness uncertainties and implications for beam arrangements and dose constraints in proton therapy. *Semin Radiat Oncol.*, 28(3):256–263, 2018.

[27] Burcu Altıparmak Güleç and Fatma Yurt. Treatment with radiopharmaceuticals and radionuclides in breast cancer: Current options. *Eur J Breast Health*, 17:3, 2021.

[28] Olivier Haas. *Radiotherapy Treatment Planning*. Springer, 1999.

[29] Youngyih Han. Current status of proton therapy techniques for lung cancer. *Radiation Oncology Journal*, 37:4, 2019.

[30] https://blogs.nvidia.com/blog.

[31] https://cancer.stonybrookmedicine.edu/RadiationTherapyProcess.

[32] https://chem.libretexts.org/Bookshelves.

[33] https://dceg.cancer.gov/.

[34] https://developer.nvidia.com/cuda toolkit.

[35] https://education.jlab.org/glossary/electroncapture.html.

[36] https://fondazionecnao.it/en/hadrontherapy.

[37] https://fr.wikipedia.org/wiki/Synchrotron/.

[38] https://geant4.web.cern.ch.

[39] https://physiosunit.com/axis-and-planes-of-human body/.

[40] https://www.bupa.co.uk/health-information/your appointment/ctscan.

[41] https://www.cancerresearchuk.org/.

[42] https://www.chegg.com/.

[43] https://www.cyberphysics.co.uk/topics/medical/CTScanner.htm.

[44] https://www.cyberphysics.co.uk/topics/radioact/Radiodecay.htm.

[45] https://www.embibe.com/exams/cyclotron/.

[46] https://www.i seecomputing.com/.

[47] https://www.intel.it/content/.

[48] https://www.ncbi.nlm.nih.gov/.

[49] https://www.nuclear-power.com/nuclear power.

[50] https://www.nupecc.org/.

[51] https://www.radiation dosimetry.org/.

[52] https://www.safework.nsw.gov.au/.

[53] https://www.tutorialspoint.com/cuda.

[54] https://www.w3schools.blog/cyclotron.

[55] http://team3rocksz.blogspot.com/.

[56] http://www.fmboschetto.it/tde4/acceleratori.html.

[57] http://www.samsunghospital.com/home/proton.

[58] Piero Fossati Ana Perpar Markus Stock Petra Georg Antonio Carlino Joanna Gora Giovanna Martino Eugen B. Hug. Carbon ion dose constraints in the head and neck and skull base: Review of medaustron institutional protocols. *Int J Part Ther.*, 8(1):25–35, 2021.

[59] IAEA. *Interaction of radiation with matter*. IAEA, 2015.

[60] ICRP. *1990 Recommendations of the International Commission on Radiological Protection*. ICRP Publication 60, 1991.

[61] ICRU. The international commission on radiation units and measurements, report 83. *Journal of the ICRU, Oxford Press*, 10:1, 2010.

[62] L Opalka Carlos Granja B Hartmann Jan Jakubek. 3d measurement of the radiation distribution in a water phantom in a hadron therapy beam. *Journal of Instrumentation*, 07:01, 2012.

[63] Adam M. Johansen and Ludger Evers. *Monte Carlo Methods, lecture notes*. University of Bristol, Department of Mathematics, 2007.

[64] Malvin H. Kalos and Paula A. Whitlock. *Monte Carlo Methods*. Wiley - VCH, 2008.

[65] Soichi Sugiyama Kuniaki Katsui Yuki Tominaga Takahiro Waki Norihisa Katayama Hidenobu Matsuzaki Shin Kariya Masahiro Kuroda Kazunori Nishizaki Susumu Kanazawa. Dose distribution of intensity-modulated proton therapy with and without a multi-leaf collimator for the treatment of maxillary sinus cancer: a comparative effectiveness study. *Radiation Oncology*, 14:209, 2019.

[66] Tom Kennedy. *Monte Carlo Methods*. Spring, 2016.

[67] Sung Jin Kim Dong Ho Kim Sung Kyu Kim. Comparison of pencil beam, collapsed cone and montecarlo algorithm in radiotherapy treatment planning for 6 mv photon. *Department of Physics, Yeungnam University, Gyeongsan*.

[68] Michael F. L'Annunziata. *Radioactivity Introduction and History, from the Quantum to Quarks*. Elsevier, 2016.

[69] SARIT APPEL JAIR BAR DROR ALEZRA MAOZ BEN-AYUN TATIANA RABIN-ALEZRA NIR HONIG 1TAMAR KATZMAN SUMIT CHATTERJI ZVI SYMON RICHARD LAWRENCE. Image-guidance triggered adaptive replanning of radiation therapy for locally advanced lung cancer: an evaluation of cases requiring plan adaptation. *Br J Radiol*, 93, 2020.

[70] Petrucci Harwood Herring Madura. *General Chemistry:Principles & Modern Applications (9th Edition)*. New Jersey: Pearson Education, 2007.

[71] P.-H. Mackeprang D. Vuong W. Volken D. Henzen D. Schmidhalter M. Malthaner S. Mueller D. Frei W. Kilby D. M. Aebersold M. K. Fix P. Manser. Benchmarking monte-carlo dose calculation for mlc cyberknife treatments. *Radiation Oncology*, 14:172, 2019.

[72] Cynthia H. McCollougha and Beth A. Schueler. Calculation of effective dose. *Department of Diagnostic Radiology, Mayo Clinic*, 2000.

[73] Marios Myronakis Mengying Shi and Matthew Jacobson. Gpu-accelerated monte carlo simulation of mv-cbct. *Physics in Medicine & Biology*, 65:23, 2020.

[74] Paul Symonds Charles Deehan John A. Mills Cathy Meredith. *Walter and Miller's Textbook of Radiotherapy*. Elsevier, 2012.

[75] Laura Vanderwaeren Rüveyda Dok Kevin Verstrepen Sandra Nuyts. Clinical progress in proton radiotherapy: Biological unknowns. *Cancers*, 13:4, 2021.

[76] The University of Liverpool. *3D Segrè chart*. Department of Physics, 2000.

[77] Ugo Amaldi Manjit Dosanjh Jacques Balosso Jens Overgaard. *A Facility for Tumour Therapy and Biomedical Research in South-Eastern Europe*. CERN Yellow Reports, 2019.

[78] Isabel Di Pasquale. *MSc Thesis: Treatment Planning in Proton Therapy using VPatient 3D and Monte Carlo Simulation*. Politecnico di Torino, 2021-2022.

[79] Michele M. Kim Arash Darafsheh Jan Schuemann Ivana Dokic Olle Lundh Tianyu Zhao José Ramos-Méndez Lei Dong Kristoffer Petersson. Development of ultra-high dose rate (flash) particle therapy. *IEEE Transactions on Radiation and Plasma Medical Sciences*, 2021.

[80] James M. Galvin D.Sc. Ying Xiao Ph.D. Yan Chen Ph.D. Greg Bednarz Ph.D. Darek Michalski Ph.D. Yair Censor Ph.D. Chris Houser B.S. Murshed Hossain PhD M. Saiful Huq Ph.D. *The Optimization of Inverse Planning and IMRT*. Jefferson Medical School.

[81] Savel Pierre. *"Atomic Energy." The Discovery of Artificial Radioactivity*. 1964.

[82] pit claudel.fr.

[83] Raystation. *ROBUST OPTIMIZATION IN RAYSTATION*. RaySearch Laboratories, 2017.

[84] Macarena Cubillos-Mesías Michael Baumann Esther G. C. Troost Fabian Lohaus Steffen Löck Christian Richter and Kristin Stützer. Impact of robust treatment planning on single- and multi-field optimized plans for proton beam therapy of unilateral head and neck target volumes. *Radiation Oncology*, 12:190, 2017.

[85] Riccardo Ridolfi. Study of the track reconstruction in the foot experiment for hadrontherapy. *University of Bologna*, 2018.

[86] Ann Barrett Jane Dobbs Stephen Morris Tom Roques. *Practical Radiotherapy Planning*. Hodder Arnold, 2009.

[87] P. Pearce S. Verdu-Andres U. Amaldi R. Bonomi A. Degiovanni M. Garlasch A. Garonna R. Wegner C. Mellace. High-gradient test of a 3 ghz single-cell cavity. *Proceedings of Linear Accelerator Conference LINAC2010, Tsukuba, Japan*, 2010.

[88] Yuan Zhou Yang Li Yoshiki Kubota Makoto Sakai and Tatsuya Ohno. Robust angle selection in particle therapy. *Frontiers*, 2021.

[89] Saini J Traneus E Maes D Regmi R Bowen SR Bloch C Wong T. Advanced proton beam dosimetry part i: review and performance evaluation of dose calculation algorithms. *Transl Lung Cancer Res*, 7:2, 2018.

[90] Indiana University. *Mesons, Baryons and Tetraquarks*.

[91] Jan Unkelbach and Harald Paganetti. Robust proton treatment planning: Physical and biological optimization. *Semin Radiat Oncol.*, 28:2, 2018.

[92] R.E. Drzymala R. Mohan L. Brewster M. Goitein W. Harms M. Urie. Dose-volume histograms. *International Journal of Radiation Oncology*, 21:71–78, 1991.

[93] Unkelbach Jan Alber Markus Bangert Mark Bokrantz Rasmus Chan Timothy C Y Deasy Joseph O Fredriksson Albin Gorissen Bram L van Herk Marcel Liu Wei Mahmoudzadeh Houra Nohadani Omid Siebers Jeffrey V Witte Marnix Xu Huijun. *Robust radiotherapy planning*. University of Zurich, 2018.

[94] Frank Verhaegen and Jan Seuntjens. Monte carlo modelling of external radiotherapy photon beams. *Physics in Medicine & Biology*, 48:21, 2003.

[95] M. Vretenar. *Linear Accelerators*. CERN, 2014.

[96] Niklas Wahl. *An introduction to inverse treatment planning / dose optimization.* HITRI, 2021.

[97] Joao Seco William R. Hendee and Frank Verhaegen. *Monte Carlo Techniques in Radiation Therapy.* CRC Press, Taylor & Francis Group, 2013.

[98] Ines Winz. *A Decision Support System for Radiation Therapy Treatment Planning.* University of Auckland, 2014.

[99] Liang Zhao Qiuyan Wan Yongqiang Zhou Xia Deng Congyin Xie Shixiu Wu. The role of replanning in fractionated intensity modulated radiotherapy for nasopharyngeal carcinoma. *Radiotherapy and Oncology*, 98:23–27, 2010.

[100] C. Zhou et al X. Zhou, W. Wang. Long-term outcomes of replanning during intensity-modulated radiation therapy in patients with nasopharyngeal carcinoma: An updated and expanded retrospective analysis. *Radiotherapy and Oncology*, 170:136–142, 2022.

[101] Wei-Rong Yao Shou-Ping Xu Bo Liu Xiu-Tang Cao Gang Ren Lei Du Fu-Gen Zhou Lin-Chun Feng Bao-Lin Qu Chuan-Bin Xie and Lin Ma. Replanning criteria and timing definition for parotid protection-based adaptive radiation therapy in nasopharyngeal carcinoma. *BioMed Research International*, 2015.

[102] Yelda Elcim Bahar Dirican Omer Yavas. Dosimetric comparison of pencil beam and monte carlo algorithms in conformal lung radiotherapy. *RADIATION ONCOLOGY PHYSICS*, 19(5):616–624, 2018.

[103] Xiaodong Zhang. A review of the robust optimization process and advances with monte carlo in the proton therapy management of head and neck tumors. *International Journal of Particle Therapy*, 2021.

[104] Jakob Ödén. *Proton plan evaluation: a framework accounting for treatment uncertainties and variable relative biological effectiveness.* Stockholm University, 2017.